Bulletin of Mathematical Biology (2021) 83:92
https://doi.org/10.1007/s11538-021-00917-0

SPECIAL ISSUE: CELEBRATING J. D. MURRAY

A Random Walk Approach to Transport in Tissues and Complex Media: From Microscale Descriptions to Macroscale Models

Jay A. Stotsky[1] · Jia Gou[2] · Hans G. Othmer[1]

Received: 5 October 2020 / Accepted: 1 June 2021

Abstract

The biological processes necessary for the development and continued survival of any organism are often strongly influenced by the transport properties of various biologically active species. The transport phenomena involved vary over multiple temporal and spatial scales, from organism-level behaviors such as the search for food, to systemic processes such as the transport of oxygen from the lungs to distant organs, down to microscopic phenomena such as the stochastic movement of proteins in a cell. Each of these processes is influenced by many interrelated factors. Identifying which factors are the most important, and how they interact to determine the overall result is a problem of great importance and interest. Experimental observations are often fit to relatively simple models, but in reality the observations are the output of complicated functions of the physicochemical, topological, and geometrical properties of a given system. Herein we use multistate continuous-time random walks and generalized master equations to model transport processes involving spatial jumps, immobilization at defined sites, and stochastic internal state changes. The underlying spatial models, which are framed as graphs, may have different classes of nodes, and walkers may have internal states that are governed by a Markov process. A general form of the solutions, using Fourier–Laplace transforms and asymptotic analysis, is developed for several spatially infinite regular lattices in one and two spatial dimensions, and the theory is developed for the analysis of transport and internal state changes on general graphs. The goal in each case is to shed light on how experimentally observable macroscale transport coefficients can be explained in terms of microscale properties

Dedicated to James D. Murray on his 90th birthday. Jim was a pioneer in Mathematical Biology, and as a mentor to many his leadership and vision have had an enormous impact on the development of the field.

✉ Hans G. Othmer
othmer@math.umn.edu

[1] School of Mathematics, University of Minnesota, 270A Vincent Hall, Minneapolis, USA

[2] Department of Mathematics, University of California, 900 University Ave. Skye Hall, Riverside CA 92521, USA

Published online: 16 July 2021

of the underlying processes. This work is motivated by problems arising in transport in biological tissues, but the results are applicable to a broad class of problems that arise in other applications.

Keywords Continuous-time random walk · Multiscale model · Drosophila · Multistate random walk · First passage time

1 Introduction

Within any organism, various spatially distributed networks with widely distinct characteristics exist—the nervous system, the cardiovascular system, and air passages in the lungs of higher organisms are but a few examples. When biochemical processes occur within these biological networks, the network structure can play a significant role in determining the outcome of such processes. For instance, if a biochemical signal secreted by a set of cells has to travel through this network to reach distant cells, transport properties of the network play a crucial role in determining the strength and dynamic behavior of the signal. In order to understand complicated cell-level and tissue-level processes such as morphogenesis, it is crucial to assess the effects of interactions between the complex spatial structures and the properties of associated signal transduction networks that translate chemical signals into cellular responses. This problem is particularly challenging as it is difficult to interpret tissue or organism-scale experiments in terms of microscopic details of reactions and transport, and conversely, it is a challenge to extrapolate local microscale measurements of transport to tissue-level behavior.

A widely-studied example arises in the analysis of transport and transduction of bone morphogenetic protein (BMP) signals during morphogenesis of the wing disk of the fruit fly *Drosophila melanogaster*. Wing disks (Fig. 1a) arise in the embryo at the intersection of a circumferential stripe of the protein wingless (Wg) and an anterior–posterior (AP) stripe of Decapentaplegic (Dpp) (Gou et al. 2020). The disk has two layers of cells separated by a lumen (Fig. 1b), one a layer of columnar epithelial cells

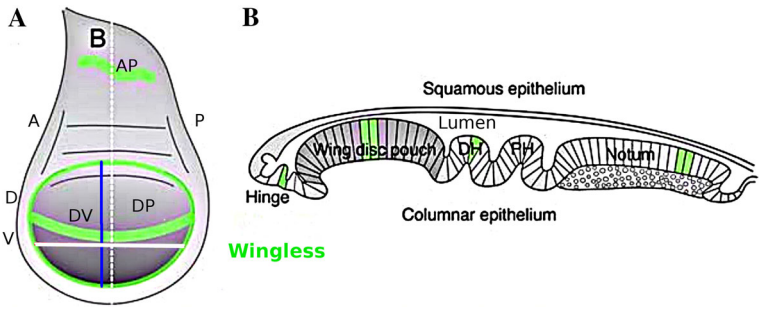

Fig. 1 **A** Wing disk A: anterior, P: posterior, D: dorsal, V: ventral, AP & DV: anterior–posterior and dorsal–ventral boundaries, DP: disk pouch. **B** side view along B in (**A**). Modified from Widmann and Dahmann (2009)

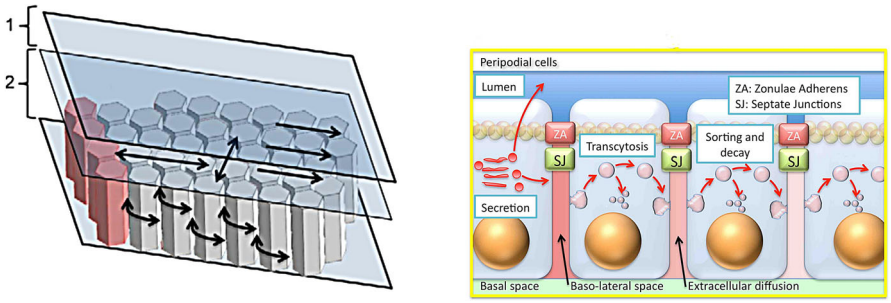

Fig. 2 Left: A schematic of a portion of the wing disk, showing the luminal section (1) at the top, , the cellular array below (2), and the source of Dpp at the left. Right: A cross section of a disk showing the transport processes that affect the morphogen distribution (Othmer et al. 2009). ZA are aka AJ

with the apical side at the lumen and the basal side at the basal lamina, the other a peripodial epithelium overlying the lumen (Fig. 2). The lateral membranes of adjacent columnar cells are connected via adherens junctions (AJs), which are complexes of E-cadherins and adapter proteins, and via septate junctions (SJs) that lie basal to the AJs and separate the extracellular fluid into apical and baso-lateral layers (Gibson and Gibson 2009; Harris and Tepass 2010; Choi 2018).

The wing disk is perhaps the best understood system in which transport of a molecule—in this case the BMP family member Dpp—involves a number of very distinct steps in a geometrically complex tissue. The secretion of Dpp from a stripe of cells along the AP boundary colored red in Fig. 2(left) gives rise to a spatial distribution of Dpp transverse to the AP boundary, but how the distribution is established is still an open question.

Various local processes and paths are involved in the transport of Dpp in the wing disk, and it has been observed that Dpp dispersal occurs both in the lumenal and the baso-lateral space. Dpp is uniformly distributed in the lumen, while in the baso-lateral region a graded Dpp distribution was found (Gibson et al. 2002; Mundt 2013; Harmansa et al. 2017). Extracellular Dpp can bind to membrane receptors, which can restrict its long-range transport by retaining it on cell surfaces (Haerry et al. 1998). It can then be internalized via endocytosis for either lysosomal degradation or recycling to the membrane, as well as for transcellular transport (Entchev et al. 2000; Akiyama et al. 2008). For instance, as was shown for Wg (Yamazaki et al. 2016), Dpp might also undergo apico-basal transport in the columnar cells, which promotes the communication between the apical and baso-lateral regions.

Spatial profiles of Dpp measured via imaging techniques such as FRAP, are usually described with a reaction–diffusion model based on diffusion and first-order decay (Kicheva et al. 2007; Wartlick et al. 2011). Fitting this model to FRAP data from one set of experiments yielded a diffusion coefficient of $0.1\,\mu m^2/s$ (Kicheva et al. 2007). In contrast, Zhou et al. (2012) measured a free diffusion coefficient of $20\,\mu m^2/s$ using fluorescence correlation spectroscopy. The discrepancy between the two values can be understood since the former is a macroscopic parameter, and in reality, the simple diffusion model integrates various local processes, such as receptor-mediated uptake, local degradation and transport in each cell. More recent work shows that

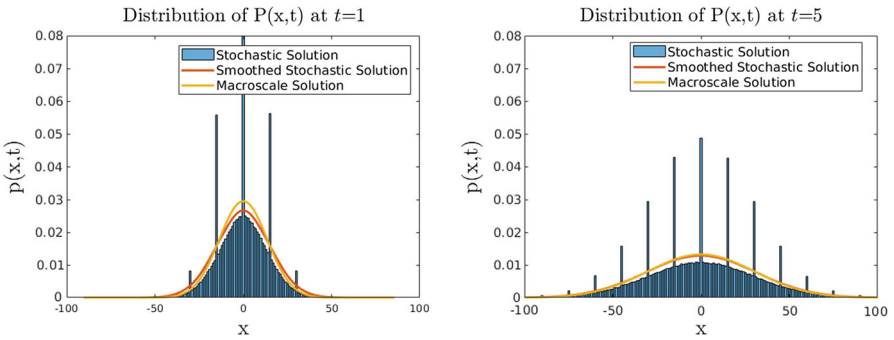

Fig. 3 Comparisons of stochastic simulations and continuum results for two times, $t = \{1, 5\}$ with $n = 15$. The cell-averaged concentration, obtained through smoothing the stochastic data, approaches the continuum macroscale solution as time progresses. The spikes are due to slower jumping rates at the cell membranes as compared with the interior, which leads to local accumulation. The waiting times at interior points are set to be 4.5 times faster than at the junctions and roughly 100 jumps occur per unit time on average

spreading of Dpp in the apical lumen, where free diffusion can occur, plays a minor role in both growth and patterning—most occurs in the baso-lateral space (Mundt 2013; Harmansa et al. 2017). Given the complexity of the geometric structure of the disk and the different local processes that may be involved in Dpp transport, a much more complicated transport model is required to describe the establishment of the Dpp profile in this system.

Herein we describe transport processes as multistate random jump processes in which the walkers are characterized by both their spatial location and their internal state. Spatial states live on lattices and general graphs, chosen so as to represent some aspects of transport in the disk, and as used here, these lattices have a translation-invariant structure that makes the problems amenable to analytical techniques. We analyze a number of examples of Markovian problems to obtain relations for certain transport coefficients in terms of the details of the underlying processes, and develop techniques for use on general graphs and non-Markovian jump processes. While we focus on analytically-tractable problems, numerical approaches can be applied to supplement what can be obtained analytically in more complex applications.

As a motivating example, consider Dpp transport in a 1D domain that is subdivided into a number of cells, each of width L. We overlay a lattice with two types of vertices on the line of cells, $n = L/\Delta x$ vertices within each cell and a distinct vertex at each membrane. We suppose that within each cell a molecule can jump from site to site at a rate μ, and at membrane points a molecule can linger longer, and either return to where it came from or jump into the neighboring cell. A stochastic simulation of the movement of a particle that begins at $x = 0$ leads to the distributions shown at two different times in Fig. 3.

Depending on the waiting-time distributions for a jump at interior points and at the membranes, the time spent at these points can be very different, as shown by the spikes at both times, but when the stochastic results are averaged the result is a normal or Gaussian distribution characteristic of a diffusion process. As we show later, if we define the diffusion coefficient within a cell as $D_m = \mu/\Delta x^2$ and set the

mean membrane residence time $\tau = \lambda_0^{-1} = \lambda^{-1}\Delta x$, then the macroscopic diffusion coefficient that characterizes the spread of the molecule's location at long times is $D_M = \frac{\lambda D_m}{\lambda + D_m/L^2}$ under a suitable scaling of the jump rates as the lattice spacing goes to zero. The yellow line in Fig. 3 shows the solution of the macroscale diffusion equation using this diffusion coefficient.

A major objective of this work is to understand in general how parameters describing microscale processes can be "lifted" to parameters for macroscale descriptions of the processes. This has been done in a continuum framework for a line of cells, but for nonlinear reactions the homogenization is not simple (Othmer 1983). This also becomes difficult when describing transport in complex geometries such as the wing disk. We show that the lattice structure often makes it possible to reduce a random process with numerous (even infinite) internal states into random processes with just a few internal states. The effect of this change is to ignore certain local details, by including information about local processes in overall transport coefficients valid at larger length and timescales.

We only deal with linear processes, which leads to linear evolution equations and thus to potentially large spectral problems, and a great deal of earlier work has dealt with similar problems (Othmer and Scriven 1971; Gadgil et al. 2005; Kang et al. 2012; Hu and Othmer 2011; Ciocanel et al. 2020). However, earlier work was focused on simple geometries, and in this article, we expand the scope of these problems to cases where there are multiple types of states that have differing connectivity patterns, and we show how exact macroscale waiting-time distributions can be derived in some cases. The computation of spatial moments for multistate random walks has also been treated earlier (Landman and Shlesinger 1979a, b, 1977; Roerdink and Shuler 1985a, b; Scher and Wu 1981), and while there is some overlap with earlier work, our approach includes both microscale spatial structure, complex geometries, and internal states for the walkers.

An outline of the paper is as follows. In the following section, we provide a brief introduction to the standard theory of continuous-time random walks (CTRWs) in continuum space. We then extend these ideas to lattice walks on graphs in which there are two distinct classes of vertices in the underlying graph, one of which we call primary junctions or vertices, and the other, which we call secondary vertices, live on edges connecting primary junctions. We also consider processes in which the walker has internal states as well, and develop evolution equations for the stochastic evolution of both spatial location and internal state. In Sect. 3, we derive the moment equations for one-dimensional lattices, and in Sect. 4 and 5, we develop different approaches to the "micro-to-macro" analysis in one-dimensional lattices. In Sect. 6, we consider hexagonal lattices and develop the evolution and moment equations for such lattices. In Appendix B, we describe a general formulation by which arbitrary graphs can be treated. For reference, Table 1 contains a list of the abbreviations used throughout.

Table 1 List of abbreviations and recurring notation

Abbreviation	Notation	Meaning
CTRW		Continuous-time random walk
WTD	$\phi(t)$ or $\psi(t)$	Waiting-time distribution
	$\Phi(t)$	Cumulative waiting-time distribution
	$\hat{\Phi}(t)$	Complementary waiting-time distribution
FPT	$\boldsymbol{f}(t)$	First-passage-time density distribution
Junction		A vertex in the primary graph $\mathscr{G}$
SV		Secondary vertices–spatial states on an edge connecting vertices in the primary graph
	$p(\boldsymbol{x}, t\|\mathbf{0})$ or $p(\boldsymbol{x}, t)$	Probability of occupying location $\boldsymbol{x}$ at time t after starting at $\boldsymbol{x} = \mathbf{0}$ at $t = 0$.
	$q(\boldsymbol{x}, t\|\mathbf{0})$ or $q(\boldsymbol{x}, t)$	Probability density of arriving at location $\boldsymbol{x}$ at time t after starting at $\boldsymbol{x} = \mathbf{0}$ at $t = 0$.
	$n(\boldsymbol{x}, t)$	Number density of particles at $\boldsymbol{x}$ and t
	$m^{(k)}(t)$	k^{th} spatial moment of $p(\boldsymbol{x}, t)$
	$T(\boldsymbol{x}, \boldsymbol{y})$	Spatial jump distribution operator for a jump process
	$\boldsymbol{K}(t)$	Internal state transition matrix
	$\boldsymbol{\Lambda}(t)$	Diagonal matrix of internal state exit rates
	$W(\boldsymbol{x}, \boldsymbol{y})$	Spatial transition operator for a differential master equation
	$\Gamma(t)$	Memory kernel for a differential master equation
	$\otimes$	Kronecker product operator
	n_k	Number of SVs on an edge
	n_s	Number of internal states of a walker or particle

Blank entries in the notation column apply when the abbreviation has no associated mathematical symbol. Likewise, the abbreviation column is empty for mathematical symbols that are not abbreviated.The dependence on the initial position $\boldsymbol{x} = \mathbf{0}$ in p and q is often omitted in the text

2 The Continuous-Time Random Walk

2.1 Single-State Walkers in a Continuum

When the underlying space is a continuum, a continuous-time random walk (CTRW) is a random jump process on R^n in which the particle or walker, which can range from a molecule to an organism, executes a sequence of spatial jumps of negligible duration. In biological contexts, a walker may have many internal states such as the configuration of a molecule that can also change, but to begin we assume that the only change in the jump process is position in space—the case of multiple internal states is treated in the following subsection. We assume that the waiting times between successive jumps at a given position are independent and identically distributed, i.e. if the jumps occur at $T_0, T_1, \ldots$ then the increments $T_i - T_{i-1}$ are independently and identically distributed, and therefore, the jump process is a semi-Markov process (Feller 1968; Karlin and Taylor 1975).

Let $\boldsymbol{\Psi}(\boldsymbol{x}, t|\boldsymbol{y}, 0)$ be the joint conditional probability density that a walker at $\boldsymbol{y}$ at time $t = 0$ remains at $\boldsymbol{y}$ until it jumps at t^- and lands at $\boldsymbol{x}$. The waiting time $\mathscr{T}$ between jumps is governed by the waiting-time distribution (WTD)

$$\phi(\boldsymbol{y}, t) = \int_{R^n} \boldsymbol{\Psi}(\boldsymbol{x}, t|\, \boldsymbol{y}, 0) d\boldsymbol{x} \tag{1}$$

and the spatial distribution of jumps is given by

$$T(\boldsymbol{x}, \boldsymbol{y}) = \int_0^\infty \boldsymbol{\Psi}(\boldsymbol{x}, t|\, \boldsymbol{y}, 0) dt. \tag{2}$$

The cumulative and complementary waiting-time distributions, Φ and $\hat{\Phi}$, respectively, are

$$\Phi(\boldsymbol{y}, t) = \int_0^t \phi(\boldsymbol{y}, s)\, ds = Pr\{\mathscr{T} \leq t\} \tag{3}$$

and

$$\hat{\Phi}(\boldsymbol{y}, t) = \int_t^\infty \phi(\boldsymbol{y}, s)\, ds = 1 - \Phi(t) = Pr\{\mathscr{T} \geq t\}. \tag{4}$$

The fact that we condition on the assumption that the current time at position $\boldsymbol{y}$ can be taken as $t = 0$ means that the jump distribution, $T(\boldsymbol{x}, \boldsymbol{y})$, is independent of the waiting time. In the above we incorporated the current position, $\boldsymbol{y}$, in the waiting-time distribution and this will be used later for lattice walks, but in this section we will omit this. Thus, if the jumps are governed by a Poisson process with parameter λ, the cumulative distribution is $\Phi(t) = 1 - e^{-\lambda t}$ and the waiting-time distribution is $\phi(t) = \lambda e^{-\lambda t}$. This is the only smooth distribution for which the jump process is Markovian (Feller 1968).

CTRWs are particularly useful since experimental observables, such as the moments of the displacement distribution and their dependence on time, can be related to the quantities, ϕ and T that specify the CTRW. In turn, ϕ and T are specified in terms of the microscale properties of the system being studied. To relate observables to ϕ and T we require an evolution equation for the density function $p(\boldsymbol{x}, t|\, 0)$, which is defined such that $p(\boldsymbol{x}, t|\, 0)dx$ is the probability that the position of a jumper which begins at the origin at $t = 0$ lies in the interval $(\boldsymbol{x}, \boldsymbol{x} + d\boldsymbol{x})$ at time t. We derive this equation via equations for some auxiliary quantities.

Let $q_k(\boldsymbol{x}, t)d\boldsymbol{x}\, dt$ be the joint probability that a walker starting at the origin takes its kth step in the interval $(t, t + dt)$ and lands in the interval $(\boldsymbol{x}, \boldsymbol{x} + d\boldsymbol{x})$. Then for any $\boldsymbol{x} \neq \boldsymbol{0}$, $t > 0$, q_k satisfies the first-order integro-difference equation

$$q_{k+1}(\boldsymbol{x}, t|\boldsymbol{0}) = \int_0^t \int_{R^n} \phi(t - \tau) T(\boldsymbol{x}, \boldsymbol{y}) q_k(\boldsymbol{y}, \tau|\boldsymbol{0})\, d\boldsymbol{y}\, d\tau, \qquad k = 1, 2, \ldots \tag{5}$$

The density function for arriving in the interval $(\boldsymbol{x}, \boldsymbol{x} + d\boldsymbol{x})$ in time interval $(t, t + dt)$ after any number of steps is the sum of these, from which we obtain the integral

equation

$$q(\boldsymbol{x}, t|\boldsymbol{0}) = \sum_{k=0}^{\infty} q_k(\boldsymbol{x}, t|\boldsymbol{0}) = q_0(\boldsymbol{x}, t|\boldsymbol{0}) + \int_0^t \int_{R^n} \phi(t-\tau) T(\boldsymbol{x}, \boldsymbol{y}) q(\boldsymbol{y}, \tau|\boldsymbol{0})\, d\boldsymbol{y}\, d\tau. \tag{6}$$

Since the walker starts at $\boldsymbol{x} = \boldsymbol{0}$, $q(\boldsymbol{x}, t|\boldsymbol{0})$ must satisfy the initial condition $q(\boldsymbol{x}, 0|\boldsymbol{0}) = \delta(\boldsymbol{x})$ and therefore

$$q(\boldsymbol{x}, t|\boldsymbol{0}) = \delta(\boldsymbol{x})\delta(t) + \int_0^t \int_{R^n} \phi(t-\tau) T(\boldsymbol{x}, \boldsymbol{y}) q(\boldsymbol{y}, \tau|\boldsymbol{0})\, d\boldsymbol{y}\, d\tau. \tag{7}$$

To obtain the density function $p(\boldsymbol{x}, t|\boldsymbol{0})$, observe that it is the product of the probability of arriving in $(\boldsymbol{x}, \boldsymbol{x} + d\boldsymbol{x})$ at some time $\tau < t$ and the probability that no transition occurs in the remaining time $t - \tau$. As a result,

$$\begin{aligned} p(\boldsymbol{x}, t|\boldsymbol{0}) &= \int_0^t \hat{\Phi}(t-\tau) q(\boldsymbol{x}, \tau|\boldsymbol{0})\, d\tau \\ &= \int_0^t \hat{\Phi}(t-\tau) \{\delta(\boldsymbol{x})\delta(\tau) + \int_0^\tau \int_{R^n} \phi(\tau - s) T(\boldsymbol{x}, \boldsymbol{y}) q(\boldsymbol{y}, s|\boldsymbol{0})\, d\boldsymbol{y}\, ds\}\, d\tau \\ &= \hat{\Phi}(t)\delta(\boldsymbol{x}) + \int_0^t \int_{R^n} \left(\int_s^t \hat{\Phi}(t-\tau)\phi(\tau - s)\, d\tau \right) T(\boldsymbol{x}, \boldsymbol{y}) q(\boldsymbol{y}, s|\boldsymbol{0}) d\boldsymbol{y}\, ds. \end{aligned} \tag{8}$$

From this, one finds that $p(\boldsymbol{x}, t|0)$ satisfies the following renewal equation (Othmer et al. 1988)

$$p(\boldsymbol{x}, t|0) = \hat{\Phi}(t)\delta(\boldsymbol{x}) + \int_0^t \int_{R^n} \phi(t-\tau) T(\boldsymbol{x}, \boldsymbol{y}) p(\boldsymbol{y}, \tau|0)\, d\boldsymbol{y}\, d\tau \tag{9}$$

which is sometimes called the *integral master equation* (Mainardi et al. 2000).

Although $p(\boldsymbol{x}, t|\boldsymbol{0})$ gives the probability density for a single particle to be located at $\boldsymbol{x}$ at time t, in experiments it is more common to observe a concentration distribution associated with many particles. If the initial number density distribution of non-interacting walkers is $f(\boldsymbol{x})$, then at time t, the number density, $n(\boldsymbol{x}, t)$ satisfies

$$n(\boldsymbol{x}, t) = \hat{\Phi}(t) f(\boldsymbol{x}) + \int_0^t \int_{R^n} \phi(t-\tau) T(\boldsymbol{x}, \boldsymbol{y}) n(\boldsymbol{y}, \tau)\, d\boldsymbol{y}\, d\tau. \tag{10}$$

The necessary and sufficient condition for conservation of walkers is that the jump distribution satisfies

$$\int_{R^n} T(\boldsymbol{x}, \boldsymbol{y})\, d\boldsymbol{x} = 1.$$

To obtain a differential form of the integral master equation, we define the Laplace transform of an exponentially bounded $f(t)$ as

$$\tilde{f}(s) = \mathscr{L}\{\langle f(t)\rangle\} \equiv \int_0^\infty e^{-st} f(t)\, dt$$

and take the Laplace transform of (10). This leads to

$$\tilde{n}(\boldsymbol{x}, s) = \frac{1-\tilde{\phi}(s)}{s} f(\boldsymbol{x}) + \tilde{\phi}(s) \int_{R^n} T(\boldsymbol{x}, \boldsymbol{y}) \tilde{n}(\boldsymbol{y}, s)\, d\boldsymbol{y} \tag{11}$$

which can be rearranged to

$$\left\{\frac{1-\tilde{\phi}(s)}{s\tilde{\phi}(s)}\right\} \{s\tilde{n}(\boldsymbol{x}, s) - f(\boldsymbol{x})\} = -\tilde{n}(\boldsymbol{x}, s) + \int_{R^n} T(\boldsymbol{x}, \boldsymbol{y}) \tilde{n}(\boldsymbol{y}, s)\, d\boldsymbol{y}. \tag{12}$$

The second bracketed quantity on the left side is the transform of $\dfrac{\partial n(\boldsymbol{x}, t)}{\partial t}$, while the leading factor defines the function

$$\Gamma(t) \equiv \mathscr{L}^{-1}\left\{\frac{1-\tilde{\phi}(s)}{s\tilde{\phi}(s)}\right\},$$

which is called the memory function (Mainardi et al. 2000). Thus the inverse transform of (12) is

$$\int_0^\infty \Gamma(t-\tau) \frac{\partial n(\boldsymbol{x}, \tau)}{\partial \tau} d\tau = -n(\boldsymbol{x}, t) + \int_{R^n} T(\boldsymbol{x}, \boldsymbol{y}) \boldsymbol{n}(\boldsymbol{y}, t)\, d\boldsymbol{y}. \tag{13}$$

For an exponential WTD of the form $\phi(t) = \lambda exp(-\lambda t)$, $\Gamma(t) = \delta(t)/\lambda$ and (13) reduces to

$$\frac{\partial n(\boldsymbol{x}, t)}{\partial t} = -\lambda n(\boldsymbol{x}, t) + \lambda \int_{R^n} T(\boldsymbol{x}, \boldsymbol{y}) n(\boldsymbol{y}, t)\, d\boldsymbol{y}. \tag{14}$$

This is the differential form of the master equation (Othmer et al. 1988). A number of examples of choices for $T(\boldsymbol{x}, \boldsymbol{y})$ that lead to either a diffusion equation or a telegrapher's equation are given in Othmer et al. (1988). A choice that will be used later defines a CTRW on a lattice or graph.

In the above, we consider a general jump function $T(\boldsymbol{x}, \boldsymbol{y})$, but if the jumps depend only on the difference $\boldsymbol{\xi} \equiv \boldsymbol{x} - \boldsymbol{y}$ the foregoing equations can be rewritten slightly. For example (14) can be written as

$$\frac{\partial \boldsymbol{n}(\boldsymbol{x}, t)}{\partial t} = \lambda \int_{R^n} T(\boldsymbol{\xi}, \boldsymbol{0}) \{\boldsymbol{n}(\boldsymbol{x} - \boldsymbol{\xi}, t) - \boldsymbol{n}(\boldsymbol{x}, t)\}\, d\boldsymbol{\xi}. \tag{15}$$

Since $T(\boldsymbol{x} - \boldsymbol{y}, 0) = T(\boldsymbol{x}, \boldsymbol{y})$ in this case, we can omit the second argument of T and just write $T(\boldsymbol{x} - \boldsymbol{y})$.

2.2 Walkers with Multiple Internal States and Binding

In biological transport problems, there are often various types of reaction, such as binding, catalysis, and degradation, that occur. One way to include these in the present formulation is to describe a walker in a CTRW as having internal states, each of which describes a distinct internal characteristic of the walker. For example, the internal state may describe the conformation of a protein, or it could describe a molecular type when interconversions occur according to a first-order reaction.

In a later example, binding will only occur in a subset of the spatial locations, thus some properties are attached to the spatial point, not to the internal state of the walker. On the other hand, if there is a probability of spontaneous interconversion between internal states (or death) that is the same for all spatial sites, that is built into the internal dynamics of the walker.

When walkers have a finite number n_s of internal states that evolve according to a Markov chain, the transitions can be included in the foregoing equations by defining the WTDs for internal state changes and the probability of a jump between states. We assume that changes in internal states and spatial position do not occur simultaneously, and thus, the effects of the processes are additive. Suppose that the internal states are $S = (S_1, \cdots, S_{n_s})$ and that they evolve according to a Markov chain with evolution equation

$$\frac{dS}{dt} = RS, \tag{16}$$

where R_{ij} is the transition rate between states j and i. Then the probability of a jump from state j to i is

$$k_{ij} = \frac{R_{ij}}{\sum_{l \neq j} R_{lj}} \tag{17}$$

and the parameter of the Poisson process governing the WTD in state j is the sum of the exit rates from state j, which is

$$\lambda_j = \sum_{l \neq j} R_{lj}. \tag{18}$$

In this case, where the space jumps and internal state changes are themselves Markovian processes, the waiting-time distributions for the composite process may be found explicitly. For the composite process of space jumps and internal state changes, the waiting-time density $\phi_{c_i}(t)$ for a space jump while in the ith state [1], conditioned on no change in the ith state, is the product of the WTD for a pure jump process times the probability of no change in the ith internal state. Thus

$$\phi_{c_i}(t) = \lambda e^{-\lambda t} \times \left(1 - \int_0^t \lambda_i e^{-\lambda_i \tau} d\tau\right) = \lambda e^{-(\lambda + \lambda_i)t}, \tag{19}$$

and the density for a jump in space, given no change in any internal state, is simply the product of these taken over all internal states.

[1] The subscript c indicates the composite process rather than the pure space jump process.

Since the position and state changes cannot occur simultaneously, their effects are additive, and letting $\boldsymbol{q}_k$ be the n_s-vector of states as a function of time and space, the generalization of (5) for arrival at $(\boldsymbol{x}, S)$ at time t is

$$\boldsymbol{q}_{k+1}(\boldsymbol{x}, t) = \int_0^t \left\{ \left[\int_{R^n} \boldsymbol{\phi}_c(t-\tau) T(\boldsymbol{x}, \boldsymbol{y}) \boldsymbol{q}_k(\boldsymbol{y}, \tau) d\boldsymbol{y} \right] + \boldsymbol{K} \Lambda(t-\tau) \boldsymbol{q}_k(\boldsymbol{x}, \tau) \right\} d\tau. \tag{20}$$

Here $\boldsymbol{\phi}_c(t) = diag\{\phi_{c_i(t)}\}$ and $\Lambda(t) = diag\{\lambda_i e^{-(\lambda+\lambda_i)t}\}$. The elements of Λ represent the waiting-time densities for the state changes multiplied by the probability that no space jump occurs in $[0, t]$, and the entries of K represent the probabilities of jumps between states, given that one occurs. $\boldsymbol{K}$ is the analog in the set of internal states of the jump kernel T in physical space. Note that for brevity of notation, we have omitted the conditioning on the initial condition in $\boldsymbol{q}$ and $\boldsymbol{p}$.

The vector version of (8) for occupancy in the state $(\boldsymbol{x}, S)$ at time t becomes

$$\begin{aligned} \boldsymbol{p}(\boldsymbol{x}, t) = \delta(\boldsymbol{x})\delta(t) S_0 + \int_0^t \left\{ \left[\int_{R^n} \boldsymbol{\phi}_c(t-\tau) T(\boldsymbol{x}, \boldsymbol{y}) \boldsymbol{p}(\boldsymbol{y}, \tau) d\boldsymbol{y} \right] \right. \\ \left. + \boldsymbol{K} \Lambda(t-\tau) \boldsymbol{p}(\boldsymbol{x}, \tau) \right\} d\tau, \end{aligned} \tag{21}$$

where S_0 is the vector of the initial internal states. The state of a multiparticle system is now defined by the n_s-vector $\boldsymbol{n}(\boldsymbol{x}, t) = (n_1(\boldsymbol{x}, t), \cdots, n_{n_s}(\boldsymbol{x}, t))$ and the corresponding vector master equation is

$$\frac{\partial \boldsymbol{n}(\boldsymbol{x}, t)}{\partial t} = -(\lambda \boldsymbol{I} + \boldsymbol{\Lambda}(0)) \boldsymbol{n}(\boldsymbol{x}, t) + \lambda \int_{R^n} T(\boldsymbol{x}, \boldsymbol{y}) \boldsymbol{n}(\boldsymbol{x} - \boldsymbol{\xi}, t)\, d\boldsymbol{\xi} + \boldsymbol{K} \boldsymbol{\Lambda}(0) \boldsymbol{n}(\boldsymbol{x}, t). \tag{22}$$

2.3 Generalization of the Waiting-Time Distributions

In order to generalize to non-Markovian subprocesses, we consider the combination of two stochastic processes whose individual renewal equations are

$$\begin{aligned} q_{k+1}^{(1)}(\boldsymbol{x}, t) &= \int_0^t \int_{\mathbb{R}^n} \phi(t-\tau) T(\boldsymbol{x}, \boldsymbol{y}) q_k^{(1)}(\boldsymbol{y}, \tau) d\boldsymbol{y} d\tau \\ \boldsymbol{q}_{k+1}^{(2)}(t) &= \int_0^t \boldsymbol{K} \boldsymbol{\Lambda}(t-\tau) \boldsymbol{q}_k^{(2)}(\tau) d\tau, \end{aligned}$$

where Λ is a matrix of waiting-time densities for the pure internal state process and $\boldsymbol{K}$ is the matrix of jump probabilities as before. To combine two, possibly non-Markovian, processes into a generalized master equation, we write

$$\boldsymbol{q}_{k+1}(\boldsymbol{x}, t) = \int_0^t \int_{\mathbb{R}^n} \boldsymbol{\phi}_c(t-\tau) T(\boldsymbol{x}, \boldsymbol{y}) \boldsymbol{q}_k(\boldsymbol{y}, \tau) d\boldsymbol{y} d\tau + \int_0^t \boldsymbol{K} \boldsymbol{\Lambda}_c(t-\tau) \boldsymbol{q}_k(\boldsymbol{x}, \tau) d\tau, \tag{23}$$

where $\boldsymbol{\phi}_c$ and $\boldsymbol{\Lambda}_c$ are diagonal matrices of waiting-time densities for the composite process that incorporates the probability of no jump in the complementary process, similar to above. Thus

$$\phi_{c_j}(t) = \phi(t)\left(1 - \int_0^t \Lambda_j(\tau)d\tau\right) \quad \text{and} \quad \Lambda_{c,j}(t) = \Lambda_j(t)\left(1 - \int_0^t \phi(\tau)d\tau\right).$$

Next, we sum over $k = 0, \ldots, \infty$ in Eq. (23) to obtain

$$\begin{aligned}\boldsymbol{q}(\boldsymbol{x}, t) = \delta(\boldsymbol{x})\delta(t)S_0 + \int_0^t \int_{\mathbb{R}^n} \boldsymbol{\phi}_c(t-\tau)T(\boldsymbol{x}, \boldsymbol{y})\boldsymbol{q}(\boldsymbol{y}, \tau)d\tau \\ + \int_0^t \boldsymbol{K}\boldsymbol{\Lambda}_c(t-\tau)\boldsymbol{q}(\boldsymbol{x}, \tau)d\tau.\end{aligned}$$

Making use of the relation between $\boldsymbol{p}$ and $\boldsymbol{q}$ in Eq. (8) leads to an integral equation for $\boldsymbol{p}$:

$$\begin{aligned}\boldsymbol{p}(\boldsymbol{x}, t) = \delta(\boldsymbol{x})\hat{\boldsymbol{\Phi}}_c(t)S_0 + \int_0^t \int_{\mathbb{R}^n} \boldsymbol{\phi}_c(t-\tau)T(\boldsymbol{x}, \boldsymbol{y})\boldsymbol{p}(\boldsymbol{y}, \tau)d\tau \\ + \int_0^t \boldsymbol{\kappa}(t-\tau)\boldsymbol{p}(\boldsymbol{x}, \tau)d\tau.\end{aligned}$$

The reaction matrix kernel $\boldsymbol{\kappa}(t)$ introduced in this equation is defined via an inverse Laplace transform:

$$\boldsymbol{\kappa}(t) = \mathscr{L}^{-1}\left[\tilde{\hat{\boldsymbol{\Phi}}}_c(s)\boldsymbol{K}_c\tilde{\boldsymbol{\Lambda}}_c(s)\tilde{\hat{\boldsymbol{\Phi}}}_c^{-1}(s)\right]$$

wherein the diagonal matrix of complementary waiting-time distributions, $\hat{\boldsymbol{\Phi}}_c$ is defined as

$$\hat{\Phi}_{c_i}(t) = 1 - \Phi_{c_i}(t) = 1 - \int_0^t \left(\phi_{c_i}(\tau) + \Lambda_{c_i}(\tau)\right)d\tau.$$

Following the derivation in Eqs. (13)–(15), we obtain the evolution equation for the number density of several non-interacting particles as

$$\begin{aligned}\int_0^t \boldsymbol{\Gamma}(t-\tau)\frac{\partial \boldsymbol{n}}{\partial t}d\tau = -\boldsymbol{n}(\boldsymbol{x}, t) + \int_0^t \int_{\mathbb{R}^n} \boldsymbol{\mu}(t-\tau)T(\boldsymbol{x}, \boldsymbol{y})\boldsymbol{n}(\boldsymbol{y}, \tau)d\boldsymbol{y}d\tau \\ + \int_0^t \boldsymbol{\nu}(t-\tau)\boldsymbol{n}(\boldsymbol{x}, \tau)d\tau\end{aligned} \tag{24}$$

with the kernels, $\boldsymbol{\Gamma}$, $\boldsymbol{\mu}$, and $\boldsymbol{\nu}$ defined in terms of inverse Laplace transformations as follows.

$$\begin{aligned}\boldsymbol{\Gamma}(t) &= \mathscr{L}^{-1}\left[\frac{1}{s}\left[\tilde{\boldsymbol{\phi}}_c(s) + \tilde{\boldsymbol{\Lambda}}_c(s)\right]^{-1}\tilde{\hat{\boldsymbol{\Phi}}}_c(s)\right]\\ \boldsymbol{\mu}(t) &= \mathscr{L}^{-1}\left[\left[\tilde{\boldsymbol{\phi}}_c(s) + \tilde{\boldsymbol{\Lambda}}_c(s)\right]^{-1}\tilde{\boldsymbol{\phi}}_c(s)\right]\\ \boldsymbol{\nu}(t) &= \mathscr{L}^{-1}\left[\left[\tilde{\boldsymbol{\phi}}_c(s) + \tilde{\boldsymbol{\Lambda}}_c(s)\right]^{-1}\tilde{\hat{\boldsymbol{\Phi}}}_c(s)\boldsymbol{K}_c\tilde{\boldsymbol{\Lambda}}_{\boldsymbol{c}}(s)\tilde{\hat{\boldsymbol{\Phi}}}_c^{-1}(s)\right].\end{aligned} \tag{25}$$

As shown earlier, when both transport and reaction are governed by Poisson processes, the resulting master equation is a system of ODEs, but what we see here is that non-Poissonian WTDs will generally lead to a more complicated integro-differential equations. We also note that in many cases, $\boldsymbol{\Gamma}$ cannot be defined as a function, but must be understood as a singular distribution (e.g., a Dirac delta function). As an example, the Erlang distribution $\phi(t) = \lambda^2 t e^{-\lambda t}$ has a singular memory kernel, $\Gamma(t) = \lambda^{-2}\delta'(t) + 2\lambda^{-1}\delta(t)$ where $\delta'(t)$ is the distributional derivative of the Dirac delta (c.f. Othmer et al. 1988). In particular, if $\phi(0) = 0$, $\Gamma(t)$ will typically be a singular distribution and the evolution equation for $p(x,t)$ will depend on higher-order derivatives of $p(x,t)$ with respect to time.

In what follows, we do not explicitly outline the manipulations needed when combining various stochastic processes. However, in each case in which we introduce a waiting-time distribution, it should be assumed that it is in fact the waiting-time distribution for the combined process whenever needed.

2.4 Lattice Walks

In many problems, the underlying space can be treated as a lattice, obtained for example, by discretizing an underlying continuum space or as a model of cellular tissues. Here we deal with infinite 1D and 2D lattices in which every lattice point has the same number of neighbors. The lattice can be defined by an undirected graph $\mathscr{G}$, all of whose vertices are of the same degree, and we call such graphs regular. The spatial points in an n-dimensional lattice are typically integer multiples of n basis vectors that define the spacing between vertices. The evolution equation for the probability p_i of a walker being at the ith vertex at time t, assuming an exponential WTD, is

$$\frac{dp_i}{dt} = \lambda \sum_{j\in\mathscr{N}(i)} T_{i.j}\left\{p_j(t) - p_i(t)\right\}, \tag{26}$$

where $T_{i,j}$ is the probability of a jump from vertex j to vertex i and $\mathscr{N}(i)$ is the set of all vertices that are connected to i by a single edge. The adjacency matrix $\mathscr{A}$ of graph $\mathscr{G}$ is the doubly infinite matrix whose entries are 0 or 1, with $\mathscr{A}_{ij} = 1$ if vertex i is connected to vertex j by a single edge. Since the graph is undirected, $\mathscr{A}$ is symmetric. If jumps to all incident edges are assumed to be equiprobable, then Eq. (26) can be

written

$$\frac{dp_i}{dt} = \frac{\lambda}{d} \sum_{j \in \mathcal{N}(i)} \mathscr{A}_{i.j} \left\{ p_j(t) - p_i(t) \right\}, \tag{27}$$

where d is the degree of any vertex in $\mathscr{G}$.[2] Here we have used the fact that

$$\sum_{j \in \mathcal{N}(i)} \mathscr{A}_{i.j} = d$$

and the fact that $\mathscr{A}$ is symmetric. For example, if $\mathscr{G}$ is a circular ring of N vertices, the evolution of $\boldsymbol{p}(t) = (p_1(t), \cdots, p_N(t))^T$ is the solution of

$$\frac{d\boldsymbol{p}}{dt} = \frac{\lambda}{2} \boldsymbol{\Delta} \boldsymbol{p}, \tag{28}$$

where $\boldsymbol{\Delta}$ is the $N \times N$ graph Laplacian

$$\boldsymbol{\Delta} = \begin{bmatrix} -2 & 1 & 0 & \cdots & 1 \\ 1 & -2 & 1 & \cdots & 0 \\ \vdots & \vdots & \cdots & \vdots & \vdots \\ 1 & 0 & \cdots & 1 & -2 \end{bmatrix}.$$

When there are n_s identical internal states of the walker the state vector is an $n_s N$-component vector and the evolution equation becomes

$$\frac{d\boldsymbol{p}}{dt} = \left\{ \boldsymbol{\Delta} \otimes \frac{\lambda}{2} \boldsymbol{I}_m + \boldsymbol{I}_N \otimes \boldsymbol{K} \boldsymbol{\Lambda}(\boldsymbol{0}) \right\} \boldsymbol{p}, \tag{29}$$

where I_N and I_{n_s} are identity matrices of size $N \times N$ and $n_s \times n_s$, $\boldsymbol{K}$ and $\boldsymbol{\Lambda}$ have the same meaning as in Sect. 2.1, and $\boldsymbol{A} \otimes \boldsymbol{B}$ is the tensor product of the matrices $\boldsymbol{A}$ and $\boldsymbol{B}$[3].

2.5 Lattices with Multiple Vertex Types and Internal States

In the preceding example, all vertices are equivalent, and the WTD for jumps between them, in what will be called the *primary* undirected graph $\mathscr{G}$, is the same at every vertex. However, many biological systems require more detailed models with more than one type of vertex. For example, consider a horizontal slice through the columnar cells in Fig. 2 and define the primary graph $\mathscr{G}$ by placing a vertex or *junction* in each cell. Secondary structure is introduced by assigning a node to the space between cells,

[2] In a finite regular graph boundary vertices have a different degree, but the boundary conditions determine how the degree changes. See (Othmer and Scriven 1971) for the structurally identical problem of diffusion between coupled cells in a finite regular lattice with various boundary conditions.

[3] The convention used in defining the tensor product is given in "Appendix A" and in Othmer and Scriven (1971).

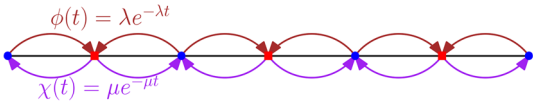

Fig. 4 Graphical depiction of the setup for a random walk with an SV between junctions with distinct transition rates between the SVs and junctions. Junctions have a waiting-time density $\phi(t) = \lambda e^{-\lambda t}$ while SVs have a waiting-time density $\chi(t) = \mu e^{-\mu t}$. The arrows indicate the transitions, colored according to whether they begin at a junction (blue circle) or SV (red square)

with the result that one obtains a graph in which the edges of $\mathscr{G}$ have vertices between junctions. In general, we call these new vertices *secondary vertices* or SVs, and in effect, introduction of SVs creates a new, extended graph $\mathscr{G}_e$. Later we will show in examples how the primary graph reflects the macrostructure of a system, whereas the extended graph incorporates the microstructure.

To illustrate how the evolution equations for such lattices change, consider the following example.

Example 1: A circular ring with two vertex types

Suppose that $N = 2M$ and that even-numbered vertices are junctions in the primary graph $\mathscr{G}$ while odd-numbered vertices represent the secondary structure. Suppose that all junctions have the same Poisson parameter λ, while the SVs have transition rates labeled μ. Thus there are M pairs of successive vertices, and we label each vertex by V_j^i, $i = 1, 2$ with $j = 1, \ldots, M$. A diagram of the allowable transitions at each point is given in Fig. 4. The evolution equations can be written as

$$\begin{aligned} \frac{dp_j^{(1)}}{dt} &= -\lambda p_j^{(1)} + \frac{\mu}{2} \sum_{k \in \mathscr{N}(j,1)} p_k^{(2)}(t) \\ \frac{dp_j^{(2)}}{dt} &= -\mu p_j^{(2)} + \frac{\lambda}{2} \sum_{k \in \mathscr{N}(j,2)} p_k^{(1)}(t), \end{aligned} \tag{30}$$

where $\mathscr{N}(j,k)$ denotes the neighborhood of vertex k in the jth pair. Define

$$\boldsymbol{p}_i = \begin{pmatrix} p_i^{(1)} \\ p_i^{(2)} \end{pmatrix},$$

and then, (30) can be written

$$\frac{d\boldsymbol{p}_i(t)}{dt} = \boldsymbol{A}\boldsymbol{p}_i + \boldsymbol{B}_{-1}\boldsymbol{p}_{i-1} + \boldsymbol{B}_1\boldsymbol{p}_{i+1}, \tag{31}$$

where

$$\boldsymbol{A} = \begin{bmatrix} -\lambda & \frac{\mu}{2} \\ \frac{\lambda}{2} & -\mu \end{bmatrix} \quad \text{and} \quad \boldsymbol{B}_{-1} = \begin{bmatrix} 0 & \frac{\mu}{2} \\ 0 & 0 \end{bmatrix} \quad \text{and} \quad \boldsymbol{B}_1 = \begin{bmatrix} 0 & 0 \\ \frac{\lambda}{2} & 0 \end{bmatrix}.$$

Notice that up to a scaling factor, $\boldsymbol{B}_1 = \boldsymbol{B}_{-1}^T$. Equation (31) can be written in block format as

$$\frac{d}{dt}\begin{pmatrix} \boldsymbol{p}_1 \\ \vdots \\ \\ \vdots \\ \boldsymbol{p}_M \end{pmatrix} = \begin{pmatrix} \boldsymbol{A} & \boldsymbol{B}_1 & & & \boldsymbol{B}_{-1} \\ \boldsymbol{B}_{-1} & \boldsymbol{A} & \boldsymbol{B}_1 & & \\ & \boldsymbol{B}_{-1} & \boldsymbol{A} & \boldsymbol{B}_1 & \\ & & \ddots & \ddots & \ddots \\ \boldsymbol{B}_1 & & & \boldsymbol{B}_{-1} & \boldsymbol{A} \end{pmatrix} \begin{pmatrix} \boldsymbol{p}_1 \\ \vdots \\ \\ \vdots \\ \boldsymbol{p}_M \end{pmatrix}. \tag{32}$$

This matrix has a block structure that suggests the discrete Laplacian for the single-state system. In fact, if $\lambda = \mu$ the equation can be written a

$$\frac{d\boldsymbol{P}}{dt} = \frac{\mu}{2}\Delta \boldsymbol{P}$$

where $\boldsymbol{P}$ is the $2M$ vector of states and Δ is the Laplacian for the ring. The structure in (32) will appear in subsequent examples as well, and in this sense, we expect that even a very complex multistate system with many internal states may at a large scale exhibit diffusive behavior. In this simple case, such behavior can further be motivated by considering the case when $\mu = \mu_0 \epsilon^{-1}$ and letting ϵ go to zero. In that case, the explicit solution for $p_i^{(2)}(t)$, ignoring initial conditions, can be written as

$$p_i^{(2)}(t) = \lim_{\epsilon \to 0} \int_0^t e^{-\mu_0 \epsilon^{-1}(t-\tau)} \frac{\lambda}{2} \left(p_i^{(1)}(t) + p_{i+1}^{(\tau)}(\tau) \right) d\tau = 0.$$

This is merely a reflection of the fact that with a large μ, particles spend negligible amounts of time on the type 2 points. Thus, particles essentially jump directly between type 1 points, and the effect of the intervening points drops out. (A similar mechanism also explains the spikes seen in Fig. 3, and those spike states have slower dynamics than the surrounding states and thus accumulate probability.) In this limit, one can therefore describe the evolution of the systems by

$$\frac{d\boldsymbol{p}^{(1)}}{dt} = 2\lambda \Delta \boldsymbol{p}^{(1)}$$

where $\boldsymbol{p}^{(1)}$ is the vector of all M type 1 points. The factor of 4 when compared with the previous result arises since each jump (really two jumps in rapid succession) now covers twice the distance, and since $D \sim \langle \Delta x^2 \rangle / \Delta t$, doubling the distance per jump quadruples the diffusivity.

Hence, we have found that the dynamics reduce to Laplacian dynamics in both the case that $\lambda = \mu$ and when λ and μ are of greatly different magnitudes. This suggests that perhaps after sufficient time has elapsed to level out local probability gradients, the system behavior may exhibit a diffusive character for arbitrary values of λ and μ. As we show in the subsequent sections, this is indeed true for many systems, and in a rough sense, part of what we discuss is a method of understanding the diffusive behavior of systems as a function of these local jump parameters and later on, the topology of the network. We note, however, that one should not always expect such nice behavior. As demonstrated in the comb example in Sect. 4 (and also many examples in the literature, e.g., Metzler and Klafter 2000; Othmer et al. 1988), non-diffusive behavior can arise too. However, these other limiting behaviors appear naturally in the CTRW framework- no special modifications need be introduced.

The foregoing results can be extended to a system with finitely many types of SVs, each with a different waiting-time distribution. Let $\{\boldsymbol{X_I}\}_{\boldsymbol{I}\in\mathbb{Z}^d}$ denote the positions of junctions of a d-dimensional lattice whose connectivity is encoded in the graph $\mathscr{G}$, and suppose that each edge is populated with n_k SVs, which could represent the discretization of the channel joining a pair of tertiary junctions (junctions at which three edges meet) in the hexagonal lattice, that must be traversed in order to move between any given pair of junctions (*cf.* Fig. 5). In biological settings, SVs can be used to represent processes such as diffusion in the space between cells or sites for surface binding and unbinding on a membrane. We assume that each step can be represented as a linear operator, both for simplicity and because the linear case covers a wide variety of applications. Implicit in this assumption is the requirement that particles do not interact with each other. In the context of binding reactions mentioned above, this requires that the substrate which the diffusing particle can bind to is present in great abundance relative to the concentration of the diffusing particles (Lin and Othmer 2017).

In addition to SVs, we also suppose that there are n_s internal states that characterize a walker, as depicted in Fig. 5. These internal states are distinguished from the n_k SVs by the fact that they do not represent changes in position along an edge. Instead, they allow us to consider systems involving first-order reactions of several chemical species or possibly even generalized master-equation-type formulations (Isaacson 2009; Hu and Othmer 2011; Gadgil et al. 2005). We also assume that, there are n_e edges incident to each junction. This results in $n_T = n_s(1 + n_e n_k)$ degrees of freedom associated with each junction.

Recalling the definitions from Sect. 2.1, we introduce the n_T-dimensional vector-valued occupation and arrival probabilities $\boldsymbol{p}(\boldsymbol{X}, t)$ and $\boldsymbol{q}(\boldsymbol{X}, t)$ for particles starting from $\boldsymbol{X} = \boldsymbol{0}$ at $t = 0$. Spatial transitions between adjacent SVs and between SVs and junctions are described by an $n_T \times n_T$-matrix function $\boldsymbol{T}(\boldsymbol{X} - \boldsymbol{X}')$ which is the analog for a multistate lattice, of the spatial jump operator $T(x, y)$ defined in Eq. (2). In the definition of $\boldsymbol{T}(\boldsymbol{X} - \boldsymbol{X}')$, $\boldsymbol{X}$ and $\boldsymbol{X}'$ are junctions on the lattice, and for a given $\boldsymbol{X}$, $\boldsymbol{T}(\boldsymbol{X} - \boldsymbol{X}')$ is typically only nonzero when $\boldsymbol{X}' = \boldsymbol{X}$ or when $\boldsymbol{X}$ and $\boldsymbol{X}'$ are connected by an edge. The waiting-time distributions for each of these jumps form a diagonal matrix, denoted by $\boldsymbol{\phi}(t)$.

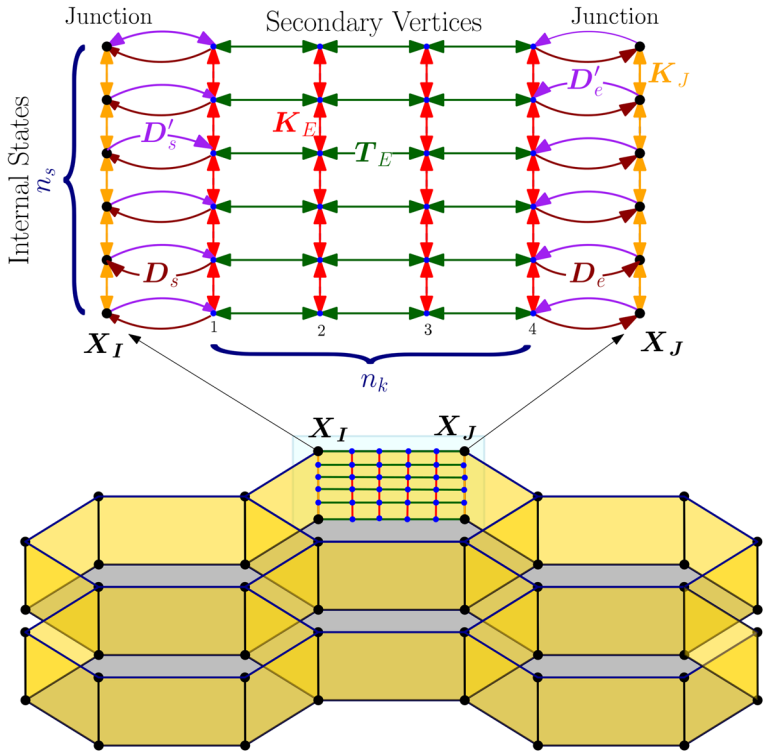

Fig. 5 Transitions allowed in a hexagonal lattice random walk having n_k SVs and n_s internal states. The larger dots represent the internal states at a junction and the smaller dots are the internal states at the n_k SVs. The lattice in this case is a 2D lattice with several internal states, but the edges in 1D or 3D (or higher) lattices behave in the same way with regard to the transitions between spatial states and the n_s internal states. The arrows are color-coded according to the matrix that contains each transition. Note that in practice, the internal states need not correspond with a physical height as they appear in this image

As an example, consider Fig. 4. For this two-state problem, $\boldsymbol{T}$ is nonzero only for $X - X' = \{-1, 0, 1\}$, and for these values,

$$\boldsymbol{T}(0) = \begin{pmatrix} 0 & \frac{1}{2} \\ \frac{1}{2} & 0 \end{pmatrix}, \quad \boldsymbol{T}(-1) = \begin{pmatrix} 0 & \frac{1}{2} \\ 0 & 0 \end{pmatrix}, \quad \boldsymbol{T}(1) = \begin{pmatrix} 0 & 0 \\ \frac{1}{2} & 0 \end{pmatrix}$$

and

$$\boldsymbol{\phi}(t) = \begin{pmatrix} \phi(t) & 0 \\ 0 & \chi(t) \end{pmatrix}.$$

In more general settings, transitions between internal states must also be described, and for this we use matrices $\boldsymbol{K}$ and $\boldsymbol{\Lambda}(t)$. These are generalizations of the $\boldsymbol{K}$ and $\boldsymbol{\Lambda}$ defined above, because they now allow for possibly different reactions to occur at each SV.

Finally, we have the evolution equations:

$$\begin{aligned}\boldsymbol{q}\,(\boldsymbol{X},t) &= \delta(t)\boldsymbol{\delta}_{k_0,\ell_0}\delta(\boldsymbol{X}) + \int_0^t \left[\sum_{\boldsymbol{X}'\in\mathcal{N}(\boldsymbol{X})} \boldsymbol{T}(\boldsymbol{X}-\boldsymbol{X}')\boldsymbol{\phi}(t-\tau)\boldsymbol{q}(\boldsymbol{X}',\tau)\right] d\tau \\ &\quad + \int_0^t \boldsymbol{K}\boldsymbol{\Lambda}(t-\tau)\boldsymbol{q}(\boldsymbol{X},\tau)d\tau \\ \boldsymbol{p}\,(\boldsymbol{X},t) &= \hat{\boldsymbol{\Phi}}(t)\boldsymbol{\delta}_{k_0,\ell_0}\delta(\boldsymbol{X}) + \int_0^t \hat{\boldsymbol{\Phi}}(t-\tau)\int_0^\tau \\ &\quad \left[\sum_{\boldsymbol{X}'\in\mathcal{N}(\boldsymbol{X})} \boldsymbol{T}(\boldsymbol{X}-\boldsymbol{X}')\boldsymbol{\phi}(\tau-s)\boldsymbol{q}(\boldsymbol{X}',s)\right] ds\, d\tau \\ &\quad + \int_0^t \hat{\boldsymbol{\Phi}}(t-\tau)\int_0^\tau \boldsymbol{K}\boldsymbol{\Lambda}(\tau-s)\boldsymbol{q}(\boldsymbol{X},s)ds\, d\tau\end{aligned} \tag{33}$$

where the vectors $\boldsymbol{\delta}_{k_0,\ell_0}$ specify the initial internal state (ℓ_0) and the initial SV (k_0) for the process, and $\mathcal{N}(\boldsymbol{X})$ is the set of lattice points adjacent to $\boldsymbol{X}$.

The nonzero elements of the diagonal matrix $\hat{\boldsymbol{\Phi}}$ of complementary waiting times (recall Eq. (4)) are defined as

$$\hat{\Phi}_{k,\ell}(t) = 1-\int_0^t \psi_{k,\ell}(t) = 1-\int_0^t \left(\sum_{\boldsymbol{X}'\in\mathcal{N}(\boldsymbol{X})} \mathbf{1}^T\boldsymbol{T}(\boldsymbol{X}')\boldsymbol{\phi}(\tau)\boldsymbol{\delta}_{k,\ell} + \mathbf{1}^T\boldsymbol{K}\boldsymbol{\Lambda}(\tau)\boldsymbol{\delta}_{k,\ell}\right) d\tau, \tag{34}$$

The factor, $\mathbf{1}$ is a vector of ones of length n_T.

To obtain a differential master equation for this system, a Laplace transformation is applied to Eq. (33) to obtain

$$\begin{aligned}&\tilde{\boldsymbol{p}}\,(\boldsymbol{X},s|\,\{k_0,\ell_0\}) \\ &= \tilde{\hat{\boldsymbol{\Phi}}}(s)\boldsymbol{\delta}_{k_0,\ell_0}\delta(\boldsymbol{X}) + \left[\sum_{\boldsymbol{X}'\in\mathcal{N}(\boldsymbol{X})} \tilde{\hat{\boldsymbol{\Phi}}}(s)\boldsymbol{T}(\boldsymbol{X}-\boldsymbol{X}')\tilde{\boldsymbol{\phi}}(s) + \tilde{\hat{\boldsymbol{\Phi}}}(s)\boldsymbol{K}\tilde{\boldsymbol{\Lambda}}(s)\right]\left(\tilde{\hat{\boldsymbol{\Phi}}}(s)\right)^{-1} \\ &\quad \tilde{\boldsymbol{p}}(\boldsymbol{X}',s,\{k_0,\ell_0\}).\end{aligned} \tag{35}$$

As long as assumptions about the lack of particle–particle interactions remain valid, an equation for the number density, $\boldsymbol{n}(\boldsymbol{x},t)$ can now be obtained. The manipulations involved are similar to those in Landman et al. (1977), eventually yielding

$$\tilde{\boldsymbol{\Gamma}}(s)\left(s\tilde{\boldsymbol{n}}(\boldsymbol{X},s)-\boldsymbol{f}(\boldsymbol{X})\right)=-\tilde{\boldsymbol{n}}(\boldsymbol{X},s)+\sum_{\boldsymbol{X}'\in\mathscr{N}(\boldsymbol{X})}\tilde{\boldsymbol{\Gamma}}(s)\boldsymbol{T}(\boldsymbol{X}-\boldsymbol{X}')\tilde{\boldsymbol{\phi}}(s)(\tilde{\tilde{\boldsymbol{\Phi}}}(s))^{-1}\tilde{\boldsymbol{n}}(\boldsymbol{X}',s)$$
$$+\tilde{\boldsymbol{\Gamma}}(s)\boldsymbol{K}\tilde{\boldsymbol{\Lambda}}(s)\left(\tilde{\tilde{\boldsymbol{\Phi}}}(s)\right)^{-1}\tilde{\boldsymbol{n}}(\boldsymbol{X},s) \tag{36}$$

where $\tilde{\boldsymbol{\Gamma}}(s)=\frac{1}{s}\left(\tilde{\tilde{\boldsymbol{\Phi}}}(s)(\tilde{\boldsymbol{\psi}}(s))^{-1}\right)$ is the diagonal memory function matrix. If all of the distributions are Poisson distributed with distinct rates, the above equation simplifies to become

$$\frac{\partial \boldsymbol{n}}{\partial t}=-(\boldsymbol{\phi}(0)+\boldsymbol{\Lambda}(0))\boldsymbol{n}(\boldsymbol{x},t)+\sum_{\boldsymbol{X}'\in\mathscr{N}(\boldsymbol{X})}\boldsymbol{T}(\boldsymbol{X}-\boldsymbol{X}')\boldsymbol{\phi}(0)\boldsymbol{n}(\boldsymbol{X}',t)+\boldsymbol{K}\boldsymbol{\Lambda}(0)\boldsymbol{n}(\boldsymbol{X},t).$$

This is the analog of Eq. (22) for multistate lattice random walks.

Since $\boldsymbol{T}$ and $\boldsymbol{\phi}$ fully determine the evolution of $\boldsymbol{p}$, we next focus on their properties through several examples. General forms for the structure of $\boldsymbol{T}$ and $\boldsymbol{K}$ are given in Appendix C.

Example 2: Secondary Vertices

Let us consider an extension of Ex. 1 in Sect. 2.5. That previous system can be thought of as having junctions and SVs with a single SV between each pair of adjacent junctions. Here we extend that example and consider a system with n_k SVs between each junction. The case with $n_k = 3$ is illustrated in Fig. 6. We also now consider the lattice to be of infinite extent rather than over a ring of length $2M$. Although this problem is still relatively straightforward, the goal is to clearly show how different types of transition matrices that arise in more complex problems, namely, $\boldsymbol{T}_{SV}$, $\boldsymbol{D}_s$, $\boldsymbol{D}_e$, $\boldsymbol{D}'_s$, and $\boldsymbol{D}'_e$, defined below, are constructed. As before, let the WTDs for the SVs be $\chi(t)=\mu e^{-\mu t}$ and the WTDs for the junctions be $\phi(t)=\lambda e^{-\lambda t}$. The governing ODEs on each junction and edge are of the form

$$\begin{pmatrix}\frac{d}{dt}p_i^{(0)}\\ \frac{d}{dt}p_i^{(1)}\\ \vdots\\ \frac{d}{dt}p_i^{(n_k)}\end{pmatrix}=-\begin{pmatrix}\lambda & & & \\ & \mu & & \\ & & \mu & \\ & & & \ddots & \\ & & & & \mu\end{pmatrix}\begin{pmatrix}p_i^{(0)}\\ p_i^{(1)}\\ p_i^{(2)}\\ \vdots\\ p_i^{(n_k)}\end{pmatrix}+\frac{1}{2}\begin{pmatrix}0 & \mu & 0 & & \\ \lambda & 0 & \mu & & \\ & \mu & 0 & \mu & \\ & & \ddots & \ddots & \ddots \\ & & & \mu & 0\end{pmatrix}\begin{pmatrix}p_i^{(0)}\\ p_i^{(1)}\\ p_i^{(2)}\\ \vdots\\ p_i^{(n_k)}\end{pmatrix}$$
$$+\frac{1}{2}\begin{pmatrix}\mu p_{i-1}^{(n_k)}\\ 0\\ \vdots\\ 0\\ \lambda p_{i+1}^{(0)}\end{pmatrix} \tag{37}$$

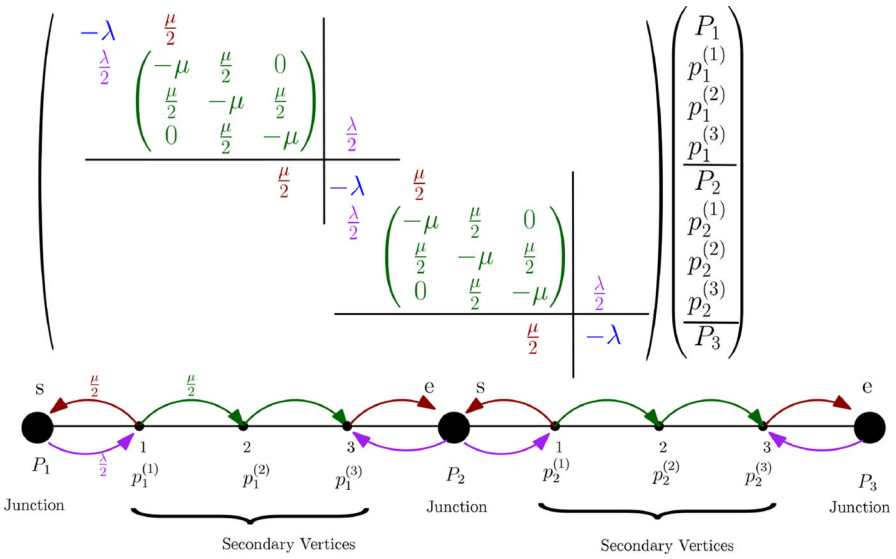

Fig. 6 A depiction of Ex. 2 with $n_k = 3$ over several junctions. Green arrows depict transitions in $\boldsymbol{T}_{SV}$, purple arrows in $\boldsymbol{D}'$ and dark red arrows in $\boldsymbol{D}$. The letters "s" and "e" label the start and end of each edge. The coloring of the entries in the matrix also indicates which types of transitions each entry corresponds to. All blank entries in the matrix are 0

where $p_i^{(0)}(t)$ are the junction probabilities and $p_i^{(k)}(t)$ for $k > 0$ are the probabilities at each SV.

We now rewrite Eq. (37) to highlight certain types of transitions that occur in this system and other problem we will encounter. Let us write the solution vector $\boldsymbol{p}$ as

$$\boldsymbol{p} = \begin{pmatrix} \vdots \\ \boldsymbol{p}_{i-1} \\ \boldsymbol{p}_i \\ \boldsymbol{p}_{i+1} \\ \cdots \end{pmatrix}$$

where each $\boldsymbol{p}_i$ is written in terms of the junction and SV states as

$$\boldsymbol{p}_i = \begin{pmatrix} \boldsymbol{p}_{i,J} \\ \boldsymbol{p}_{i,SV} \end{pmatrix}.$$

Since there is only a single internal state (but many SVs) in this case, there are three types of transitions that must be considered: jumps between adjacent SVs, jumps from an SV to a junction, and jumps from a junction to an SV. We will organize these categories of jumps into transition matrices denoted $\boldsymbol{T}_{SV}$, $\boldsymbol{D}$, and $\boldsymbol{D}'$, respectively. Since transitions from an SV to a junction can occur from either end of an edge ($k = 1$ or $k = n_k$ here), we define two different matrices $\boldsymbol{D}_s$ and

$\boldsymbol{D}_e$ associated with the transitions from the two ends [4]. Since the rate of jumps is μ at each SV, and there is a 1/2 probability of jumping to the right or left, we have $\boldsymbol{D}_{s,e} \in \mathbb{R}^{1\times n_k}$ and (see Fig. 6)

$$\boldsymbol{D}_s = \left(\tfrac{\mu}{2}\ 0\ \ldots\ 0\right), \qquad \boldsymbol{D}_e = \left(0\ \ldots\ 0\ \tfrac{\mu}{2}\right).$$

The matrices $\boldsymbol{D}_s$ and $\boldsymbol{D}_e$ can be thought of as linear operators acting on the SVs along an edge to yield the flux of a particle to land on the junctions attached to that edge.

Next, we consider jumps from junctions to SVs. Since each junction is connected to two edges, there are two types of transitions: transitions from junction i to the n_k^{th} SV on edge $i-1$, and transitions from junction i to the first SV on edge i. Thus, we define $\boldsymbol{D}'_e$ to describe jumps to edge $i-1$ and $\boldsymbol{D}'_s$ to describe jumps to edge i, Since the rate of jumping from a junction is λ, and there is a 1/2 probability of jumping right or left, we have $\boldsymbol{D}'_{s,e} \in \mathbb{R}^{n_k\times 1}$ and (see Fig. 6)

$$\boldsymbol{D}'_s = \begin{pmatrix} \frac{\lambda}{2} \\ 0 \\ \vdots \\ 0 \end{pmatrix}, \qquad \boldsymbol{D}'_e = \begin{pmatrix} 0 \\ \vdots \\ 0 \\ \frac{\lambda}{2} \end{pmatrix}$$

Similar to $\boldsymbol{D}_{s,e}$, $\boldsymbol{D}'_{s,e}$ may be thought of as linear operators that give the flux of particles from a junction to the SVs on edges attached to it.

Lastly, we must define the matrix of transitions between SVs on the edge. Since transitions between neighboring points are possible in Eq. (37), this yields an $n_k \times n_k$ transition matrix,

$$\boldsymbol{T}_{SV} = \frac{1}{2}\begin{pmatrix} 0 & \mu & 0 & & & \\ \mu & 0 & \mu & & & \\ & \mu & 0 & \mu & & \\ & & \ddots & \ddots & \ddots & \\ & & & & \mu & 0 \end{pmatrix}$$

which incidentally, is also the transition matrix for a random walk with WTD $\chi(t)$ and absorbing boundaries at $n = 0$ and $n = n_k + 1$.

The previous matrices describe transitions associated with a single junction and edge, and now, we must incorporate this description into the topology of the primary graph. In particular, we must describe how junction i and edge i are connected to the edges and junctions that they are adjacent to. To formulate this as a matrix problem, define the matrices $\boldsymbol{A}_s$ and $\boldsymbol{A}_e$ as permutations of the

[4] The subscripts s and e are meant to indicate the start ($k = 1$) and end ($k = n_k$) of an edge. However, this is merely for labeling purposes and does not mean that the transport is directed.

infinite-dimensional identity matrix over the lattice as follows

$$\boldsymbol{A}_s = \begin{pmatrix} \ddots & \ddots & & & & & \\ & 0 & 1 & & & & \\ & & 0 & 1 & & & \\ & & & 0 & 1 & & \\ & & & & 0 & \ddots & \\ & & & & & \ddots & \end{pmatrix},$$

$$\boldsymbol{A}_e = \boldsymbol{A}_s^T = \begin{pmatrix} \ddots & & & & & & \\ \ddots & 0 & & & & & \\ & 1 & 0 & & & & \\ & & 1 & 0 & & & \\ & & & 1 & 0 & & \\ & & & & \ddots & \ddots & \end{pmatrix}. \tag{38}$$

From Eq. (37), we see that probability, $p_i^{(n_k)}$, of being located at the n_k^{th} SV of edge i depends directly on $p_{i+1}^{(0)}$. By definition, transitions from the n_k^{th} SV to a junction are described by $\boldsymbol{D}_e$, and $\boldsymbol{A}_e$ describes the connection between edge i and junction $i+1$. Thus, one can see that $\boldsymbol{A}_e \otimes \boldsymbol{D}_e$ is the appropriate matrix to describe these transitions across the entire lattice. Likewise, we see that $\boldsymbol{A}_s \otimes \boldsymbol{D}'_e$ describes jumps from junction i to the n_k^{th} SV on edge $i-1$.
After constructing the transition matrices involving $\boldsymbol{D}_s$ and $\boldsymbol{D}'_s$, and gathering all the terms together, this ultimately leads to a global transition matrix:

$$\boldsymbol{W} = \left(\begin{array}{cc|cc|cc|cc|c} 0 & \boldsymbol{D}_s & 0 & \boldsymbol{0} & & & & & \\ \boldsymbol{D}'_s & \boldsymbol{T}_{SV} & \boldsymbol{D}'_e & \boldsymbol{0} & & & & & \\ \hline 0 & \boldsymbol{D}_e & 0 & \boldsymbol{D}_s & 0 & \boldsymbol{0} & & & \\ \boldsymbol{0} & \boldsymbol{0} & \boldsymbol{D}'_s & \boldsymbol{T}_{SV} & \boldsymbol{D}'_e & \boldsymbol{0} & & & \\ \hline & & 0 & \boldsymbol{D}_e & 0 & \boldsymbol{D}_s & 0 & \boldsymbol{0} & \\ & & \boldsymbol{0} & \boldsymbol{0} & \boldsymbol{D}'_s & \boldsymbol{T}_{SV} & \boldsymbol{D}'_e & \boldsymbol{0} & \\ \hline & & & & \ddots & & \ddots & & \ddots \end{array}\right) = \boldsymbol{I} \otimes \begin{pmatrix} 0 & \boldsymbol{D}_s \\ \boldsymbol{D}'_s & \boldsymbol{T}_{SV} \end{pmatrix}$$
$$+\boldsymbol{A}_s \otimes \begin{pmatrix} 0 & \boldsymbol{0} \\ \boldsymbol{D}'_e & \boldsymbol{0} \end{pmatrix} + \boldsymbol{A}_e \otimes \begin{pmatrix} 0 & \boldsymbol{D}_e \\ \boldsymbol{0} & \boldsymbol{0} \end{pmatrix}$$

where $\boldsymbol{I}$ is an infinite-dimensional identity matrix on the lattice. We also rewrite the evolution equation in Eq. (37), now over the entire lattice rather than a single junction and edge, as

$$\frac{d}{dt}\boldsymbol{p} = -\boldsymbol{\Lambda}\boldsymbol{p} + \boldsymbol{W}\boldsymbol{p} \tag{39}$$

where

$$\boldsymbol{\Lambda} = \boldsymbol{I} \otimes diag(\lambda, \mu, \cdots, \mu).$$

The first term on the right-hand side, $-\boldsymbol{\Lambda}\boldsymbol{p}$, reflects the fact that jumps from junctions occur at a rate λ and from SVs at a rate μ. As in Ex. 1, $-\boldsymbol{\Lambda} + \boldsymbol{W}$ has a kind of block Laplacian type of structure.

Further analysis of this system will be done in Sect. 4.2, but here we describe a few properties that will be clarified later. First, for fixed n_k, if $\mu \gg \lambda$, then we expect that the transitions between the SVs and from SVs to junctions will take a negligible amount of time compared to transitions from junctions to SVs. Given this, the transport at large enough length and timescales will evolve as though it were a random walk with no SVs and a waiting time $\lambda e^{-\lambda t}$ for a particles to jump between two adjacent junctions.

The second property we note is that setting $dp_i^{(k)}/dt = 0$ for all i and k, we can solve for steady-state solutions. If we suppose that the particle is confined to edge i and junction i, the steady-state solution can be found as

$$p_{ss}^{(k)} = \begin{cases} \frac{\mu}{n_k\lambda+\mu} & k = 0 \\ \frac{\lambda}{n_k\lambda+\mu} & k = 1, \ldots, n_k \end{cases}$$

This type of analysis for steady-state solutions has been used elsewhere (Roerdink and Shuler 1985a, b) to obtain the long-time asymptotic mean and variance for certain multistate random walk processes. Accordingly, some of our long-time asymptotics can be found from the analysis presented there. However, the methods developed throughout this paper can also be used to find the full solution, and not just long-time asymptotics.

Although the previous example ultimately just leads to a reformulation of Eq. (37) over the lattice, the categorization of transitions into different classes will prove useful in more complicated problems where the evolution equations are otherwise difficult to write out. The main categories of transitions which may occur are: internal state changes at junctions ($\boldsymbol{K}_J$), junction-to-SV ($\boldsymbol{D}'$), SV-to-junction ($\boldsymbol{D}$), and SV-to-SV spatial and internal jumps ($\boldsymbol{T}_{SV}$ and $\boldsymbol{K}_{SV}$). The transitions at the junctions and SVs described by these matrices are then connected to the topology of the underlying lattice through structural matrices $\boldsymbol{A}_s$ and $\boldsymbol{A}_e$ which are permutations of the infinite-dimensional identity matrix on the lattice. In more general settings, there may be $m = 1, 2, \ldots, n_e$ types of edges each associated with its own structural matrices $\boldsymbol{A}_{s,m}$ and $\boldsymbol{A}_{e,m}$, and $n = 1, 2, \ldots, n_e$ types of vertices each associated with its own $\boldsymbol{K}_J$.

3 Moments of the Density Distribution

In general, equations such as (9) cannot be solved analytically, but often the quantities of interest are the low-order moments of the spatial distribution rather than $p(\boldsymbol{x}, t)$

itself. To illustrate how these can be found, consider a scalar equation in a 1D homogeneous medium. We define the moments of $p(x,t|0)$ as

$$m^{(n)}(t) = \langle x^n(t)\rangle = \int_{-\infty}^{+\infty} x^n p(x,t|0)\,dx$$
$$= \int_{-\infty}^{+\infty}\int_0^t \int_{-\infty}^{+\infty} x^n T(x-y)\phi(t-\tau)p(y,\tau|0)\,dy\,d\tau\,dx, \qquad (40)$$

and let

$$m_k = \int_{-\infty}^{+\infty} x^k T(x)\,dx$$

be the kth moment of the jump kernel T about zero. Then after a change of variables, one finds that (40) can be written as

$$m^{(n)}(t) = \int_0^t \sum_{k=0}^{n} \binom{n}{k} m_k \phi(t-\tau) m^{(n)}(t)\,d\tau, \qquad (41)$$

and therefore, all the moments of $x(t)$ can be obtained by solving a sequence of linear integral equations of convolution type.

It is often convenient to work with the Laplace transformed equations for the moments since this allows for the use of Laplace transform limit theorems to obtain the asymptotic time dependence of the moments. The Laplace transformed solutions for the first two moments are

$$\tilde{m}^{(1)}(s) = \frac{m_1}{s}\frac{\bar{\phi}(s)}{1-\bar{\phi}(s)}$$
$$\tilde{m}^{(2)}(s) = \left(2m_1\tilde{m}^{(1)}(s) + \frac{m_2}{s}\right)\frac{\bar{\phi}(s)}{1-\bar{\phi}(s)}. \qquad (42)$$

If the first moment of T vanishes, then these simplify to

$$\tilde{m}^{(1)}(s) = 0$$
$$\tilde{m}^{(2)}(s) = \frac{m_2}{s}\frac{\bar{\phi}(s)}{1-\bar{\phi}(s)}. \qquad (43)$$

In simple cases, the moments can be found directly. For example suppose that $m_1 = 0$ and that $\phi(t) = \lambda e^{-\lambda t}$. Then one finds that

$$m^{(2)}(t) = m_2 \int_0^t \mathscr{L}^{-1}\left(\frac{\lambda}{s}\right) d\tau = m_2\lambda t, \qquad (44)$$

and therefore, the underlying process is asymptotically a diffusion process with diffusion coefficient $D = m_2\lambda/2$. Furthermore, analogous results hold for homogeneous[5] 1D lattice random walks with the integrals in m_k replaced by summation over the lattice.

Anomalous diffusion is said to occur when the large-time limit of the mean square displacement grows either sub- or superlinearly. If the second moment varies as

$$m^{(2)}(t) \sim \gamma t^{\beta}$$

for $\beta \neq 1$ and $t \to \infty$, it is called *subdiffusion* if $\beta < 1$ and *superdiffusion* if $\beta > 1$ (Metzler and Klafter 2000). The former occurs when particles spread slowly, and in particular, if the mean waiting time between jumps is infinite. If $m_1 = 0$, then from (43), if $\tilde{\phi} \sim 1 - \bar{\tau}^{-1}s^{\rho}$ for $\rho \in (0, 1)$, $\bar{\tau} > 0$, and $s \to 0$, then $\langle x^2(t)\rangle \sim m_2 t^{\rho}$ for $t \to \infty$, i.e., movement is asymptotically subdiffusive. An example for which all moments of ϕ are infinite arises from the WTD

$$\phi(t) = \frac{1}{(1+t)^2}.$$

The transform of ϕ is

$$\bar{\phi}(s) = \left(\frac{\pi}{2} - Si(s)\right)\cos s + Ci(s)\sin s$$

where Si and Ci are the sine and cosine integral functions (Ruel 1958). From the asymptotic expansion of the integrals, one finds that

$$m^{(2)}(t) \sim \log t,$$

and thus, the process is also subdiffusive. The superdiffusive case arises when the walk is highly persistent in time, or for walks having a fat-tailed jump distribution. The simplest example of the first case arises when the walker never turns, which leads to a wave equation for which the mean square displacement scales as t^2. An application to bacteria that exhibit long runs is discussed in Matthaus et al. (2009).

3.1 First and Second Moments for Systems

The evolution equations for the first and second moments of a stochastic system consisting of N_c cells coupled by diffusion with first-order reactions in the cells were derived in Gadgil et al. (2005). The deterministic governing equations for this system can be written as

$$\frac{d\mathbf{n}}{dt} = \boldsymbol{\Omega}\mathbf{n},$$

[5] Homogeneous in a lattice as in a continuum, means that $T(x, y)$ and $\phi(t|y)$ do not vary with current position of a particle, as in the continuum case.

where $\mathbf{n}$ is the vector of molecule numbers for all cells, the $n_s N_c \times n_s N_c$ matrix $\boldsymbol{\Omega} \equiv \boldsymbol{\Delta} \otimes \boldsymbol{D} + \boldsymbol{I} \otimes \boldsymbol{K}\boldsymbol{\Lambda}(0)$, and $\boldsymbol{I}$ and $\boldsymbol{\Delta}$ are the identity matrix and graph Laplacian for the underlying lattice, respectively. Evolution equations for the mean and second moments were then derived through a generating function approach.

Generating functions of the form

$$g(z,t) = \sum_{n=0}^{\infty} z^{n_1} z^{n_2} \dots z^{n_{n_s}} p(n_1, n_2, \dots, n_{n_s}, t)$$

were used in Gadgil et al. (2005) to describe the number of molecules in a particular state. In the present context, we have matrix-valued generating functions for the position and internal state of a single particle, with argument z corresponding to lattice indices rather than particle numbers. For a single-particle, one-dimensional transport problem, we have

$$g_{k,\ell}(z,t) = \sum_{j=-\infty}^{\infty} z^j p_{k,\ell}(j,t), \tag{45}$$

where $j \in \mathbb{Z}$ is a lattice point. The quantities, $p_{k,\ell}(j,t)$, are the probabilities that the particle is located in internal state ℓ at SV k, along edge j of the lattice at time t (e.g., consider the $k = 0, \dots, n_k$ internal states as a discretization of an edge, as in Fig. 5 or later in Fig. 7). The negative powers are needed as it is assumed that the lattice has infinite extent in both directions. We also note that

$$\lim_{z \to 1^-} g_{k,\ell}(z,t)$$

is the total probability that the particle is located in SV k with internal state ℓ.

Let us assume that jumps only occur between neighboring points. Then for a drift–diffusion process, $\boldsymbol{T}$, which is equal to

$$\boldsymbol{T}(X) = \boldsymbol{D}_0 \delta(X) + \boldsymbol{D}^+ \delta(X - \Delta X) + \boldsymbol{D}^- \delta(X + \Delta X),$$

where $\boldsymbol{D}^+$ and $\boldsymbol{D}^-$ are equal for purely diffusive transport, but differ when there is even a transient drift. As before, the reaction matrix is $\boldsymbol{K}$, or we may write $\boldsymbol{K}\delta(\boldsymbol{X})$ to indicate that no transport occurs during reactions. To construct the generating function, we equate $n\Delta X$ with z^n, where ΔX is the lattice spacing, and write

$$\boldsymbol{\Omega}(z) = \left(\boldsymbol{K}\boldsymbol{\Lambda}(0) + \boldsymbol{D}_0 + \boldsymbol{D}^+ + \boldsymbol{D}^-\right) + \boldsymbol{D}^+ (z-1) + \boldsymbol{D}^- \left(z^{-1} - 1\right).$$

Systems with multiple connections and dimensions require one function like $(z-1)$ or $(z^{-1}-1)$ for each neighboring junction in the lattice. These functions coordinate the topology of the lattice in the generating function formalism and correspond to $\boldsymbol{A}_{t,m}$, the structural matrices specifying the lattice connectivity used before. Further discussion can be found in the general formulation given in Appendix C.1.

Differentiating the vector $\boldsymbol{g}(z,t)$, whose elements are $g_{k\ell}(z,t)$, with respect to t and z and setting $z \to 1$ yields the spatial moments

$$\frac{d}{dt}\boldsymbol{g} = \lim_{z\to 1}\frac{\partial}{\partial t}\boldsymbol{g}(z,t) = (\boldsymbol{K\Lambda}(0) + \boldsymbol{D}_0 + \boldsymbol{D}^+ + \boldsymbol{D}^-)\boldsymbol{g} \tag{46}$$

$$\frac{d}{dt}\boldsymbol{m}^{(1)} = L\lim_{z\to 1}\frac{\partial^2}{\partial z\partial t}\boldsymbol{g}(z,t) = (\boldsymbol{K\Lambda}(0) + \boldsymbol{D}_0 + \boldsymbol{D}^+ + \boldsymbol{D}^-)\boldsymbol{m} + L(\boldsymbol{D}^+ - \boldsymbol{D}^-)\boldsymbol{g} \tag{47}$$

$$\frac{d}{dt}\boldsymbol{v} = L^2\lim_{z\to 1}\frac{\partial^3}{\partial z^2\partial t}\boldsymbol{g}(z,t) = (\boldsymbol{K\Lambda}(0) + \boldsymbol{D}_0 + \boldsymbol{D}^+ + \boldsymbol{D}^-)\boldsymbol{v} + 2L(\boldsymbol{D}^+ - \boldsymbol{D}^-)\boldsymbol{m} + 2L^2\boldsymbol{D}^-\boldsymbol{g} \tag{48}$$

where L is the distance between two junctions, $\boldsymbol{m}$ are the k-th moments, and $\boldsymbol{v}$ is realted to the second moment by

$$\boldsymbol{v}(t) = \boldsymbol{m}^{(2)}(t) - \boldsymbol{m}^{(1)}(t).$$

Note that these spatial moments do not take into account microstructural geometry of edges, specifically the location of SVs relative to the junctions of the lattice. The inclusion of microscale details is discussed in Appendix C.1, although there we use a lattice Fourier transform approach rather than a generating function[6].

We also see that the resulting elements of $\boldsymbol{g}$, $\boldsymbol{m}$, and $\boldsymbol{v}$ are for particles at a specific SV and in a specific internal state. However, experimental measurements are usually not at this level of resolution, and we will discuss this point further in subsequent sections.

Although these results hold for single-particle transport, the multiple particle case described by the general formulation from Gadgil et al. (2005) could in principle be applied. Additionally, for a d-dimensional lattice, the generating function $\boldsymbol{g}$ is of the form

$$\boldsymbol{g}(z_1,\ldots,z_d,t) = \sum_{j_1=-\infty}^{\infty}\cdots\sum_{j_d=-\infty}^{\infty} z_1^{j_1}z_2^{j_2}\ldots z_d^{j_d}\,\boldsymbol{p}(j_1,\ldots,j_d,t)$$

where the elements of $\boldsymbol{g}$ and $\boldsymbol{p}$ again describe SVs and internal states at each junction. The derivations of $\boldsymbol{m}$ and $\boldsymbol{v}$ are similar to the one-dimensional case with one important difference. In multiple dimensions, one gets several distinct vectors, $\boldsymbol{m}_j$ and $\boldsymbol{v}_{jk}$ with $j,k = 1,\ldots d$. This occurs since differentiation is now taken with respect to z_j,

[6] Both are formally equivalent if one replaces z by $e^{i\omega}$ in $\boldsymbol{g}(z,t)$). One advantage of the Fourier transform method is that the lattice spacings can be included as multiplying factors in the Fourier transform, e.g., $e^{i\Delta X\omega}$ whereas the generating function approach is defined only for integer powers of z. What this means is that the moments defined above must be multiplied by appropriate length factors related to the lattice spacing to obtain the correct results, whereas in the Fourier transform approach, these factors are included automatically.

$j = 1, \ldots, d$. Furthermore, $\boldsymbol{v}_{jk}$ is now defined as

$$\boldsymbol{v}_{jk}(t) = \begin{cases} m_{jk}^{(2)}(t) - m_k^{(1)}(t) & j = k \\ m_{jk}^{(2)}(t) & j \neq k. \end{cases}$$

3.2 The Moments in a One-Dimensional System

In the following example, we derive the moment equations for a one-dimensional lattice with SVs.

Example 3

In Ex. 2, we obtained the transition matrix $\boldsymbol{T}$ for that system and the evolution Eq. (39)

$$\frac{d}{dt}\boldsymbol{p} = -\boldsymbol{\Lambda}\boldsymbol{p} + \boldsymbol{W}\boldsymbol{p}. \tag{49}$$

With the definitions of $\boldsymbol{\Lambda}$ and $\boldsymbol{W}$ from Ex. 2 of Sect. 2.5, we can write $\boldsymbol{W}$ as

$$\begin{aligned} \boldsymbol{W}(X) &= (\boldsymbol{K} + \boldsymbol{D}_0)\delta(X) + \boldsymbol{D}^{+}\delta(X - \Delta X) + \boldsymbol{D}^{-}\delta(X + \Delta X) \\ &= \begin{pmatrix} 0 & \boldsymbol{D}_s \\ \boldsymbol{D}_s' & \boldsymbol{T}_E \end{pmatrix}\delta(X) + \begin{pmatrix} 0 & \boldsymbol{D}_e \\ 0 & 0 \end{pmatrix}\delta(X - \Delta X) + \begin{pmatrix} 0 & 0 \\ \boldsymbol{D}_e' & 0 \end{pmatrix}\delta(X + \Delta X). \end{aligned}$$

We now solve for the lower-order moments of this system, and to do so, we use a Fourier–Laplace transform. This yields the 4×4 matrix equation

$$\begin{aligned} &\begin{pmatrix} s\tilde{p}^{(0)}(\omega, s) \\ s\tilde{p}^{(1)}(\omega, s) \\ s\tilde{p}^{(2)}(\omega, s) \\ s\tilde{p}^{(3)}(\omega, s) \end{pmatrix} - \begin{pmatrix} p^{(0)}(0) \\ p^{(1)}(0) \\ p^{(2)}(0) \\ p^{(3)}(0) \end{pmatrix} \\ &= \left[-\boldsymbol{\Lambda} + \begin{pmatrix} 0 & \boldsymbol{D}_s + e^{-i\Delta X\omega}\boldsymbol{D}^{e} \\ \boldsymbol{D}_s' + e^{i\Delta X\omega}\boldsymbol{D}_e' & \boldsymbol{T}_E \end{pmatrix} \right] \begin{pmatrix} \tilde{p}^{(0)}(\omega, s) \\ \tilde{p}^{(1)}(\omega, s) \\ \tilde{p}^{(2)}(\omega, s) \\ \tilde{p}^{(3)}(\omega, s) \end{pmatrix} \end{aligned}$$

where $\tilde{p}^{(k)}(\omega, s)$ are the Fourier–Laplace transformed probabilities $p^{(k)}(X, t)$. Assuming an initial condition, $p^{(k)}(0) = 1/4$, we now solve for $\tilde{p}^{(k)}(\omega, s)$. The next step is to either invert $\tilde{p}^{(k)}(\omega, s)$ to obtain $p^{(k)}(X, t)$, or if we are interested in the spatial moments, we can make use of certain identities that allow for their direct computation in Fourier space. In particular, applying the operator

$$\left((-i)\frac{\partial}{\partial\omega}\right)^{r}\Bigg|_{\omega\to 0}$$

to $\tilde{p}^{(k)}$ yields the Laplace transform of the rth spatial moment of $p^{(k)}(x,t)$. For instance, if $r=0$, we obtain the probability of a particle being in SV k on any edge. For $r=1$, we obtain the mean position of particles in SV k, and for $r=2$ the second moment of particles in SV k.
This dependence on the SV state k can be a complication since most experimental results would report a single mean or variance result rather than multiple results for each internal state of some given system. For SVs, we make use of the fact that given a junction at X, the position of SV k is then $X+(k/4)\Delta X$, see Fig. 6. Thus, the overall first moment is

$$m^{(1)}(t)=\sum_{k=0}^{3}\sum_{X\in\mathbb{Z}}\left(X+\frac{k}{4}\Delta X\right)p^{(k)}(X,t)=\sum_{k=1}^{3}\left(m^{(1,k)}(t)+\frac{k}{4}\Delta X m^{(0,k)}(t)\right)$$

where $m^{(r,k)}(t)$ are the rth moments for particles in state k. Note that since there are multiple states, $m^{(0,k)}$, the probability of a particle being in state k is less than unity for each individual SV, but

$$\sum_{k=0}^{3}m^{(0,k)}(t)=1$$

since particles are conserved in this system. Making use of Fourier transform identities, we find that

$$\begin{aligned}\tilde{m}^{(1)}(s)&=\sum_{k=0}^{3}\left((-i)\frac{\partial\tilde{p}^{(k)}(\omega,s)}{\partial\omega}+\frac{k}{4}\Delta X\tilde{p}^{(k)}(0,s)\right)\\&=\frac{3\Delta X}{8s}\end{aligned}\tag{50}$$

with inverse Laplace transform, $m^{(1)}(t)=3\Delta X/8$.
We apply the same technique for the second moment and obtain the following.

$$\begin{aligned}\tilde{m}^{(2)}(s)&=\sum_{k=0}^{3}\sum_{X\in\mathbb{Z}}\left[X^2+2X\frac{k\Delta X}{4}+\left(\frac{k\Delta X}{4}\right)^2\right]p^{(k)}(X,s)\\&=\sum_{k=0}^{3}\left((-i)^2\frac{\partial^2\tilde{p}^{(k)}(\omega,s)}{\partial\omega^2}+2(-i)\frac{k\Delta X}{4}\frac{\partial\tilde{p}^{(k)}(\omega,s)}{\partial\omega}+\left(\frac{k\Delta X}{4}\right)^2\tilde{p}^{(k)}(0,s)\right)\\&=\frac{\Delta X^2\left(14s^3+(39\lambda+31\mu)s^2+4\mu(17\lambda+3\mu)s+8\lambda\mu^2\right)}{32s^2\left(2s^2+2(\lambda+3\mu)s+\mu(3\lambda+\mu)\right)}.\end{aligned}\tag{51}$$

To leading order, this yields

$$m^{(2)}(t) \sim \frac{\Delta X^2}{4} \frac{\lambda\mu}{\lambda+\mu} t = \frac{\Delta X^2}{4} \left(\frac{1}{\mu} + \frac{3}{\lambda} \right)^{-1} \equiv Dt.$$

Thus, to make an analogy to electronic circuits, the individual exit rates for each state combine like resistors in parallel for SVs that are in series. In contrast, for a set of four single-state, 1D lattices aligned in parallel with jump rate λ for the first and μ for the remainder, $m^{(2)}(t) = \frac{1}{4}(\lambda + 3\mu)\, t$. Thus, SVs in parallel combine like resistors in series. Of course, the analogy becomes harder to follow in cases where there are both internal states and SVs since there are paths in parallel and in series in those cases.

In the above example, the results for all t can also be found explicitly in terms of eigenvalues and eigenfunctions of $\boldsymbol{\Omega}$ (Gadgil et al. 2005). Though the results are somewhat lengthy, the explicit solution, after Fourier and Laplace transformation, for this problem can easily be found by symbolic calculation in Mathematica, for instance. Later, we will discuss a technique that in some cases allows for a simplification of the moment calculation so that it need not be enumerated for every internal state, but can be estimated around each vertex. A general description of the moment computations can be found in Appendix C.1.

4 From "Micro" to "Macro" Moments

As we saw in the preceding section, the macroscale moments, $m^{(r)}$, which are the typical experimental observables, involve sums over the moments for each internal state, $m^{(r,k)}$, and require details of the local geometry. However, this approach becomes cumbersome as more internal states and geometrical features are involved, and suggests that a more direct approach is needed. This is further supported by the observation that, in experiments, it is often difficult to accurately measure concentration distributions over short time and length scales, and thus, in some cases experimental results may only be valid for sufficiently large length and timescales. For instance, tissue-scale diffusivity values would not be expected to hold at very short length scales when a diffusing substance is still confined to a specific cell in the tissue. Thus, a simplified means of obtaining the dynamics over intermediate- and long-term time and length scales is appropriate.

Here we discuss a more direct method of determining these macroscale properties that obviates the need to sum over the SVs. In particular, we reduce the size of the state space of the multistate CTRW by deriving effective waiting-time distributions for jumps between junctions. In this sense, a single jump corresponds to a path beginning at a given junction and terminating at an adjacent junction or returning to the starting point without visiting an adjacent junction. The path is in turn made up of jumps between SVs and internal states on a given edge. As will be shown, the effective waiting-

time distributions for these compound jumps are closely related to the solutions of first-passage-time problems.

Example 4: The Alternating 1D Lattice Revisited

To observe how these effective transition rates may be computed, we return to Ex. 1 on the lattice with alternating junctions and SVs (see Fig. 4). Recall that the evolution equations for this random walk are of the form

$$\frac{dp_i^{(1)}}{dt} = -\lambda p_i^{(1)} + \frac{\mu}{2} \sum_{j \in \mathcal{N}(i,1)} p_j^{(2)}(t)$$
$$\frac{dp_i^{(2)}}{dt} = -\mu p_i^{(2)} + \frac{\lambda}{2} \sum_{j \in \mathcal{N}(i,2)} p_j^{(1)}(t),$$

with index $i \in \mathbb{Z}$. As before, we consider the type 1 points to represent the junctions of a graph, and the type 2 points as SVs along edges of this graph.
If we assume a particle starts at a type 1 point, then we see from the form of the equations that the occupancy probabilities at a type 2 point depends solely upon the probabilities over time at the two type 1 points it is adjacent to. This is because in order to reach type 2 point i that particle has to first reach one of the neighboring type 1 points at i or $i+1$. Thus, we may determine formulas that give the probability at each 2 point as a function of the probabilities at the adjacent type 1 points. Starting with the evolution equation for $p_i^{(2)}(t)$ which has initial condition, $p_i^{(2)}(0) = 0$ since the particles starts on a type 1 point, we have the following:

$$\frac{dp_i^{(2)}}{dt} = -\mu p_i^{(2)} + \frac{\lambda}{2}(p_{i-1}^{(1)}(t) + p_i^{(1)}(t)) \quad \overset{\mathscr{L}}{\Rightarrow} \quad (s+\mu)\tilde{p}_i^{(2)}(s) = \frac{\lambda}{2}(\tilde{p}_{i-1}^{(1)}(s) + \tilde{p}_i^{(1)}(s)) \tag{52}$$

where the arrow indicates Laplace transformation. For the type 1 points, we have

$$\begin{aligned} \frac{dp_i^{(1)}}{dt} &= -\lambda p_i^{(1)} + \frac{\mu}{2}(p_i^{(2)}(t) + p_{i+1}^{(2)}(t)) \quad \overset{\mathscr{L}}{\Rightarrow} \quad (s+\lambda)\tilde{p}_i^{(1)}(s) \\ &= \delta_{i,0} + \frac{\mu}{2}(\tilde{p}_i^{(2)}(s) + \tilde{p}_{i+1}^{(2)}(s)), \end{aligned} \tag{53}$$

where $\delta_{i,0}$ gives the initial condition of the particle in the type 1 state at $X_0 = 0$. Combining these yields a system of equations for $\tilde{p}_i^{(1)}(s)$ where $\tilde{p}_i^{(2)}(s)$ has been eliminated. After simplifying, we have

$$\tilde{p}_i^{(1)}(s) = \frac{1}{\lambda + s}\delta_{i,0} + \frac{\mu\lambda}{4(s+\mu)(s+\lambda)}\left(\tilde{p}_{i-1}^{(1)} + 2\tilde{p}_i^{(1)} + \tilde{p}_{i+1}^{(1)}\right) \tag{54}$$

or, after inverting the Laplace transform

$$p_i^{(1)}(t) = e^{-\lambda t}\delta_{i,0} + \int_0^t \frac{\lambda\mu}{4(\lambda-\mu)}\left(e^{-\mu(t-\tau)} - e^{-\lambda(t-\tau)}\right) \left(p_{i-1}^{(1)}(\tau) + 2p_i^{(1)}(\tau) + p_{i+1}^{(1)}(\tau)\right) d\tau. \tag{55}$$

This is the integral master equation for a random jump process, but while the initial system had two types of points and was Markovian, this new process has a single type of point, and, having a non-Poisson waiting-time distribution, is semi-Markovian. We also see that $p_i^{(1)}$ appears on the right- and left-hand sides of Eq. (55). This obfuscates the meaning of a jump, since jumps that return a particle to its origin could occur in this setting, but the remedy is quite straightforward here – simply rearrange terms in Laplace space before inverting so that p_1^i is isolated on the left. This leads to

$$\tilde{p}_i^{(1)}(s) = \frac{s+\mu}{(s+\lambda)(s+\mu) - \frac{1}{2}\lambda\mu}\delta(X) + \tilde{f}(s)\left(\tilde{p}_{i-1}^{(1)}(s) + \tilde{p}_{i+1}^{(1)}(s)\right) \tag{56}$$

where

$$\tilde{f}(s) = \frac{1}{4}\frac{\mu\lambda}{(s+\lambda)(s+\mu) - \frac{1}{2}\lambda\mu}, \tag{57}$$

or, after inverting the Laplace transform,

$$f(t) = \frac{1}{2}\frac{\lambda\mu e^{-\frac{\lambda+\mu}{2}t}}{\sqrt{\lambda^2+\mu^2}}\sinh\left(\frac{\sqrt{\lambda^2+\mu^2}}{2}t\right). \tag{58}$$

Note that $f(t)$ is not quite a WTD since it integrates to 1/2. In fact, one can think of $f(t)$ as $\frac{1}{2}\phi(t)$ where the factor of 1/2 is from the jump distribution operator (e.g., $T(X_{i\pm1}, X_i) = 1/2$) which accounts for the fact that there is a 50% chance of jumping to the left and 50% to the right at any given step. This in turn leads to an integral master equation of the form

$$p_i^{(1)}(t) = \hat{\Psi}(t)\delta_{i0} + \int_0^t f(t-\tau)\left(p_{i-1}^{(1)}(\tau) + p_{i+1}^{(1)}(\tau)\right) d\tau$$

where

$$\hat{\Psi}(t) = e^{-\frac{\lambda+\mu}{2}t}\left(\cosh\left(\frac{t}{2}\sqrt{\lambda^2+\mu^2}\right) + \frac{\mu-\lambda}{\sqrt{\lambda^2+\mu^2}}\sinh\left(\frac{t}{2}\sqrt{\lambda^2+\mu^2}\right)\right)$$

At first, this last rearrangement may seem like an unnecessary complication, but it enables us to understand the waiting time $f(t)$ in terms of a standard jump process where each jump implies a change of position. Only when self-jumps are removed can the terms in the transition matrix be understood as the waiting

times for a jump to occur. As will be discussed in the following section, the modified waiting-time distribution is also equal to the first-passage-time for a particle to travel between type 1 points.

Notice that $\hat{\Psi}(t)$ is *not* the complementary cumulative waiting-time distribution of $f(t)$. This is because even though we have written a master equation for $p^{(1)}(t)$ alone, in reality the system still has two states, and thus, at any given moment, some of the particles will reside in type 1 states, and some in type 2 states. Thus, $\hat{\Psi}$ includes this additional information and differs from $\hat{\Phi}$, as discussed below.

Of course, given $f(t)$, we can compute $\hat{\Phi}$ as

$$\hat{\Phi}(t) = 1 - \int_0^t f(\tau)d\tau = e^{-\frac{\lambda+\mu}{2}t}\left(\cosh\left(\frac{t}{2}\sqrt{\lambda^2+\mu^2}\right) + \frac{\lambda+\mu}{\sqrt{\lambda^2+\mu^2}}\sinh\left(\frac{t}{2}\sqrt{\lambda^2+\mu^2}\right)\right).$$

In order to understand the distinction between $\hat{\Psi}$ and $\hat{\Phi}$, we begin by summing over $i \in \mathbb{Z}$ in Eq. (56). This yields an equation in Laplace transform space for the zeroth-order moment, $\tilde{m}^{(0)}(s)$ of $\tilde{p}^{(1)}(s)$. Upon simplifying,

$$\tilde{m}^{(0)}(s) = \frac{\tilde{\hat{\Psi}}(s)}{1 - 2\tilde{f}(s)}$$

and, after inverse Laplace transformation, $m^{(0)}(t) = 1/(\mu+\lambda)\left(\mu + \lambda e^{-(\mu+\lambda)t/2}\right)$. Thus, the probability of a particle being on a type 1 point varies in time, since, depending on the values of μ and λ, there is a nonzero probability that the particle can be located on a type 2 point at any given time.

On the other hand, if we replace $\tilde{\Psi}$ by $\tilde{\Phi}$, the same steps yield: $m^{(0)}(t) = 1$, or the particle remains on type 1 states with probability 1. At first glance, it appears that we have eliminated (seemingly erroneously) the possibility of a particle to ever land on a type 2 state. However, there is a more subtle interpretation of this change. By going from $\hat{\Psi}$ to $\hat{\Phi}$, we have changed the meaning of the quantity, $p_i^{(1)}(t)$ being computed. Originally, $p_i^{(1)}(t)$ was the probability of being located on the ith type 1 point, but the new probability is that of having reached the ith type 1 point, but not yet having reached an another type 1 point. In other words, with $\hat{\Phi}$, each $p_i(t)$ refers to the combined probability of all paths that occupy the type 1 point at i at time t, and also those that have reached i at a prior time, but not reached the type 1 points at $i \pm 1$.

Depending on the application, it can be useful to use $\hat{\Psi}$ or $\hat{\Phi}$. If we are to reduce this problem solely to a random jump process on type 1 points, then $\hat{\Phi}$ should be used—for instance, if we attempt to compute moments without resorting to details about the type 2 points. On the other hand, if we wish at the end to also compute occupation probabilities for the SVs, then $\hat{\Psi}$ should be used since it

includes information about how particles are distributed between type 1 and type 2 points.

Given this explicit solution over the type 1 points, we can also examine how variation of the parameters μ and λ affect the outcome. For instance of $\mu \gg \lambda$, then the process reduces to a single-state process with exit rate λ from each point. For instance, using $\Phi(t)$ and the fact that $\phi(t) = 2f(t)$, we can derive an differential master equation,

$$\frac{1}{\mu\lambda}\frac{d^2p_i}{dt^2} + \left(\frac{1}{\mu} + \frac{1}{\lambda}\right)\frac{dp_i}{dt} = \frac{1}{2}(p_{i-1}(t) - 2p_i(t) + p_{i+1}(t))$$

This equation appears similar to a discretization of the telegrapher's equation; however, as discussed in Othmer et al. (1988), supposing $\lambda = \mu$, there is no scaling of λ with time that results in the telegrapher's equation. Rather, in this case, diffusive behavior results if we set $\Delta X = X_i - X_{i-1}$ and let $\Delta X \to 0$ while $\lambda \to \infty$ and $\lambda \Delta X^2 = \text{const.}$.

4.1 First-Passage-Time Problems

The first-passage-time (FPT) density of a stochastic process is the probability density function, $\boldsymbol{f}(t, \boldsymbol{x}_1|\boldsymbol{x}_0)$ that characterizes the time it takes the trajectory of a random process, having started at a point $\boldsymbol{x}_0$, to reach a point, $\boldsymbol{x}_1$ for the first time (c.f. Montroll and Weiss 1965). In the special case that $\boldsymbol{x}_0 = \boldsymbol{x}_1$, the FPT density describes the time it takes a particle to return to $\boldsymbol{x}_0$ after having made at least one jump away. We now show how $f(t)$ above can be understood as a FPT density.

In general, FPT densities can be found as the fluxes of particles leaving a domain subject to absorbing boundary conditions (Kampen 1992). Let us consider the first-passage-time from the type 1 point i, to reach the adjacent type 1 points located at X_{i+1} or X_{i-1}. To solve this problem, we apply absorbing boundary conditions at $X_{i\pm1}$, e.g., $p^{(1)}_{i-1}(t) = 0$ and $p^{(1)}_{i+1}(t) = 0$, and write out the evolution equations for the random walk on the interval between these points, which includes an SV on either side of the type 1 point at the origin.

$$\begin{aligned}
\frac{dp_i^{(2)}}{dt} &= -\mu p_i^{(2)} + \frac{\lambda}{2}p_i^{(1)}(t), & p_{i-1}^{(2)}(0) &= 0 \\
\frac{dp_i^{(1)}}{dt} &= -\lambda p_i^{(1)} + \frac{\mu}{2}(p_{i-1}^{(2)}(t) + p_i^{(2)}(t)), & p_i^{(1)}(0) &= 1 \\
\frac{dp_{i+1}^{(2)}}{dt} &= -\mu p_{i+1}^{(2)} + \frac{\lambda}{2}p_i^{(1)}(t), & p_{i+1}^{(2)}(0) &= 0.
\end{aligned} \tag{59}$$

Upon solving Eq. (59) for $p_i^{(1)}$, $p_i^{(2)}$, and $p_{i+1}^{(2)}$, the FPT densities at $X_{i\pm1}$ are then found as the fluxes of particles at the type 1 points at $i \pm 1$. These fluxes are simply

the convolution of $\phi(t)$ with $p_i^{(2)}(t)$ and $p_{i+1}^{(2)}(t)$, and therefore,

$$f_{+1}(t) = \frac{\mu}{2}\int_0^t e^{-\mu(t-\tau)} p_{i+1}^{(2)}(\tau)d\tau.$$
$$f_{-1}(t) = \frac{\mu}{2}\int_0^t e^{-\mu(t-\tau)} p_i^{(2)}(\tau)d\tau.$$

Due to symmetry, $f_{+1}(t) = f_{-1}(t)$ and we may solve the above equations for the first-passage-time density,

$$f(t) = \frac{1}{2}\frac{\lambda\mu e^{-\frac{\lambda+\mu}{2}t}}{\sqrt{\lambda^2+\mu^2}}\sinh\left(\frac{\sqrt{\lambda^2+\mu^2}}{2}t\right).$$

We see that $f(t)$ is precisely the modified WTD from Eq. (58). The effective WTD for this problem is thus $\phi(t) = 2f(t)$.

Having derived the form of the first-passage-time distribution to travel between adjacent type 1 points, we have reduced the problem to a random walk on a 1D lattice with waiting time $2f(t)$. To find the moments, it is convenient to apply a Laplace transformation to the integral master equation. The result of Eq. (43) can then be applied to yield

$$m^{(2)}(t) = \mathscr{L}^{-1}\left[\frac{L^2}{s}\frac{2f(s)}{1-2f(s)}\right] = \frac{L^2}{2}\frac{\lambda\mu}{\lambda+\mu}t - L^2\frac{\lambda\mu}{(\lambda+\mu)^2}\left(1-e^{-(\lambda+\mu)t}\right).$$

Recall that in previous examples, we had a factor of ΔX^2 multiplying the second moment. The factor of L^2 which appears here reflects the fact that we specify that the lattice spacing $L = \Delta X$, and this appears as the nth power in an nth-order moment.

In Appendices D.1 and 2, we show that the FPT procedure can be generalized to more complicated random walks.

4.2 A 1D CTRW with Many SVs

Let us continue with the preceding example, but now with an arbitrary number, n_k, of SVs, as in Fig. 7. The system of equations describing the probabilities associated with each junction and SV are of the form

$$\begin{pmatrix} \frac{d}{dt}p_i^{(0)} \\ \frac{d}{dt}p_i^{(1)} \\ p_i^{(2)} \\ \vdots \\ \frac{d}{dt}p_i^{(n_k)} \end{pmatrix} = -\begin{pmatrix} \lambda & & & \\ & \mu & & \\ & & \mu & \\ & & & \ddots \\ & & & & \mu \end{pmatrix}\begin{pmatrix} p_i^{(0)} \\ p_i^{(1)} \\ p_i^{(2)} \\ \vdots \\ p_i^{(n_k)} \end{pmatrix} + \frac{1}{2}\begin{pmatrix} 0 & \mu & 0 & & \\ \lambda & 0 & \mu & & \\ & \mu & 0 & \mu & \\ & & \ddots & \ddots & \ddots \\ & & & \mu & 0 \end{pmatrix}\begin{pmatrix} p_i^{(0)} \\ p_i^{(1)} \\ p_i^{(2)} \\ \vdots \\ p_i^{(n_k)} \end{pmatrix}$$

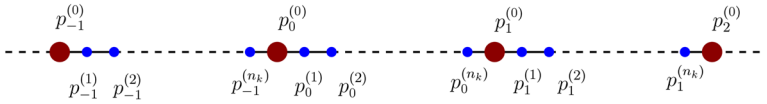

Fig. 7 Depiction of the random walk problem described in Sect. 4.2. Red dots are junctions and blue dots refer to SVs along each edge

$$+\frac{1}{2}\begin{pmatrix}\mu p_{i-1}^{(n_k)}\\ 0\\ \vdots\\ 0\\ \lambda p_{i+1}^{(0)}\end{pmatrix} \tag{60}$$

for index, $i \in \mathbb{Z}$.

This problem can serve as a simple model for diffusive transport in a series of cells. The transport of molecules in cell interiors can be modeled as jumps on the n_k SVs, and the junctions represent cell membranes. Since the cell membranes are then represented by a single junction point, this case corresponds to a situation where adjacent cells are closely packed together. Further extensions can be included when the intracellular gap between adjacent cells must be considered, as in Sect. 5.1.

Computing the moments in this case would generally be quite complicated, since it requires averaging over every internal state. Thus, to obtain an approximation for a simplified system, we first compute how long it takes to travel the length of an edge, from junction X_i to X_{i+1}. Once the effective waiting-time distribution for this transport to occur is found, we can then treat this system as a standard one-dimensional CTRW on a lattice.

To solve for the effective WTD at junctions, we compute the first-passage-time density to traverse an edge, i.e. to travel from one side of a cell to the other. Consider a particle starting from membrane i (the left side of cell i, or equivalently the right membrane of cell $i-1$ in this model) and traveling to membrane $i-1$, or $i+1$. Since the process terminates upon arrival at either membrane, we impose absorbing boundary conditions at $X_{i\pm1}$. In terms of the microscale SVs, these absorbing conditions are applied to $p_{i-1}^{(0)}$ and $p_{i+1}^{(0)}$.

We can use a recursion method to find the solution to this problem, as was done in Teimouri and Kolomeisky (2013). We also note that due to the symmetry about X_i, $p_i^{(k)} = p_{i-1}^{(n_k-k)}$ for each k, and without loss of generality, we only have to consider transport from X_i to X_{i+1} with modified boundary condition at X_i. In particular, there is an absorbing boundary condition at X_{i+1}, and a reflecting boundary condition at X_i. The reflecting condition is obtained by simplifying the equation for $p_i^{(0)}$ on the full lattice with the assumption that $p_i^{(1)} = p_{i-1}^{(n_k)}$. That this yields a reflecting boundary can be verified via a method of images argument (Chandrasekhar 1943). The absorbing

condition at X_{i+1} and the reflecting condition at X_i can be written as

$$\begin{aligned}\tilde{p}_{i+1}^{(0)} =&0\\ \tilde{p}_i^{(0)} =&\frac{1}{s+\lambda}+\frac{\mu}{s+\lambda}\tilde{p}_i^{(1)}\end{aligned} \tag{61}$$

Between X_i and X_{i+1}, Equation (60) can be solved by assuming an *ansatz*, $\tilde{p}_i^{(k)} = a^k$ for $k = 1, 2, 3, \ldots$ and leaving $\tilde{p}_i^0$ unspecified at first. Thus, we start by solving for $\tilde{p}_i^{(k)}$ with

$$\tilde{p}_i^{(1)} =\frac{1}{s+\mu}\left(\frac{\mu}{2}\tilde{p}_i^{(2)}+\frac{\lambda}{2}\tilde{p}_i^{(0)}\right) \qquad k=1 \tag{62}$$

$$\tilde{p}_{i+1}^{(0)} =0 \qquad k=0 \tag{63}$$

After some algebraic simplifications

$$\tilde{p}_i^{(k)} = A_1(s)w_-(s)^k + A_2(s)w_+(s)^k \quad k = 1, 2, 3, \ldots, n_k$$

with

$$w_-(s) = \left(\left(\frac{s}{\mu}+1\right)-\sqrt{\left(\frac{s}{\mu}+1\right)^2-1}\right),$$

$$w_+(s) = \left(\left(\frac{s}{\mu}+1\right)+\sqrt{\left(\frac{s}{\mu}+1\right)^2-1}\right)$$

and where $A_1(s)$ and $A_2(s)$ are specified by the boundary conditions. Finally, we enforce the boundary condition at $k = 0$ to find $\tilde{p}_i^{(0)}$.

Ultimately, the result only depends on μ, λ, n_k, and s, and if we compute the FPT, $\tilde{f}(s)$, for a particle to arrive at the boundary at X_{i+1}, we obtain

$$\begin{aligned}\tilde{f}(s) &= \frac{\mu}{2}p_i^{n_k}(s)\\ &= \frac{1}{2}\frac{\lambda\mu(w_+-w_-)w_+^{n_k-1}w_-^{n_k-1}}{w_+^{n_k}\left(2s^2+2s(\mu+\lambda)+\mu\lambda-\mu(s+\lambda)w_-\right)-w_-^{n_k}\left(2s^2+2s(\mu+\lambda)+\mu\lambda-\mu(s+\lambda)w_+\right)}\end{aligned} \tag{64}$$

Since i was left unspecified, this relation is true for each junction, and we ultimately obtain a system of equations for $\tilde{p}_i^{(0)}$ where the dependence on the SVs has been removed,

$$\tilde{p}_i^{(0)} = \tilde{f}(s)\left(\tilde{p}_{i-1}^{(0)}+\tilde{p}_{i+1}^{(0)}\right).$$

Thus, $\tilde{f}(s)$ is an effective WTD for transitions in a 1D single-state CTRW on $\mathbb{Z}$ with no SVs. It is also useful to note that the mean waiting time to travel between cell, can be found, after much algebra, as

$$\bar{t} = -2 \lim_{s \to 0} \frac{\partial \tilde{f}}{\partial s} = (n_k + 1) \frac{n_k \lambda + \mu}{\lambda \mu}.$$

The factor of 2 appears since if we compute how long it takes to travel from X_i to $X_{i \pm 1}$, we must include the rates of particles arriving at X_{i+1} and X_{i-1}, which in this case are both equal to $\tilde{f}(s)$.

The macroscale moments can be found by using the result from Eq. (43) and assuming that $L = \Delta X$ is independent of n_k. The explicit solution can be written out in Laplace space, and the asymptotic result can be found as

$$m^{(2)}(t) = \frac{L^2 \mu \lambda}{(n_k + 1)(n_k \lambda + \mu)} t.$$

Since we regard the SVs as representing a discretization of diffusion within each cell, we expect that the space between each pair of SVs is $\Delta x = L/n_k$. The average time it takes a diffusing particle to travel a distance Δx is $\sqrt{D_m \Delta t}$ where D_m is the microscopic diffusion constant within a cell. Thus, if we set $\mu = D_m/\Delta x^2 = D_m n_k^2/L^2$, we should obtain an approximation of diffusion within each cell. Furthermore, if we let $\lambda = \lambda_\infty n_k$,

$$m^{(2)}(t) = \frac{D_m \lambda_\infty t}{\lambda_\infty + D_m/L^2} \equiv 2 D_M t$$

where D_M may be treated as a macroscale diffusion coefficient. This scaling of λ is necessary because as n_k grows, the number of times a random walker will return to the origin before reaching an adjacent junction increases. If λ does not scale with n_k, this increasing number of returns to the origin leads to arbitrarily long waiting times to reach an adjacent junction, and no macroscale diffusion occurs.

Although we do not consider all of the details here, with suitable scalings of μ and λ as n_k approaches infinity, we can consider the problem not merely as a discretization of diffusion within the cell, but as a continuum problem.

4.3 CTRW with SVs and Internal States

Next we consider an extension of the previous problem in which there are two internal states: a mobile state and an immobile bound state. Let us assume that transitions from the mobile to the bound state occurs at rate k_+ and from bound to mobile at rate k_-. The resulting reaction network is diagrammed in Fig. 8.

From the discussion in Sect. 2.2, we know that Poisson processes can be additively combined to obtain a multistate differential master equation. Thus, we obtain the following system of equations

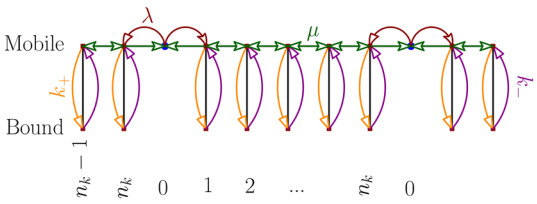

Fig. 8 Diagram of the various transitions allowed in the system discussed in a jump process involving both SVs and internal states. Note that there are no internal state transitions at the junctions since we assume that all particles are in a mobile state there

$$
\begin{aligned}
\frac{dp_{i,m}^{(0)}}{dt} &= -\lambda p_{i,m}^{(0)} + \frac{\mu}{2}\left(p_{i-1,m}^{(n_k)} + p_{i,m}^{(1)}\right) && k = 0 \\
\frac{dp_{i,m}^{(1)}}{dt} &= -(\mu + k_+)p_{i,m}^{(1)} + \frac{1}{2}\left(\lambda p_{i,m}^{(0)} + \mu p_{i,m}^{(2)}\right) + k_- p_{i,b}^{(1)} && k = 1 \\
\frac{dp_{i,m}^{(k)}}{dt} &= -(\mu + k_+)p_{i,m}^{(k)} + \frac{\mu}{2}\left(p_{i,m}^{(k-1)} + p_{i,m}^{(k+1)}\right) + k_- p_{i,b}^{(k)} && k = 2, \ldots, n_k - 1 \\
\frac{dp_{i,m}^{(n_k)}}{dt} &= -(\mu + k_+)p_{i,m}^{(n_k)} + \frac{1}{2}\left(\mu p_{i,m}^{(n_k-1)} + \lambda p_{i+1,m}^{(0)}\right) + k_- p_{i,b}^{(n_k)} && k = n_k \\
\frac{dp_{i,b}^{(k)}}{dt} &= -k_- p_{i,b}^{(k)} + k_+ p_{i,m}^{(k)} && k = 1, \ldots, n_k
\end{aligned}
\tag{65}
$$

where m and b subscripts indicate mobile and bound states. To solve this, we first note that each $p_{i,b}^{(k)}$ can be found in terms of $p_{i,m}^{(k)}$ as

$$p_{i,b}^{(k)} = \int_0^t e^{-k_-(t-\tau)} k_+ p_{i,m}^{(k)}(\tau) d\tau.$$

We can rearrange terms to obtain

$$\frac{dp_{i,m}^{(k)}}{dt} = -(-\mu + k_+)p_{i,m}^{(k)} + \frac{\mu}{2}\left(p_{i,m}^{(k-1)} + p_{i,m}^{(k+1)}\right) + k_- k_+ \int_0^t e^{-k_-(t-\tau)} p_{i,m}^{(k)}(\tau) d\tau.$$

In Laplace transform space, we obtain a recursion relation with the same boundary conditions as in the previous section, but with w_+ and w_- now set to

$$w_\pm(s) = \frac{1}{\mu}\left[\left(s + \mu + k_+ - \frac{k_+ k_-}{s + k_-}\right) \pm \sqrt{\left(s + \mu + k_+ - \frac{k_+ k_-}{s + k_-}\right)^2 - \mu^2}\right].$$

We find that to leading order, the FPT in this case is

$$f(s) \sim \frac{1}{2} - \frac{(1 + n_k)(k_+ n_k \lambda + k_-(n_k \lambda + \mu)}{k_- \lambda \mu} s$$

and the second moment is

$$m^{(2)}(t) \sim \frac{L^2 k_- \lambda \mu}{(n_k+1)((k_+ + k_-)n_k \lambda + k_- \mu)} t$$

In the limit that $n_k \to \infty$ with $\lambda \sim \lambda_\infty n_k$ and $\mu \sim (D_m/L^2)n_k^2$,

$$m^{(2)}(t) \sim \frac{D_m \lambda_\infty k_-}{(k_+ + k_-)\lambda_\infty + k_- D_m/L^2} t \equiv 2D_M t.$$

We see that if unbinding is much more rapid than binding, i.e. $k_- \gg k_+$, we recover the case with no immobilization.

Another case of interest occurs when $k_- = 0$, i.e. if binding is irreversible, or represents a degradation reaction. In this case, since all particles eventually are degraded, the long-time asymptotic moments vanish. However, if there is a source term, then a steady-state distribution can be found by taking the limit that $s \to 0$ in Laplace space. The solution for the probability of being located in a particle index j is then of the form

$$p(j,s) = \frac{1-f(s)}{s} \frac{1}{\sqrt{1-f(s)^2}} \left(\frac{(1-f(s)-\sqrt{1-f(s)^2})}{f(s)} \right)^{|j|} h(s)$$

where $h(s)$ is the Laplace transform of a source at $j = 0$. For $h(s) = h_0$, a constant source, the steady-state solution can be found as

$$\lim_{s \to 0} sp(j,s)$$

Of course, there are many variations that can be applied: immobilization and degradation as separate reactions, multiple mobile states with different jump rates, etc.

Example 5: Comb Geometry

Comb models are widely used to study transport phenomenon, especially in percolation theory (Havlin and Ben-Avraham 1987), and in studies of transport in systems where anomalous transport behavior is observed. They also arise in certain polymerization problems and in the study of transport in dendrites (Iomin 2011; Iomin and Méndez 2013; Iomin et al. 2016; Iomin 2019; Berezhkovskii et al. 2014, 2015; Hu and Othmer 2011; Bressloff and Newby 2013).

The basic comb mode shown in Fig. 9 consists of a "backbone" with periodic side branches which effectively act as traps for particles which diffuse along the backbone. If the side branches are infinitely long, the mean waiting time for particles in the side branches to return to the backbone becomes infinite, leading to anomalous transport behavior. If the side branches are of finite length, crossover behaviors occur with an initial anomalous transport phase followed by normal diffusion, albeit with a smaller

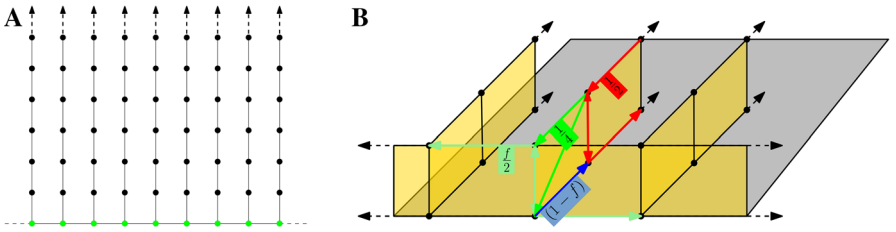

Fig. 9 **A** Basic comb geometry. Green dots represent junctions along the backbone and black dots are secondary spatial states on the teeth. **B** Depiction of the various transitions that can occur from state 1 and state 2 at each junction in the comb model with 2 internal states. The probabilities for each transition to occur are labeled adjacent to the arrows indicating each allowed transition

diffusion coefficient than that which would be observed for a particle traveling on a backbone without traps (Lubashevskii and Zemlyanov 1998).

Rather than simply solve for the density distributions of a random walk along the comb, which is known from many previous studies (Havlin and Ben-Avraham 1987; Weiss and Havlin 1986), we combine the comb geometry with the multistate transport processes discussed earlier. In particular, we will consider a two-state, persistent or biased random walk (Montroll and West 1979). A random walk in 1D will be called persistent if the particles can enter into various internal states that have unequal likelihoods of jumping forward or backwards. In the continuum sense, this leads to telegrapher's equation models in one space dimension (Othmer et al. 1988). In a biological example, this type of transport is believed to play an important role in the putative ability of fingerlike projections, known as cytonemes, to transport morphogens from source cells to target cells (Kornberg and Roy 2014; Kornberg 2014; Roy et al. 2014). Current modeling efforts (Kim and Bressloff 2018; Bressloff and Kim 2018) suggest that this type of transport can be understood in terms of a velocity jump process (Othmer 1983) similar to a telegrapher's equation, but much still remains unknown about this mode of transport and it could be a rich field for modeling.

Here, we combine persistence with a complex geometry and show how our formulation makes this type of otherwise very–complicated problem fairly straightforward to study. For the sake of simplicity, we take a two-state random walk. Junctions are located at integers along the x-axis, and the comb teeth point vertically, emanating from each junction, but only connected horizontally along the x-axis ($y = 0$) as in Fig. 9a.

At each junction, and at SVs along the teeth, we assume that there are two internal states, $\ell = 1$ and $\ell = 2$. At SVs with $y \geq 1$, particles in state 1 only can jump to state 1 at position $y + 1$ or to state 2 while remaining fixed at y. Particles in state 2 can only jump to state 2 at $y - 1$ or transition to state 1. Let us assume that $\phi(t)$ is the WTD for all of the transitions so that we can reduce the number of parameters. This can be generalized if needed. Thus, at each point on a tooth (where $y \geq 1$), we have the following transition matrices:

$$\boldsymbol{T}_{SV}(y, y') = \frac{1}{2}\left[\begin{pmatrix} 1 & 0 \\ 0 & 0 \end{pmatrix}\delta(y - y' - 1) + \begin{pmatrix} 0 & 0 \\ 0 & 1 \end{pmatrix}\delta(y - y' + 1)\right], \qquad \boldsymbol{K}_{SV} = \frac{1}{2}\begin{pmatrix} 0 & 1 \\ 1 & 0 \end{pmatrix}.$$

At $y = 1$, the form of $\boldsymbol{T}(y)$ is different, there is only a $(1-f)$ probability for a particle traveling along the backbone to enter into a tooth. Thus, for $y = 1$, we write

$$\boldsymbol{T}_{SV}(1, y') = \frac{1}{2}\begin{pmatrix} 0 & 0 \\ 0 & 1 \end{pmatrix}\delta(2 - y')$$

and define

$$\boldsymbol{D}' = \frac{1}{2}\begin{pmatrix} (1-f) & (1-f) \\ 0 & 0 \end{pmatrix}$$

as the transfer matrix for particles jumping from a tooth to the backbone. Similarly, the transfer of particles from the tooth to the backbone is given by

$$\boldsymbol{D} = \begin{pmatrix} 0 & \frac{1}{4} \\ 0 & \frac{1}{4} \end{pmatrix}.$$

It remains to specify $\boldsymbol{K}_J$ and the additional matrix, $\boldsymbol{T}_J$, which describes spatial jumps between adjacent junction points on the backbone. At $y = 0$, let us assume state 1 points can only travel to the right, change state, or travel up to $y = 1$, and a state 2 point can only travel left or change state. In matrix form, we have

$$\boldsymbol{T}_J(x, x') = \frac{1}{2}\left[\begin{pmatrix} f & 0 \\ 0 & 0 \end{pmatrix}\delta(x - x' - 1) + \begin{pmatrix} 0 & 0 \\ 0 & f \end{pmatrix}\delta(x - x' + 1)\right], \qquad \boldsymbol{K}_J = \frac{1}{2}\begin{pmatrix} 0 & f \\ f & 0 \end{pmatrix},$$

where f is the fraction of particles that did not jump to $y = 1$. Putting everything together, we write:

$$\boldsymbol{T} + \boldsymbol{K} = \boldsymbol{I} \otimes \begin{pmatrix} \boldsymbol{K}_J & \boldsymbol{D} \\ \boldsymbol{D}' & \boldsymbol{T}_{SV} + \boldsymbol{K}_{SV} \end{pmatrix} + \boldsymbol{A}_s \otimes \begin{pmatrix} \boldsymbol{T}_J(1, 0) & \boldsymbol{0} \\ \boldsymbol{0} & \boldsymbol{0} \end{pmatrix} + \boldsymbol{A}_e \otimes \begin{pmatrix} \boldsymbol{T}_J(0, 1) & \boldsymbol{0} \\ \boldsymbol{0} & \boldsymbol{0} \end{pmatrix} \tag{66}$$

where $\boldsymbol{A}_s$ and $\boldsymbol{A}_e$ are the infinite-dimensional permutation matrices from Eq. (38). Because of the infinite extent of the teeth, this problem, even after Fourier transformation along the x-direction is still of infinite dimension. Thus, we will make use of the FPT method discussed in Sect. 4.1.

After Laplace transformation of $\phi(t)$, the problem becomes an infinite-dimensional matrix vector problem. To find the relevant FPT, we must invert $\boldsymbol{I} - \tilde{\phi}(s)(\boldsymbol{T}_{SV}(y, y') + \boldsymbol{K}_{SV})$ which, in general is a difficult task when there are infinitely many states involved. However, due to the simple structure of $\boldsymbol{T}_{SV}(y, y') + \boldsymbol{K}_{SV}$, inversion is possible in this case. Let us first consider, instead of a semi-infinite tooth, one that is bidirectionally infinite. Thus, consider $y \in \mathbb{Z}$ rather than just positive-valued. Noting that the transition matrix $\boldsymbol{T}_{SV}(y, y') + \boldsymbol{K}_{SV}$ is translation-invariant along this infinite tooth (i.e. a function only of $y - y'$), then we can take a lattice Fourier transform in the y-direction to obtain

that

$$\hat{\boldsymbol{T}}_{SV}(\nu) + \boldsymbol{K}_{SV} = \frac{1}{2}\begin{pmatrix} e^{-i\nu y} & 1 \\ 1 & e^{i\nu y} \end{pmatrix}$$

Accordingly,

$$\left[\boldsymbol{I} - \tilde{\phi}(s)(\hat{\boldsymbol{T}}_{SV}(\nu) + \boldsymbol{K}_{SV})\right]^{-1} = \frac{1}{1 - \phi(s)\cos\nu}\begin{pmatrix} 1 - \frac{\tilde{\phi}(s)}{2}e^{i\nu} & \frac{\tilde{\phi}(s)}{2} \\ \frac{\tilde{\phi}(s)}{2} & 1 - \frac{\tilde{\phi}(s)}{2}e^{-i\nu} \end{pmatrix}$$

The inverse lattice Fourier transform is then found as[7]

$$\begin{aligned}\left[\boldsymbol{I} - \tilde{\phi}(s)(\boldsymbol{T}_{SV}(y) + \boldsymbol{K}_{SV})\right]^{-1} &= \frac{1}{2\pi}\int_{-\pi}^{\pi}\left[\boldsymbol{I} - \tilde{\phi}(s)(\hat{\boldsymbol{T}}_{SV}(\nu) + \boldsymbol{K}_{SV})\right]^{-1} e^{-i\nu y} d\nu \\ &= \frac{1}{\sqrt{1-\tilde{\phi}^2}}\zeta^{|y|}\begin{pmatrix} 1 - \frac{\tilde{\phi}}{2}\zeta & \frac{\tilde{\phi}}{2} \\ \frac{\tilde{\phi}}{2} & 1 - \frac{\tilde{\phi}}{2}\zeta \end{pmatrix}\end{aligned} \tag{67}$$

with

$$\zeta = \frac{1 - \sqrt{1 - \tilde{\phi}^2}}{\tilde{\phi}}.$$

With this solution over an infinite tooth, we can now calculate the first-passage-time distribution for a particle to start at $y = 1$ in state 1 and return to $y = 1$ in state 2. As discussed in Hughes (1996), Montroll and Greenberg (1964), first-passage-time distributions for a discrete time and space random walk can be found by noting that the probability of being located at some point can be calculated as the sum of the probability of arriving at the point for the first time, plus the probability of returning to that point after already having visited it one or more times previously. Recall the definition of $q_n(y, t|y_0)$ as the probability of arriving at y after n steps at time t starting from y_0. We define $f_n(y, t|y_0)$ as the probability of reaching y for the first time after n steps at time t starting from y_0. It has been shown in Montroll and Weiss (1965), Hughes (1996) that the Laplace transforms of these quantities are related by

$$\tilde{q}_n(y, s|y_0) = \delta_{n,0}\delta(y - y_0) + \sum_{m=1}^{n} \tilde{f}_m(y, s|y_0)\tilde{q}_{n-m}(y, s|y).$$

[7] In this sense, the probability $p(y)$ defined at each lattice point can be thought of as the Fourier series for the function $\hat{p}(\nu)$. Thus, the inverse lattice Fourier transform is simply the integral that gives the Fourier coefficients of $p(\nu)$.

One can make use of this result to eventually obtain that the first-passage-time distribution for a CTRW is of the form

$$\tilde{f}(y,s|y_0) = \frac{\tilde{q}(y,s|y_0) - \delta(y-y_0)}{\tilde{q}(y,s|y)}$$

recalling that $q(y,t|y_0)$ is the probability density associated with arrival at y at time t from Eq. (6) in Sect. 2.1. From the derivation in Hughes (1996), we see that this definition extends directly to multistate problems. In the current situation, set

$$\tilde{q}_{ij}(1,s|1) = \boldsymbol{\delta}_{y,1}\delta_i \left[\boldsymbol{I} - \tilde{\phi}(s)(\boldsymbol{T}_{SV} - \boldsymbol{K}_{SV})\right]^{-1} \boldsymbol{\delta}_{y,1}\delta_j$$

where δ_i and δ_j indicate the internal state ($i, j \in \{1,2\}$) for ending and starting the sojourn on a tooth, and $\boldsymbol{\delta}_{y,1}$ is the Kronecker delta concentrated at $y = 1$. With this, $\tilde{f}_{21}(s)$, which is interpreted as the first-passage-time probability density for reaching state 2 at $y = 1$ after starting at $y = 1$ in state 1, is found as

$$f_{21}(s) = \frac{\tilde{q}_{21}(1,s|1)}{\tilde{q}_{22}(1,s|1)} = \frac{\frac{\tilde{\phi}}{2}}{1 - \frac{\tilde{\phi}}{2}\zeta} = \frac{1}{2}\frac{\tilde{\phi}(s)}{1 + \sqrt{1 - \tilde{\phi}^2(s)}}.$$

The effective transition rate for particles to enter the comb in state 1 and return to the backbone in state 2 is then

$$\begin{aligned}\tilde{\boldsymbol{D}}^{\text{eff}}(s) &= \tilde{\phi}^2(s)\boldsymbol{D}\begin{pmatrix}\tilde{f}_{11}(s) & \tilde{f}_{12}(s)\\ \tilde{f}_{21}(s) & \tilde{f}_{22}(s)\end{pmatrix}\boldsymbol{D}' = \frac{(1-f)\tilde{\phi}^2(s)\tilde{f}_{21}(s)}{4}\begin{pmatrix}1 & 1\\ 1 & 1\end{pmatrix}\\ &= \frac{1-f}{8}\frac{\tilde{\phi}^3}{1+\sqrt{1-\tilde{\phi}^2}}\begin{pmatrix}1 & 1\\ 1 & 1\end{pmatrix}\end{aligned}$$

where the $\tilde{\phi}^2$ factor comes about due to the waiting times for a particle to jump to the tooth in the first step, and to the backbone in the last step. This formulation yields a problem where we need only consider transport along the backbone. The transition matrix in this case is now

$$\boldsymbol{T}_J(x,x')\tilde{\phi}(s) + \boldsymbol{K}\tilde{\phi}(s) + \tilde{\boldsymbol{D}}^{\text{eff}}(s).$$

After Fourier transformation in the x-direction, we obtain

$$\hat{\boldsymbol{T}}_J(\omega)\tilde{\phi}(s) + \boldsymbol{K}\tilde{\phi}(s) + \tilde{\boldsymbol{D}}^{\text{eff}}(s) = \begin{pmatrix}\frac{f}{2}e^{i\omega} & \frac{1}{2}\\ \frac{1}{2} & \frac{f}{2}e^{-i\omega}\end{pmatrix}\tilde{\phi} + \tilde{\boldsymbol{D}}^{\text{eff}}(s).$$

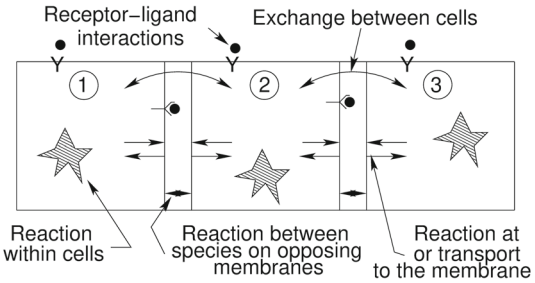

Fig. 10 An elaboration of the transport and kinetics processes involved in the wing disk. In the analysis that follows not all processes are treated, and we identify the membranes on adjacent cells. From Gou et al. (2018)

The moments then follow from Equations (D.2) and (D.3). For $\phi(t) = \rho e^{-\rho t}$, at leading order, we have

$$m^{(1)}(t) \sim \frac{f}{3-f}$$
$$m^{(2)}(t) \sim \sqrt{\frac{2\rho t}{\pi}} \frac{f(3+f)}{(3-f)(1-f)} + \mathcal{O}(1)$$

where the estimates are found using asymptotic results for the Laplace transform. Because the teeth are of infinite extent, the exit time from a tooth may be very long, hindering the transport of the particle along the backbone. This leads to anomalous diffusion and similar anomalous transport results are typical of comb models, as mentioned earlier. Furthermore, recalling the discussion in Sect. 3.1, we see that this is an example of subdiffusion, which is to be expected since the comb teeth act as traps that hinder the particle. Note that the anomalous behavior is dependent on the fact that these traps have an undefined mean waiting time since in Laplace domain space, $\tilde{f}_{21}(s)$ has an unbounded derivative near $s = 0$. When the mean waiting time is finite, the asymptotic long-term behavior is not anomalous, although there can be crossover effects where the system at first appears anomalous but eventually relaxes to normal asymptotic behavior.

5 Transport in a Series of Cells

In this section, we address in more detail the problem that motivated this study, which was to reconcile the vast disparity between experimentally determined parameters for transport in the wing disk. We do this by determining how parameters that describe microscopic processes involved in reaction and transport in the wing disk are reflected in the macroscopic diffusion and decay constants that are estimated from FRAP data. Fig 10 shows the numerous processes that are involved in transport, binding and other reactions in the disk in detail, but as observed earlier, experimentally measured profiles of Dpp measured via FRAP are usually described using a reaction–diffusion model such as Eq. 68, which is based on "free diffusion" and first-order decay (Kicheva et al. 2007; Wartlick et al. 2011).

$$\begin{aligned}\frac{\partial c}{\partial t} &= D\frac{\partial^2 c}{\partial x^2} - kc \qquad x \in (0, L_p)\\ -D\frac{\partial c}{\partial x}(x) &= j \qquad x = 0\\ -D\frac{\partial c}{\partial x}(x) &= 0 \qquad x = L_p\end{aligned} \tag{68}$$

Here $x = 0$ ($x = L_p$) is the location of the Dpp source (pouch boundary). For simplicity we consider a line of cells in which there is only axial variation of the components, and we begin with a simple system that only involves diffusion within cells and in the gaps between those cells. A more complicated model might also include membrane binding kinetics, which can be addressed with the method below as well.

5.1 Diffusion with Extracellular Gaps

We begin with a simple problem that involves diffusion only to understand the effect of the gap between cells. Consider the problem with continuum diffusion in a series of cells of width L separated by gaps of width δ, wherein the diffusion coefficients in the cell and in the gap are to be interpreted as those obtained from the earlier analysis of lattice walks. We write the governing equations as

$$\begin{aligned}\frac{\partial p_i^{(1)}}{\partial t} &= D_{m,1}\frac{\partial^2 p_i^{(1)}}{\partial x^2}, && X_i < x < \delta + X_i\\ \frac{\partial p_i^{(2)}}{\partial t} &= D_{m,2}\frac{\partial^2 p_i^{(2)}}{\partial x^2}, && X_i + \delta < x < X_i + L\\ p_i^{(1)}(X_i + \delta, t) &= p_i^{(2)}(X_i + \delta, t)\\ D_{m,1}\frac{\partial p_i^{(1)}}{\partial x}\bigg|_{x=X_i+\delta} &= D_{m,2}\frac{\partial p_i^{(2)}}{\partial x}\bigg|_{x=X_i+\delta}\end{aligned} \tag{69}$$

where $p_i^{(1)}(x, t)$ is the probability density for a particle to be located in the ith gap, and $p_i^{(2)}(x, t)$ the probability density for a particle to be located in the ith cell. Consider the left-hand cell membrane of each cell (e.g., $X_i = iL$) the junctions in this system and the right-hand cell membrane as a secondary vertex between each pair of junctions.

Then the WTDs for particles to jump between the two types of vertices are the respective FPTs for a particle starting at a membrane to reach a membrane to its left or right. The two FPTs (to travel across a gap, and to travel across a cell) are found as the fluxes to the left and right of the following system:

$$\begin{aligned}
\frac{\partial G^{(1)}}{\partial t} &= D_{m,1}\frac{\partial^2 G^{(1)}}{\partial x^2} && 0 < x < \delta \\
\frac{\partial G^{(2)}}{\partial t} &= D_{m,2}\frac{\partial^2 \partial G^{(2)}}{\partial x^2} && \delta < x < L \\
G^{(1)}(\delta, t) &= G^{(2)}(\delta, t) \\
D_{m,1}\frac{\partial G^{(1)}}{\partial x}\bigg|_{x=\delta} &= \delta(t) + D_{m,2}\frac{\partial G^{(2)}}{\partial x}\bigg|_{x=\delta}
\end{aligned} \tag{70}$$

which can be solved after Laplace transformation. The resulting fluxes at $x = 0$ and $x = L$ are then

$$\begin{aligned}
\tilde{f}_0(s) &= \frac{\sqrt{D_{m,1}}\operatorname{csch}\left(\sqrt{\frac{s}{D_{m,1}}}\delta\right)}{\sqrt{D_{m,1}s}\coth\left(\sqrt{\frac{s}{D_{m,1}}}\delta\right) + \sqrt{D_{m,2}s}\coth\left(\sqrt{\frac{s}{D_{m,2}}}(L-\delta)\right)} \\
\tilde{f}_L(s) &= \frac{\sqrt{D_{m,2}}\operatorname{csch}\left(\sqrt{\frac{s}{D_{m,2}}}(L-\delta)\right)}{\sqrt{D_{m,1}s}\coth\left(\sqrt{\frac{s}{D_{m,1}}}\delta\right) + \sqrt{D_{m,2}s}\coth\left(\sqrt{\frac{s}{D_{m,2}}}(L-\delta)\right)}
\end{aligned} \tag{71}$$

Making use of this result, we can simplify Eq. (69) to obtain, after Laplace transformation, that

$$\begin{aligned}
\tilde{P}_i^{(L)} &= \tilde{f}_0(s)\tilde{P}_{i-1}^{(R)} + \tilde{f}_L(s)\tilde{P}_i^{(R)} \\
\tilde{P}_i^{(R)} &= \tilde{f}_0(s)\tilde{P}_i^{(L)} + \tilde{f}_L(s)\tilde{P}_{i+1}^{(L)}
\end{aligned} \tag{72}$$

where $\tilde{P}_i^{(L,R)}(s)$ represent the probability densities at the left and right cell membrane of each cell.[8]

Already, we have reduced the problem to essentially a two-state CTRW, but before obtaining the diffusivity, we further collapse the system, by solving for the FPT to go between $P_i^{(L)}$ and $P_{i\pm1}^{(L)}$. This yields

$$P_i^{(L)} = \frac{\tilde{f}_0(s)\tilde{f}_L(s)}{1 - \tilde{f}_0^2(s) - \tilde{f}_L^2(s)}\left(P_{i-1}^{(L)} + P_{i+1}^{(L)}\right)$$

We have at this point transformed what was initially a continuum problem into a single-state spatially discrete CTRW for transport between cell membranes. The waiting-time distribution is the first-passage-time for a particle undergoing heterogeneous diffusion to travel a distance L after starting at $x = 0$. As such, Eq. (43) can be used to show

[8] These two quantities technically represent the probabilities associated with particles having reached membrane i (right or left) and not having yet reached a subsequent cell membrane.

that the asymptotic second moment at large t is

$$m^{(2)}(t) = \frac{2t}{\frac{1-\eta}{D_{m,2}} + \frac{\eta}{D_{m,1}}} \equiv 2D_M t$$

where $\eta = \delta/L$. This is equivalent to equation (42) in Othmer (1983) with $\lambda = 1$ (in fact the more general case with $\lambda \neq 1$ can analyzed with FPTs as well).

5.2 Macroscale Equations

With the result for pure diffusion at hand, we consider a line of cells as shown in Fig. 10, with internal reactions and degradation, and derive a macroscale equation that describes the overall process at large enough time and space scales. Within each cell there is diffusion, binding to and release from an immobile site, and degradation of the immobilized particle. The probability densities of states in cell i evolve according to the following equations,

$$\frac{\partial p_i^{(2,1)}}{\partial t} = D_{m,1}\frac{\partial^2 p_i^{(2,1)}}{\partial x^2} + k_- p_i^{(2,2)} - k_+ p_i^{(2,1)} \tag{73}$$

$$\frac{dp_i^{(2,2)}}{dt} = -k_- p_i^{(2,2)} + k_+ p_i^{(2,1)} - k_d p_i^{(2,2)}. \tag{74}$$

$$\frac{\partial p_i^{(1)}}{\partial t} = D_{m,2}\frac{\partial^2 p_i^{(1)}}{\partial x^2} \tag{75}$$

where $p^{(2,1)}$ and $p^{(2,2)}$ represent mobile and bound states in the intracellular domains, and $p^{(1)}$ represents the (mobile) extracellular state. At the boundaries between adjacent cells, the boundary conditions on $p_i^{(1)}$ and $p_i^{(2,1)}$ are the same as those discussed in the previous section.

Eq. (74) can be eliminated by solving for $p_i^{(2,2)}$ in terms of $p_i^{(2,1)}$, and as a result, Eq. (73) becomes

$$\frac{\partial p_i^{(2,1)}}{\partial t} = D_m\frac{\partial^2 p_i^{(2,1)}}{\partial x^2} + k_- k_+ \int_0^t e^{-(k_- + k_d)(t-\tau)} p_i^{(2,1)}(\tau)d\tau - k_+ p_i^{(2,1)}.$$

To further simplify this, we consider the FPT for a particle starting in state 1 at a membrane to reach an adjacent membrane in state 1. After applying a Laplace transformation, the FPT can be found as in the previous example, but with s replaced by

$$\nu(s) = s - k_+\left(\frac{k_-}{s + k_- + k_d} - 1\right),$$

in the Green's function[9]. Thus, the FPTs for a particle starting at a membrane to reach an adjacent membrane (to the left or right) are

$$\begin{aligned}\tilde{f}_0(s) &= \frac{\sqrt{D_{m,1}s}\,\mathrm{csch}\left(\sqrt{\frac{s}{D_{m,1}}}\delta\right)}{\sqrt{D_{m,1}s}\coth\left(\sqrt{\frac{s}{D_{m,1}}}\delta\right)+\sqrt{D_{m,2}\nu(s)}\coth\left(\sqrt{\frac{\nu(s)}{D_{m,2}}}(L-\delta)\right)}\\ \tilde{f}_L(s) &= \frac{\sqrt{D_{m,2}\nu(s)}\,\mathrm{csch}\left(\sqrt{\frac{\nu(s)}{D_{m,2}}}(L-\delta)\right)}{\sqrt{D_{m,1}s}\coth\left(\sqrt{\frac{s}{D_{m,1}}}\delta\right)+\sqrt{D_{m,2}\nu(s)}\coth\left(\sqrt{\frac{\nu(s)}{D_{m,2}}}(L-\delta)\right)}\end{aligned} \tag{76}$$

and as in the previous section, we obtain an equation for the membrane concentrations, $P_i^{(L)}(s)$,

$$\tilde{P}_i^{(L)}(s) = \frac{\tilde{f}_0(s)\tilde{f}_L(s)}{1-\tilde{f}_0^2(s)-\tilde{f}_L^2(s)}\left(\tilde{P}_{i-1}^{(L)}(s)+\tilde{P}_{i+1}^{(L)}(s)\right)+\hat{\Phi}(s)\delta_{i0} \tag{77}$$

with WTD

$$\tilde{F}(s) = \frac{2\tilde{f}_0(s)\tilde{f}_L(s)}{1-\tilde{f}_0^2(s)-\tilde{f}_L^2(s)}.$$

We leave the complementary waiting-time distribution, $\hat{\Phi}(t)$, which gives the probability that no jumps have occurred by time t, undefined for a moment.

We know that $\tilde{F}(s)$ is the WTD for a process with both diffusion and degradation, and in order to see how the diffusion and degradation terms appear on the macroscale, we write,

$$F(t) = \alpha g(t). \tag{78}$$

Here α is the overall probability that a particle leaving membrane i eventually reaches membrane $i+1$ or $i-1$, and $g(t)$ is the unitary WTD (i.e. it integrates to 1) for this to occur. Since degradation is involved, $\alpha < 1$, but since $g(t)$ is a unitary WTD, we can define $\hat{\Phi}$ in terms of $\tilde{g}(s)$ as

$$\hat{\Phi}(s) = \frac{1-\tilde{g}(s)}{s}.$$

The reason we use $\tilde{g}(s)$ rather than $\tilde{F}(s)$ here is that a particle must eventually jump or be degraded. Defining $\hat{\Phi}$ in terms of $F(t)$, which is non-unitary, would imply that there is a $(1-\alpha)$ chance for a particle to simply never jump, which is inconsistent with Eqs. (73) and (74). The use of a unitary WTD, $g(t)$, resolves this inconsistency. On the other hand, the presence of decay implies that the use of $g(t)$ involves a slight

[9] If particle immobilization is irreversible the following analysis simplifies somewhat, for Eq. (73) is then independent of $p_i^{(2,2)}$ and k_+ takes the place of k_d in the macroscopic parameters.

approximation since there is a nonzero probability of degradation to occur before reaching a junction. However, since we are ultimately interested in asymptotic limits that are approached only after many jumps occur, the use of an approximate WTD for the first step of the transport process has a negligible effect.

With $\hat{\Phi}$ specified, we rearrange Eq. (77), following the derivation in Sect. 2.1, to obtain the Laplace transform of the differential form of the master equation,

$$\frac{1-\tilde{g}(s)}{s\tilde{g}(s)}\left(s\tilde{p}_i-\delta_{i0}\right)=-(1-\alpha)\tilde{p}_i+\frac{\alpha}{2}\left(\tilde{p}_{i-1}-2\tilde{p}_i+\tilde{p}_{i+1}\right). \tag{79}$$

If $g(t)$ were a Poisson distribution of rate θ, this could be inverted to obtain

$$\frac{dp_i}{dt}=-\theta(1-\alpha)p_i+\frac{\alpha\theta}{2}\left(p_{i-1}-2p_i+p_{i+1}\right),$$

and this leads to an interpretation of $\alpha\theta/2$ as a discrete diffusivity and $\theta(1-\alpha)$ as a degradation rate.

However, $g(t)$ as defined via $F(t)$ is a more complex distribution whose explicit time-dependent form cannot be obtained analytically. Nonetheless, at leading order we may still approximate $g(t)$ by a Poisson distribution. To do so, we compute the Taylor expansion of $\tilde{g}(s)$ about $s=0$ up to first order as

$$\tilde{g}(s)\approx\tilde{g}(0)+\tilde{g}'(0)s=1-g'(0)s=\left(\int_0^\infty g(t)dt\right)-\left(\int_0^\infty tg(t)dt\right)s.$$

We then note that by equating this expansion with the first-order Taylor expansion of the Laplace transform of a Poisson distribution, we may approximate $g(t)$ by a Poisson distribution with rate $\theta=-1/\tilde{g}'(0)$. By the same Taylor expansion approach, we also see that $\alpha=\tilde{F}(0)$. With $\tilde{F}(s)$ as defined above, we see that

$$\begin{aligned}\alpha&=\frac{2D_{m,2}}{2D_{m,2}\cosh\left(\sqrt{\frac{\nu(0)}{D_{m,1}}}(L-\delta)\right)+\sqrt{\nu(0)D_{m,1}}\delta\sinh\left(\sqrt{\frac{\nu(0)}{D_{m,1}}}(L-\delta)\right)},\\ \theta&=\frac{2}{\left(\frac{(1-\eta)}{D_{m,2}}+\frac{\eta}{\eta D_{m,1}}\right)\left(\eta+(1-\eta)\nu'(0)\right)L^2}+\mathcal{O}(1)\end{aligned} \tag{80}$$

where

$$\nu(0)=k_+k_d/(k_d+k_-),\quad \nu'(0)=1+\frac{k_+k_m}{(k_d+k_-)^2}.$$

On a tissue-level scale, we are concerned with the evolution of p_i at length scales $L_\infty\gg L$: thus, we set $L=\epsilon L_\infty$. In the limit $\epsilon\to 0$, this leads to

$$(1-\alpha)\theta=\frac{(1-\eta)\nu(0)}{\eta+(1-\eta)\nu'(0)}=\frac{(1-\eta)k_dk_+(k_d+k_-)}{(k_d+k_-)^2+(1-\eta)k_-k_+}, \tag{81}$$

$$\alpha\theta = \frac{2}{\left(\frac{(1-\eta)}{D_{m,2}} + \frac{\eta}{\eta D_{m,1}}\right)(\eta + (1-\eta)\nu'(0))\,\epsilon^2 L_\infty^2}$$
$$= \frac{2}{\left(\frac{(1-\eta)}{D_{m,2}} + \frac{\eta}{D_{m,1}}\right)\left(\eta + (1-\eta)\left(1 + \frac{k_- k_+}{(k_d+k_-)^2}\right)\right)\epsilon^2 L_\infty^2}. \quad (82)$$

Furthermore, in this limit $p_i(t)$ can be treated as a function defined with respect to a continuous variable x (i.e. $p(x,t)$) since $\Delta X = X_i - X_{i-1} = \epsilon^2 L_\infty$ becomes very small compared to L_∞, the length scale of interest over the tissue. Noting that $1/(\epsilon^2 L_\infty^2)$ times the discrete Laplacian approaches the continuum Laplacian, we can write

$$\frac{\partial p(x,t)}{\partial t} = -\frac{(1-\eta)\nu(0)}{\eta + (1-\eta)\nu'(0)} p(x,t) + \frac{1}{\left(\frac{(1-\eta)}{D_{m,2}} + \frac{\eta}{D_{m,1}}\right)(\eta + (1-\eta)\nu'(0))} \frac{\partial^2 p(x,t)}{\partial x^2}$$
$$= -\left[\frac{(1-\eta)k_d k_+ (k_d + k_-)}{(k_d+k_-)^2 + (1-\eta)k_- k_+}\right] p(x,t)$$
$$+ \left[\frac{1}{\left(\frac{(1-\eta)}{D_{m,2}} + \frac{\eta}{D_{m,1}}\right)\left(\eta + (1-\eta)\left(1 + \frac{k_- k_+}{(k_d+k_-)^2}\right)\right)}\right] \frac{\partial^2 p(x,t)}{\partial x^2}$$
$$= -K_M p(x,t) + D_M \frac{\partial^2}{\partial x^2} p(x,t). \quad (83)$$

Thus the macroscale diffusion and degradation coefficients

$$K_M \equiv \frac{(1-\eta)k_d k_+ (k_d + k_-)}{(k_d+k_-)^2 + (1-\eta)k_- k_+}, \quad \text{and}$$
$$D_M \equiv \frac{1}{\left(\frac{(1-\eta)}{D_{m,2}} + \frac{\eta}{D_{m,1}}\right)\left(\eta + (1-\eta)\left(1 + \frac{k_- k_+}{(k_d+k_-)^2}\right)\right)} \quad (84)$$

are complex functions of the microscale parameters.

Furthermore, since there are more microscopic parameters than macroscale coefficients, there will be many combinations of the microscopic parameters that yield the same macroscopic parameters. Thus, if one attempts to fit data on the macroscale to a "standard" diffusion–degradation equation, the resulting diffusion and degradation coefficients cannot be interpreted as having simple meaning in terms of microscale processes. This presents a real challenge to those in the field, since it certainly seems possible that many microscale models could be adapted to macroscale diffusion–reaction equations as we have done here, but in each case, the macroscale diffusion and degradation coefficients are found as different functions of the microscale parameters.

In certain limits, the multiplicity is reduced somewhat. For example, if k_- and k_+ both tend to infinity at a fixed finite ratio $k_+/k_- = \beta$ (e.g., rapid equilibration of

diffusing and immobile species), the foregoing reduces to

$$K_M = \frac{k_d\beta(1-\eta)}{1+(1-\eta)\beta} \quad D_M = \frac{1}{(1+(1-\eta)\beta)\left[\frac{\eta}{D_{m,1}} + \frac{1-\eta}{D_{m,2}}\right]} \tag{85}$$

and there is one less microscopic parameter. In any case, if the microscale parameters can be perturbed, one can observe the macroscale behavior, and given the functional dependence of K_M and D_M on microscale parameters, this may prove to be a useful way of ascertaining whether a given model is plausible.

As an application of this analysis, we consider the model for Dpp transport in the Drosophila wing disk discussed in Kicheva et al. (2007). There D_M and K_M are estimated from FRAP data to be

$$D_M = 0.10 \pm 0.05 \mu m/s, \qquad K_M = 2.52 \times 10^{-4} \pm 1.29^{-4} s^{-1}.$$

The authors also note that there is a slow "irreversible" binding process, and an immobile fraction of 62.8% of all Dpp molecules. Since the microscale model has 6 unknown parameters—$D_{m,1}$, $D_{m,2}$, k_d, k_+, k_-, and η—but only three parameters—D_M, K_M, and the immobile fraction—were measured experimentally, there can be many combinations of the microscale parameters that yield the observed macroscale parameter values. In addition, a more complete description of the processes in Fig. 10 would introduce other microscopic processes and the attendant parameters, and make the problem of connecting macroscopic and microscopic parameters even more difficult. While parameter estimates from other contexts and limiting cases discussed earlier may be useful, further experiments are needed to connect the micro- and macroprocesses.

Finally, we see that by deriving the macroscale equation from a starting point that involves microscope-level details, assumptions that are needed for the validity of the macroscopic equation can be determined. For instance, in order to justify the limit $\epsilon \to 0$, it is necessary that sufficient time has elapsed so that the waiting time for a single jump between adjacent cells is small. Otherwise, the discrete nature of the system will dominate and the continuum description will not be appropriate.

6 The Hexagonal Lattice

In this section, we return to a discussion of spatially discrete CTRWs. The goal here is to formulate solutions in hexagonal lattices, which are topologically more complex. However, note that in some cases one can use the FPTs of continuum processes as WTDs for a discrete CTRW, as was done in the preceding section.

Hexagonal lattices are of particular importance since cells of many tissues tend to pack into a arrays that can be approximated by hexagonal grids. There are in fact two types of arrays that can be described in this context: those where transport occurs directly between neighboring, hexagonally shaped cells, and those in which transport occurs around the borders of such cells. The two topologies thus defined for the primary

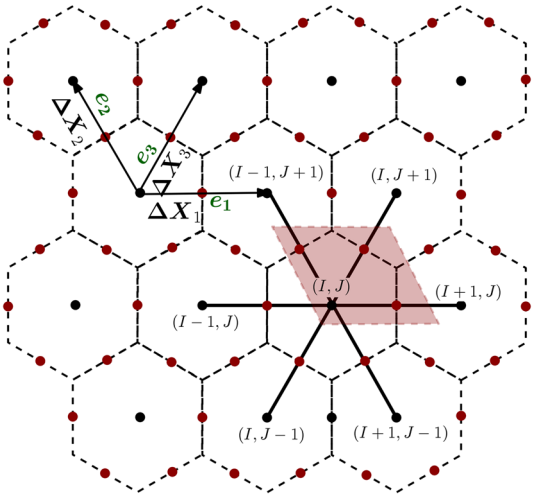

Fig. 11 Interior hexagon lattice that connects adjacent hexagon centers to one another. Each center is connected by an edge to six neighbors on adjacent edges. The vectors in the upper left show the displacements between adjacent junctions and the three types of edges are labeled as e_i. The red shaded region contains all junctions and SVs with the same index (I, J)

graphs lead to what we call the interior and exterior hexagonal lattice problems. They are related in the sense that the exterior lattice is the Voronoi diagram of the interior hexagonal lattice, and thus, the interior lattice is the Delaunay tessellation of the exterior lattice (Aurenhammer et al. 2013).

The interior lattice can be described as in Othmer and Scriven (1971) (see Fig. 11). Each junction is connected by a single edge to six adjacent junctions. The edges can be classified into three types distinguished by their orientation relative to the x-axis. In order to describe this connectivity, some labeling convention must be introduced that maps each lattice point to the edges it is linked to and each edge with the lattice points at which it terminates. One such convention is to assume that for each junction (labeled by $\boldsymbol{X}_{\boldsymbol{I}}$ with $\boldsymbol{I} = (I, J) \in \mathbb{Z}^2$), there are three edges (one of each type) with index $\boldsymbol{I}$ as well that connect to junction $\boldsymbol{I}$. As shown in Fig. 11, one can consistently label all lattice points and edges in this way. It turns out then, that junction $\boldsymbol{I}$ is connected to the three edges of label $\boldsymbol{I}$ and the type I (horizontal) edge of label $(I-1, J)$, the type II (vertical) edge of label $(I, J-1)$ and the type III (diagonal) edge of $(I-1, J-1)$. To make this consistent, it then must be the case that each edge of type I of label (I, J) is attached to lattice points (I, J) and $(I+1, J)$, and each edge of type II with label (I, J) is attached to junctions (I, J) and $(I, J+1)$. Finally, each type III edge of label (I, J) is attached to junctions (I, J) and $(I+1, J+1)$.

With this description of the geometry, let us consider an example that makes use of the interior lattice. Suppose that we have a hexagonal array of cells and some substance that can diffuse through the interior and can be transported through the boundaries of adjacent cells. Let us also assume that this substance can transiently enter an immobile state when on the cell boundaries. In a simple model, we can describe the key steps in the transport process in terms of a few waiting-time distributions. Let $\psi(t)$ be the WTD for the substance to diffuse through the cell and reach a boundary. Since this process involves diffusion within the cell, $\psi(t)$ must be considered here as a spatial average of waiting times for particles starting at different positions within the cell. Let

$\phi(t)$ be the WTD for a particle to be transported across the boundary to an adjacent cell, and $\chi(t)$ be the WTD for transitions to and from the immobile state which we will suppose only occurs on the boundary. This model can be thought of as having $n_k = 1$ (one boundary point between each adjacent pair of junctions) and $n_s = 2$ (a mobile and an immobile state). For simplicity, we will assume that all three WTDs (ψ, ϕ, and χ) are Poisson distributions with parameters λ, μ, and ξ resp. The objective is now to pose this problem in the framework of the earlier sections and solve for the probability distributions.

The matrix, $\boldsymbol{K\Lambda}$, from Equation (33) describes all internal state changes. For a single junction and set of edges, it can be written as

$$\boldsymbol{K\Lambda} = \begin{pmatrix} \boldsymbol{K}_J\boldsymbol{\Lambda}_J & \mathbf{0} & \mathbf{0} & \mathbf{0} \\ \mathbf{0} & \boldsymbol{K}_{SV}\boldsymbol{\Lambda}_{SV} & \mathbf{0} & \mathbf{0} \\ \mathbf{0} & \mathbf{0} & \boldsymbol{K}_{SV}\boldsymbol{\Lambda}_{SV} & \mathbf{0} \\ \mathbf{0} & \mathbf{0} & \mathbf{0} & \boldsymbol{K}_{SV}\boldsymbol{\Lambda}_{SV} \end{pmatrix}$$

where $\boldsymbol{K}_J\boldsymbol{\Lambda}_J$ describes internal state transitions at junctions, and $\boldsymbol{K}_{SV}\boldsymbol{\Lambda}_{SV}$ describes internal state transitions at SVs on each edge. Since the junctions are placed in the cell centers, transitions between mobile and immobile states inside the cell are described by $\boldsymbol{K}_J$. However, we have assumed that immobilization only occurs on the boundary, and therefore $\boldsymbol{K}_J$ is simply a 2×2 matrix of zeros. Transitions between internal states at SVs on each edge are described by $\boldsymbol{K}_{SV}$. There are two types of transitions that occur at an SV: 1) mobile to immobile and 2) immobile to mobile. Defining the probability of each state as $\boldsymbol{p} = (p_m, p_i)$ with m = mobile and i = immobile, $\boldsymbol{K}_{SV}$ can be written in matrix form as

$$\boldsymbol{K}_{SV}\boldsymbol{\Lambda}_{SV} = \begin{pmatrix} 0 & 1 \\ (1-f) & 0 \end{pmatrix} \begin{pmatrix} \phi & 0 \\ 0 & \chi \end{pmatrix} = \begin{pmatrix} 0 & \chi \\ (1-f)\phi & 0 \end{pmatrix}.$$

where $(1 - f)$ is the probability of transitioning to an immobile state.

The next step is to define the transition matrices $\boldsymbol{D}$, $\boldsymbol{D}'$, $\boldsymbol{T}_{SV}$ and describing spatial jumps between junctions and SVs and between adjacent SVs. Since there is only a single SV on each edge, all spatial jumps involve transitions between edges and junctions, thus $\boldsymbol{T}_{SV} = \mathbf{0}$. Furthermore, since the immobile state cannot change position, the rows of $\boldsymbol{D}$ and $\boldsymbol{D}'$ corresponding to the immobile state will be all zeros. Transitions from junctions to SVs are governed by ψ and are written in matrix form in terms of $\boldsymbol{D}'$. With $\boldsymbol{p} = (p_m, p_i)$ as above, we can write

$$\boldsymbol{D}' = \begin{pmatrix} \frac{1}{6}\psi & 0 \\ 0 & 0 \end{pmatrix}.$$

The factor of $1/6$ comes from the fact that each cell center is linked to 6 SVs, and each of them is equally likely to receive a particle from the cell center. In this case, since $n_k = 1$, the start and end SV on each edge coincide, and we do not need to distinguish between $\boldsymbol{D}'_s$ and $\boldsymbol{D}'_e$, or $\boldsymbol{D}_s$ and $\boldsymbol{D}_e$ as we did in Ex. 2. Since transitions from the cell membrane to the cell center are governed by WTD ϕ, $\boldsymbol{D}$ takes on a similar form with

ϕ in place of ψ. In particular,

$$\boldsymbol{D} = \begin{pmatrix} \frac{f}{2}\phi & 0 \\ 0 & 0 \end{pmatrix}.$$

The factor of $f/2$ accounts for the probability of particles *not* being immobilized, and that a mobile particle has a 50% chance of going to either of the junctions that the edge is connected to. This concludes the enumeration of all the transitions relevant on the edges and in the cell centers. What remains is to connect the current transition matrices with the topological structure of the hexagonal lattice, which is done via $\boldsymbol{A}_m$ and $\boldsymbol{A}'_m$.

Since $\boldsymbol{K}_J$ and $\boldsymbol{K}_{SV}$ do not involve changes of position, the relevant matrices for internal state changes over the entire lattice are formed by taking Kronecker products of these matrices with the lattice identity matrix, e.g., $\boldsymbol{I} \otimes \boldsymbol{K}_J$. The transitions in $\boldsymbol{D}$ and $\boldsymbol{D}'$ involve changes in position of the particles, and thus require non-trivial structural matrices. Generally, $\boldsymbol{A}_m$ and $\boldsymbol{A}'_m$ can be written as permutations of the identity matrix over the junctions. However, they can also be thought of as linear operators on the lattice points. In particular, for $m = 1, 2, 3$, define

$$\boldsymbol{A}_m(\boldsymbol{X}, \boldsymbol{X}') = \delta(\boldsymbol{X} - \boldsymbol{X}' - \boldsymbol{\Delta X}_m),$$

where $\delta(\cdot)$ is a Kronecker delta over the junctions, e.g., $\delta(\boldsymbol{X}) = 0$ for $\boldsymbol{X} \neq \boldsymbol{0}$ and 1 for $\boldsymbol{X} = \boldsymbol{0}$ where $\boldsymbol{X}$ is a lattice point in the hexagonal lattice. Similarly,

$$\boldsymbol{A}'_m(\boldsymbol{X}, \boldsymbol{X}') = \delta(\boldsymbol{X} - \boldsymbol{X}' + \boldsymbol{\Delta X}_m).$$

The displacements $\boldsymbol{\Delta X}_m$ are those depicted in Fig. 11. From geometric considerations, these are found as

$$\boldsymbol{\Delta X}_1 = (1, 0), \quad \boldsymbol{\Delta X}_2 = \left(\frac{1}{2}, \frac{\sqrt{3}}{2}\right), \quad \boldsymbol{\Delta X}_3 = \left(-\frac{1}{2}, \frac{\sqrt{3}}{2}\right). \tag{86}$$

Although $\boldsymbol{A}_m$ can also be written as matrices, in complicated problems it seems that the operator approach may be more intuitive since it reflects the problem geometry rather than a particular ordering of the degrees of freedom.

Putting all of the pieces together, we obtain the overall transition matrix $\boldsymbol{T}$. Let $\boldsymbol{q} = (\boldsymbol{q}_J, \boldsymbol{q}_{SV_1}, \boldsymbol{q}_{SV_2}, \boldsymbol{q}_{SV_3})$ be the probabilities for a particle starting in cell $(I_0, J_0) = (0, 0)$ to arrive in some other cell (I, J) at time t in the cell interior ($\boldsymbol{q}_J$) or at the portion of the cell membrane attributed to an edge of type i, ($\boldsymbol{q}_{SV_i}$). After Laplace

transformation, we write Eq. (33) for this system:

$$\begin{pmatrix} \tilde{\boldsymbol{q}}_J \\ \tilde{\boldsymbol{q}}_{SV_1} \\ \tilde{\boldsymbol{q}}_{SV_2} \\ \tilde{\boldsymbol{q}}_{SV_3} \end{pmatrix} = \begin{pmatrix} \delta(\boldsymbol{X}) \\ \boldsymbol{0} \\ \boldsymbol{0} \\ \boldsymbol{0} \end{pmatrix} + \boldsymbol{I} \otimes \left[\begin{pmatrix} \boldsymbol{K}_J \boldsymbol{\Lambda}_J & \boldsymbol{D} & \boldsymbol{D} & \boldsymbol{D} \\ \boldsymbol{D}' & \boldsymbol{K}_{SV} \boldsymbol{\Lambda}_{SV} & \boldsymbol{0} & \boldsymbol{0} \\ \boldsymbol{D}' & \boldsymbol{0} & \boldsymbol{K}_{SV} \boldsymbol{\Lambda}_{SV} & \boldsymbol{0} \\ \boldsymbol{D}' & \boldsymbol{0} & \boldsymbol{0} & \boldsymbol{K}_{SV} \boldsymbol{\Lambda}_{SV} \end{pmatrix} + \sum_{m=1}^{3} \left(\boldsymbol{A}_m \otimes \boldsymbol{D}_m + \boldsymbol{A}'_m \boldsymbol{D}'_m \right) \right] \begin{pmatrix} \tilde{\boldsymbol{q}}_J \\ \tilde{\boldsymbol{q}}_{SV_1} \\ \tilde{\boldsymbol{q}}_{SV_2} \\ \tilde{\boldsymbol{q}}_{SV_3} \end{pmatrix} \tag{87}$$

where

$$\boldsymbol{D}_m = \begin{pmatrix} . & \boldsymbol{D}\delta_{m,1} & \boldsymbol{D}\delta_{m,2} & \boldsymbol{D}\delta_{m,3} \\ . & . & . & . \\ . & . & . & . \\ . & . & . & . \end{pmatrix}, \quad \boldsymbol{D}'_m = \begin{pmatrix} . & \dots \\ \boldsymbol{D}'\delta_{m,1} & \dots \\ \boldsymbol{D}'\delta_{m,2} & \dots \\ \boldsymbol{D}'\delta_{m,3} & \dots \end{pmatrix},$$

with δ_{mn} the Kronecker delta concentrated at $m = n$.

To solve this infinite-dimensional matrix equation, we make use of a lattice Fourier transform to block-diagonalize the problem. For any function $f(\boldsymbol{X})$ defined over the lattice, the lattice Fourier transform is defined as

$$\hat{f}(\boldsymbol{\omega}) = \sum_{\boldsymbol{X} \in \mathscr{G}} e^{i\boldsymbol{X}\cdot\boldsymbol{\omega}} f(\boldsymbol{X}). \tag{88}$$

This definition holds whether $f(\boldsymbol{X})$ is scalar-, vector-, or matrix-valued. Since the space between junctions on a lattice is fixed, the maximum wave number that can be represented on the junctions is $\omega_{max} = (2\pi)/|\boldsymbol{\Delta X}|$ where $\boldsymbol{\Delta X}$ is the edge length. Additionally, on an infinite lattice, $\boldsymbol{\omega}$ is defined over a continuum with each element of $\boldsymbol{\omega}$ in the range $-\pi/\Delta X_i < \omega_i < \pi/\Delta X_i$. This differs from Fourier analysis of discretizations which are being refined, where $\boldsymbol{\Delta X}$ is not fixed. In those cases, the maximum wave number which can be represented by a lattice function increases as the discretization is refined.

Applying the lattice Fourier transform to the evolution to $\tilde{\boldsymbol{q}}$, we obtain an 8×8 system:

$$\begin{pmatrix} \hat{\boldsymbol{q}}_J \\ \hat{\boldsymbol{q}}_{SV_1} \\ \hat{\boldsymbol{q}}_{SV_2} \\ \hat{\boldsymbol{q}}_{SV_3} \end{pmatrix} = \begin{pmatrix} 1 \\ 0 \\ 0 \\ 0 \end{pmatrix} + \boldsymbol{I} \otimes \begin{pmatrix} \boldsymbol{K}_J & (1 + e^{-i\boldsymbol{\Delta X}_1 \cdot \boldsymbol{\omega}})\boldsymbol{D} & (1 + e^{-i\boldsymbol{\Delta X}_2 \cdot \boldsymbol{\omega}})\boldsymbol{D} & (1 + e^{-i\boldsymbol{\Delta X}_3 \cdot \boldsymbol{\omega}})\boldsymbol{D} \\ (1 + e^{i\boldsymbol{\Delta X}_1 \cdot \boldsymbol{\omega}})\boldsymbol{D}' & \boldsymbol{K}_{SV} & 0 & 0 \\ (1 + e^{i\boldsymbol{\Delta X}_2 \cdot \boldsymbol{\omega}})\boldsymbol{D}' & 0 & \boldsymbol{K}_{SV} & 0 \\ (1 + e^{i\boldsymbol{\Delta X}_3 \cdot \boldsymbol{\omega}})\boldsymbol{D}' & 0 & 0 & \boldsymbol{K}_{SV} \end{pmatrix}$$

$$\begin{pmatrix} \hat{\boldsymbol{q}}_J \\ \hat{\boldsymbol{q}}_{SV_1} \\ \hat{\boldsymbol{q}}_{SV_2} \\ \hat{\boldsymbol{q}}_{SV_3} \end{pmatrix}.$$

This matrix equation can be solved directly, but can be slightly simplified. First, $\boldsymbol{K}_J = \boldsymbol{0}$, and second, the immobile state associated with $\hat{\boldsymbol{q}}_J$ has no transitions to or from any other states, and thus can be removed to yield a 7×7 system.

The solution here yields $\hat{\boldsymbol{q}}$ from Eq. (33). However, the most important quantity is typically $\boldsymbol{p}(\boldsymbol{X}, t)$, the probability of being located at $\boldsymbol{X}$ at time t. Inversion of the Fourier and Laplace transforms is often only feasible numerically, but the solution for $\hat{\boldsymbol{p}}(\boldsymbol{\omega}, s)$ is possible once we have found $\hat{\tilde{\boldsymbol{\Phi}}}$ defined in Eq. (34). After Fourier and Laplace transform, one can show that the nonzero entries are

$$\hat{\boldsymbol{\Phi}}_{k,\ell}(s) = \frac{1}{s}\left(1 - \boldsymbol{1}^T \boldsymbol{K}\boldsymbol{\delta}_{k,\ell} - \boldsymbol{1}^T \hat{\boldsymbol{T}}(\boldsymbol{\omega} = \boldsymbol{0}, s)\boldsymbol{\delta}_{k,\ell}\right). \tag{89}$$

In this example, after simplifying (89), we obtain diagonal entries:

$$\hat{\boldsymbol{\Phi}} = \operatorname{diag}\left(\tfrac{1}{\lambda+s}\ \tfrac{1}{\mu+s}\ \tfrac{1}{\xi+s}\ \tfrac{1}{\mu+s}\ \tfrac{1}{\xi+s}\ \tfrac{1}{\mu+s}\ \tfrac{1}{\xi+s}\right)$$

Finally, we may solve (33) for $\boldsymbol{p}$. The exact solutions may be found using Mathematica's symbolic solver; however, it is often useful to obtain simpler summary statistics that describe the distribution. Here we give one sample that is straightforward to compute. The proportion of particles in the cell centers can be found by summing $\boldsymbol{p}_c$ over the junctions. In Fourier space,

$$\sum_{\boldsymbol{X}} p_c(\boldsymbol{X}, t) = \lim_{\boldsymbol{\omega}\to\boldsymbol{0}} \hat{p}_c(\boldsymbol{\omega}, t).$$

Applying this result to our solution in the Laplace domain,

$$\lim_{\boldsymbol{\omega}\to\boldsymbol{0}} \hat{p}_c(\boldsymbol{\omega}, s) = \frac{1}{s}\frac{2s(\xi+s) + \mu(\xi+2s)}{2s(\xi+s) + \mu(\xi+2s) + \lambda(\mu+2(\xi+s))}$$

The steady-state limit may be found using the Laplace transform final value theorem (Bracewell et al. 1986) as

$$\lim_{s\to 0} sp(\boldsymbol{0}, s) = \frac{\mu\xi}{\mu\xi + \lambda\mu + 2\lambda\xi}.$$

We can observe how this compares with the steady-state probabilities, $p_{c,ss}$, reported for a segment in Ex. 2. We see here that the analogous result is obtained when $\xi \to \infty$,

$$p_{c,ss} = \frac{\mu}{\mu + 2\lambda},$$

or, in other words, when mobilization (unbinding) occurs rapidly compared to the other transitions. However, because of the hexagonal topology, in that case even though there is only a single SV per edge, the denominator has 2λ rather than λ as it would for the 1D case. This same result is observed for a square lattice with a single SV and the same immobilization/mobilization transition at that SV.

A key point here is that by describing a complicated transport process in terms of fundamental steps, we found results that reflect how macroscale observables, here the steady-state solution, depend on microstructural mechanisms. Next, we turn to computation of the mean and variance of the hexagonal lattice problem.

6.1 The Moments for Transport in the Hexagonal Lattice

For the interior hexagonal lattice in Fig. 11, let us assume that a particle starts inside a cell (that is, on a junction). Then we may use Eq. (C.7) to find the first moment of the transport process, which due to the symmetry of this problem should be zero. This fact is confirmed upon computation.

The second moment, found by using Eq. (C.9), is nonzero. In order to compute this result, we must specify how each internal state and each SV are positioned relative to the junction that shares the same index, (I, J). To determine this, we use $\boldsymbol{\Delta X}_i$ from above, and note that the SVs are located precisely halfway along each edge. This gives us sufficient information to compute $\boldsymbol{x}$ for each SV and internal state. All that remains is to apply Eq. (C.9) and substitute each term with one specific to the hexagonal lattice system at hand. The large-t asymptotic result for the second moment is

$$m^{(2)}(t) = \frac{\lambda\mu f\xi t}{4\left(f\mu\xi + \lambda((1-f)\mu + \xi)\right)}$$

for both x-direction transport and y-direction transport. The moments for particles to be in the mobile or immobile state can easily be found by summing over the degrees of freedom associated with the mobile or immobile states.

Recall that λ, μ, and ξ are the rate constants associated with diffusion, boundary binding, and immobilization. Thus, we see that if mobilization/immobilization happens rapidly compared to diffusion and binding, e.g., that $\xi \to \infty$, then

$$m^{(2)}(t) = \frac{\lambda\mu f t}{4\left(f\mu + \lambda\right)}.$$

Similarly, if diffusion is very rapid compared to binding and immobilization, then $\lambda \to \infty$ and

$$m^{(2)}(t) = \frac{\mu\xi f t}{4((1-f)\mu + \xi)}.$$

If binding is very rapid compared to immobilization and diffusion, $\mu \to \infty$ and

$$m^{(2)}(t) = \frac{\lambda\xi f t}{4(f\xi + (1-f)\lambda)}.$$

Finally, if binding is rapid compared with diffusion and very little immobilization occurs, e.g., $f = 1$, we obtain

$$m^{(2)}(t) = \frac{\lambda t}{4}$$

independent of ξ. This is the result for pure diffusion in this lattice structure.

For the exterior hexagonal lattice, the local displacements are found by similar calculations since $\boldsymbol{\Delta X}_i$ are equivalent to those for the interior lattice. The details are described in "Appendix B". In that case, consider an initial condition with a particle at junction $\boldsymbol{X} = \mathbf{0}$. This condition leads to a first moment equal to zero, and the asymptotic second moment is found using Eq. (C.9):

$$m^{(2)}(t) = \frac{\lambda \mu f \xi t}{12\left(f\mu\xi + \lambda((1-f)\mu + \xi)\right)}.$$

Remark 1 Note that the scale factors $1/4$ and $1/12$ corresponds to the case that $\boldsymbol{\Delta X}_i$ are the same length for the interior and exterior lattices (see Fig. 11). However, in the exterior hexagonal lattice with $n_k = 1$, the length of each jump is $1/\sqrt{3}$ times the length of each jump in the interior lattice. In a diffusive process, the average time $\bar{t}$ required to travel a distance $\bar{x}$ scales quadratically, e.g., $D\bar{t} \sim \bar{x}^2$. If one rescales λ, μ, and ξ in the exterior lattice by a factor of 3 to account for shorter distances, one obtains precisely the result on the interior lattice. However, the rescaling we have supposed is only sensible for μ and λ. The coefficient, ξ was not hypothesized to depend on diffusion, but instead is a kinetic immobilization rate constant. Thus, although there may be some analogies between transport on interior and exterior hexagonal lattices, there are situations where the analogy breaks down.

Remark 2 In general, the second moment and the variance can differ since the variance involves both the first and second moment as

$$\sigma^2(t) = m^{(2)}(t) - \left(m^{(1)}(t)\right)^2.$$

This distinction is especially important in biased CTRWs (Shlesinger 1974; Othmer et al. 1988); however, when the transport is unbiased, then $m^{(1)}(t) = 0$ and the variance and second moment are equal.

Remark 3 With the use of first-passage-times, the moment calculation can be simplified somewhat. Rather than needing to handle details about the positions of SVs relative to each other, FPTs can be used to reduce this system to a single-state CTRW (for the junctions). Of course, collapsing all the information about the local geometry leads to a slight approximation; however, if the timescales of interest are larger than λ, μ, and ξ, the approximation will be accurate.

7 Conclusion

Transport processes in complex media such as biological tissues often involve several sub-processes that play a crucial role in setting the experimental data, and without incorporating the microscopic processes, macroscopic models may shed little light on the meaning of the data. As evidenced by the example involving transport in the wing disk, the macroscopic coefficients have detailed information embedded in them, and interpretation of the experimental data must be based on the microscopic processes. However, the complexity of the geometry in tissues often makes it difficult to do this using continuum reaction–diffusion equations. For example, developing an analytically tractable model of transport, binding, and degradation of Dpp in the cells and extracellular space of the wing disk is nigh impossible, but as we have shown herein, approaching this problem from a graph-based model of the geometry, coupled to a discrete description of spatial and internal states of a walker, enables one to obtain the coefficients of a macroscopic reaction–transport model based on the underlying microscopic processes. Our analysis is based on lattices in which all junctions have the same degree, all edge lengths are equal, and the lattice is infinite, which allows the use of Fourier transforms to analyze the resulting equations, but the incorporation of secondary vertices along edges and internal states of the walkers provides the means for describing several levels of microstructure in the models. In this description, the extracellular space in the wing disk is approximated by the set of edges in a graph, which simplifies the description, and while this does not capture all the details of the underlying structure, it is a significant step toward "lifting" microscopic information to a macroscopic description.

One potential complication is that microscale models are often difficult to define, and are not necessarily "better" or "worse" than an ad hoc macroscale model. However, when there is uncertainty about the macroscale model, understanding how microscale details eventually coalesce into readily observable macroscale behavior may help to separate promising theories from specious ones. In the wing disk, there are many experimental tools available to perturb various cellular-level biochemical and mechanical cues that are involved in normal growth and development. By perturbing these microscale parameters through genetic modifications or other means, and observing the resulting Dpp distribution, one can determine how K_M and D_M should depend on those parameters. These results can then be compared with the K_M and D_M determined via the methods presented here to assess whether the model is sensible. For instance, it is not immediately obvious that D_M in Eq. (84) should depend on the degradation rate, k_d, but retrospectively this is easily explained: rapid degradation will rapidly remove immobile particles leading to a larger proportion of mobile particles. This increases the macroscale diffusivity and the macroscale degradation coefficient.

Several previous studies (Goldhirsch and Gefen 1986, 1987) have presented ideas related to the development here with regard to compressing degrees of freedom in a random walk and computing moments. However, in those investigations the internal states consisted only of discrete spatial positions within various blocks making up a larger network. Neither the continuous-time aspects, nor the multistate aspects were studied. Moments of multistate random walks were also in Landman and Shlesinger (1979b), Landman and Shlesinger (1979a), Roerdink and Shuler (1985b), Roerdink

and Shuler (1985a), Scher and Wu (1981), and Gadgil et al. (2005). Here we have extended the approaches in these studies and have shown how to systematically work with multistate systems that would be quite cumbersome to deal with in the frameworks developed previously. We have also shown how the theory developed in Othmer and Scriven (1971) can be applied to random processes that are not locally homogeneous.

The connection between micro- and macroscale properties is also extensively studied in homogenization theory (Pavliotis and Stuart 2008) and renewal theory (Cox 1967). In fact many of the problems we analyzed can be posed as systems of renewal equations, and some recent results have been obtained regarding the derivation of macroscale transport coefficients (Ciocanel et al. 2020). One difference between our method and classically homogenization theory is in the type of approximation used to extract the macroscale dynamics. In classical homogenization theory, one often *begins* by assuming an *ansatz* of the form

$$p_\epsilon(t, x, x/\epsilon, \dots) = \sum_{i=0}^{\infty} \epsilon^i \, p_i(t, x, x/\epsilon, \dots)$$

and then obtaining limiting equations as $\epsilon \to 0$. In a number of cases, this process has been rigorously verified. On the other hand, it is not true in all cases that the *ansatz* is valid, or frequently, the presence of boundary layers means that the expansion is only valid up to low order. In contrast, with our method, the asymptotic limit only need be considered in the last step of our method after deriving first-passage-time distributions which preserve the exact internal dynamics.

Finally, in this study we primarily considered examples in which the local state space of the random walk was discrete in nature, even when infinitely many states existed, such as in the comb problem. In a sequel, to this paper we will develop a detailed continuum computational model of the wing disk, which will enable us to compare predictions made herein with a microscopic continuum description. In effect, we will be able to model the time evolution of the Dpp distribution in the disk and determine in what parameter regimes the macroscopic parameters determined from the graph-based model coincide with those of the continuum model. It will also enable us to study variations in cell size and other factors that may affect morphogen distributions, and to determine when such problems can be reduced to lattice-based random walks by solving for certain continuum first-passage-time distributions.

Acknowledgements Supported in part by NIH Grants # GM29123 and 54-CA-210190 and NSF Grants DMS # 178743 and 185357.

Appendix A: Definition of the Kronecker Product

We define the tensor product of vectors as

$$\mathbf{x} \otimes \mathbf{y} \equiv (x_1\mathbf{y}, \dots, x_N\mathbf{y})^T = (x_1 y_1, \dots, x_1 y_n \dots, x_N y_1, \dots, x_N y_n)^T,$$

and if $\mathbf{R}$ is an $N \times N$ matrix and $\mathbf{T}$ an $n \times n$ one, their tensor product is the $Nn \times Nn$ matrix

$$\mathbf{R} \otimes \mathbf{T} = \begin{bmatrix} R_{11}T & \dots & R_{1N}T \\ \cdot & & \cdot \\ \cdot & & \cdot \\ \cdot & & \cdot \\ R_{N1}T & \dots & R_{NN}T \end{bmatrix}.$$

As we have seen throughout, multistate random walks can be conveniently written as matrix–vector problems involving Kronecker products. An important property of matrices and vectors formed as Kronecker products is that one can compute Fourier transforms on the first and second terms of the Kronecker product separately. For instance if $\boldsymbol{F}$ is a discrete Fourier transform matrix with Hermitian adjoint $\boldsymbol{F}'$,

$$(\boldsymbol{F} \otimes \boldsymbol{I})(\boldsymbol{A} \otimes \boldsymbol{B})\left(\boldsymbol{F}' \otimes \boldsymbol{I}\right) = \boldsymbol{F}\boldsymbol{A}\boldsymbol{F}' \otimes \boldsymbol{B} = \tilde{\boldsymbol{A}} \otimes \boldsymbol{B}.$$
$$(\boldsymbol{I} \otimes \boldsymbol{F})(\boldsymbol{A} \otimes \boldsymbol{B})\left(\boldsymbol{I} \otimes \boldsymbol{F}'\right) = \boldsymbol{A} \otimes \boldsymbol{F}\boldsymbol{B}\boldsymbol{F}' = \boldsymbol{A} \otimes \tilde{\boldsymbol{B}}.$$

Kronecker products provide an easy way to describe certain multidimensional problems in terms of simpler one-dimensional problems (Othmer and Scriven 1971). Each additional dimension is, roughly speaking, included by appending an additional Kronecker product to the previous transition matrix. This also applies in cases where the dimension of the state space is increased by adding internal state transitions to a spatial jump process.

Appendix B: The Exterior Hexagonal Lattice

In an exterior hexagonal lattice, there are three orientations of edges that occur, and two types of junctions: those centered at upwards facing trijunctions (type I), and those at downwards facing trijunctions (type II), see Fig. 12. Let us assume here that $\boldsymbol{T}_{SV}$ and $\boldsymbol{K}_{SV}$ are the same for each edge, and that $\boldsymbol{K}_J$ is the same for all junctions. Likewise we assume that $\boldsymbol{D}_s$, $\boldsymbol{D}_e$, $\boldsymbol{D}'_e$, and $\boldsymbol{D}'_s$ do not vary depending on the edge or junction being considered.

With two types of junctions that alternate, an easy way of assigning which edges start or end at which junctions is to require that all edges start at a type I junction and end at a type II junction (see the edges labeled "e" and "s" in Fig. 12). It is also helpful to specify some type of labeling system on the junctions and edges. To do so, we consider the combination of three edges around a type I vertex, and the type II junction attached at the end of the vertical edges to be labeled with the same label, (I, J) (see Fig. 12). The lattice position associated with this structure is given as $\boldsymbol{X}$, the position of the type I vertex. Of course, the positions of each SV on an edge can be found as some displacement, $\boldsymbol{x}$ from $\boldsymbol{X}$.

With this description, type I edges are vertical edges that pair type I and type II points with the same lattice index, e.g., $\boldsymbol{\Delta I}_1 = \boldsymbol{0}$. Type II edges are diagonal edges that pair type I lattice points and type II lattice points that differ with $\boldsymbol{\Delta I}_2 = (0, -1)$ from

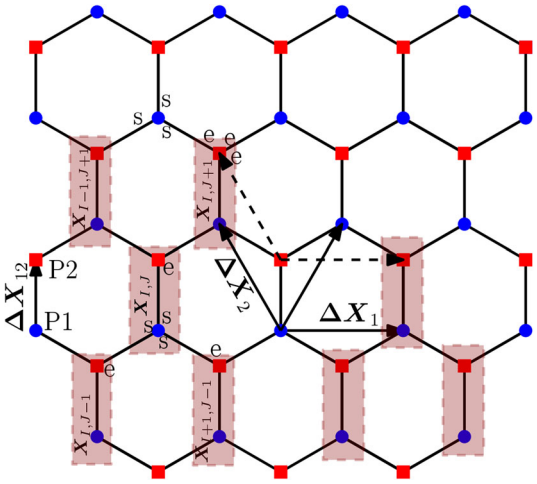

Fig. 12 Geometric quantities associated with the hexagonal lattice are depicted. Blue points are type I and Red points are type II. The quantity $\boldsymbol{\Delta X}_{12}$ is the displacement vector between a type I and type II point, and $\boldsymbol{\Delta X}_1$, $\boldsymbol{\Delta X}_2$, and $\boldsymbol{\Delta X}_3$ represent lattice displacement vectors between adjacent cells on the lattice. The red boxes indicate pairs of type I and type II points with the same lattice index, (I, J). The labels "s" and "e" indicate the starts and ends of edges

start to end. Finally, type III edges pair type I and type II points with $\boldsymbol{\Delta I}_3 = (1, -1)$ from start to end.

Since type I points are attached to the start of each edge and type II to the end of each edge, if we structure the probability density vector as $\boldsymbol{p} = (\boldsymbol{p}_I, \boldsymbol{p}_{II}, \boldsymbol{p}_{e_1}, \boldsymbol{p}_{e_2}, \boldsymbol{p}_{e_3})^T$, we may write the overall transition matrix $\boldsymbol{T} + \boldsymbol{K}$ as

$$\begin{aligned}\boldsymbol{T}+\boldsymbol{K} = \boldsymbol{I} \otimes &\left(\begin{array}{cc|ccc} \boldsymbol{K}_J & \boldsymbol{0} & \boldsymbol{D}_s & \boldsymbol{D}_s & \boldsymbol{D}_s \\ \boldsymbol{0} & \boldsymbol{K}_J & \boldsymbol{D}_e & \boldsymbol{0} & \boldsymbol{0} \\ \hline \boldsymbol{D}'_s & \boldsymbol{D}'_e & \boldsymbol{T}_{SV}+\boldsymbol{K}_{SV} & \boldsymbol{0} & \boldsymbol{0} \\ \boldsymbol{D}'_s & \boldsymbol{0} & \boldsymbol{0} & \boldsymbol{T}_{SV}+\boldsymbol{K}_{SV} & \boldsymbol{0} \\ \boldsymbol{D}'_s & \boldsymbol{0} & \boldsymbol{0} & \boldsymbol{0} & \boldsymbol{T}_{SV}+\boldsymbol{K}_{SV} \end{array}\right) \\ &+ \boldsymbol{A}_{e,1} \otimes \left(\begin{array}{c|ccc} \boldsymbol{0} & \boldsymbol{0} & \boldsymbol{0} & \boldsymbol{0} \\ \hline \boldsymbol{0} & \boldsymbol{0} & \boldsymbol{D}_e & \boldsymbol{0} \end{array}\right) + \boldsymbol{A}^T_{e,1} \otimes \left(\begin{array}{c|ccc} \boldsymbol{0} & \boldsymbol{0} & \boldsymbol{0} & \boldsymbol{0} \\ \hline \boldsymbol{0} & \boldsymbol{0} & \boldsymbol{0} & \boldsymbol{0} \\ \boldsymbol{0} & \boldsymbol{0} & \boldsymbol{D}'_e & \boldsymbol{0} \end{array}\right) \\ &+ \boldsymbol{A}_{e,2} \otimes \left(\begin{array}{c|ccc} \boldsymbol{0} & \boldsymbol{0} & \boldsymbol{0} & \boldsymbol{0} \\ \hline \boldsymbol{0} & \boldsymbol{0} & \boldsymbol{0} & \boldsymbol{D}_e \end{array}\right) + \boldsymbol{A}^T_{e,2} \otimes \left(\begin{array}{c|ccc} \boldsymbol{0} & \boldsymbol{0} & \boldsymbol{0} & \boldsymbol{0} \\ \hline \boldsymbol{0} & \boldsymbol{0} & \boldsymbol{0} & \boldsymbol{0} \\ \boldsymbol{0} & \boldsymbol{0} & \boldsymbol{0} & \boldsymbol{D}'_e \end{array}\right)\end{aligned} \tag{B.1}$$

We apply a lattice Fourier transformation to $\boldsymbol{X}$ to obtain

$$\hat{\boldsymbol{T}}(\boldsymbol{\omega}) + \boldsymbol{K} = \boldsymbol{I} \otimes \left(\begin{array}{cc|ccc} \boldsymbol{K}_J & \boldsymbol{0} & \boldsymbol{D}_s & \boldsymbol{D}_s & \boldsymbol{D}_s \\ \boldsymbol{0} & \boldsymbol{K}_J & \boldsymbol{D}_e & e^{i\boldsymbol{\Delta X}_2\cdot\boldsymbol{\omega}}\boldsymbol{D}_e & e^{i\boldsymbol{\Delta X}_3\cdot\boldsymbol{\omega}}\boldsymbol{D}_e \\ \hline \boldsymbol{D}'_s & \boldsymbol{D}'_e & \boldsymbol{T}_{SV}+\boldsymbol{K}_{SV} & \boldsymbol{0} & \boldsymbol{0} \\ \boldsymbol{D}'_s & e^{-i\boldsymbol{\Delta X}_2\cdot\boldsymbol{\omega}} & \boldsymbol{0} & \boldsymbol{T}_{SV}+\boldsymbol{K}_{SV} & \boldsymbol{0} \\ \boldsymbol{D}'_s & e^{-i\boldsymbol{\Delta X}_3\cdot\boldsymbol{\omega}}\boldsymbol{D}'_e & \boldsymbol{0} & \boldsymbol{0} & \boldsymbol{T}_{SV}+\boldsymbol{K}_{SV} \end{array}\right) \tag{B.2}$$

where $\boldsymbol{\Delta X}_m$ are as defined in Eq. (86). Once the local transitions in $\boldsymbol{K}_J$, $\boldsymbol{K}_{SV}$, $\boldsymbol{T}_{SV}$, $\boldsymbol{D}_m$, and $\boldsymbol{D}'_m$ are specified, substituting this matrix into Eq. (33) and solving for $\boldsymbol{q}$ and $\boldsymbol{p}$ will yield a solution for the spatial distribution of a particle over the hexagonal lattice with possible internal states and SVs between junction points. If we make use

of the same definitions for $\boldsymbol{D}$, $\boldsymbol{D}'$, $\boldsymbol{T}_{SV}$, $\boldsymbol{K}_{SV}$ and $\boldsymbol{K}_J$ from the interior lattice example in Sect. 6, with $n_k = 1$ and $n_s = 2$, we obtain a 8×8 matrix (after removing the rows and columns associated with immobile states at the junctions as in Sect. 6) that can be inverted to solve for $\boldsymbol{p}$ in Fourier–Laplace transform space. For instance, with $1 - f$ the proportion of particles that are immobilized at the boundary, the steady-state concentration at the junctions can be found as

$$\lim_{\boldsymbol{\omega}\to\boldsymbol{0}} \lim_{s\to 0} s\left(p_I(\boldsymbol{\omega}, s) + p_{II}(\boldsymbol{\omega}, s)\right) = \frac{f\mu\xi}{f\mu\xi + d((1-f)\mu + \xi)}.$$

In closing this section, we note that random walks on exterior hexagonal lattices have been studied several times previously (Montroll 1969; Hughes 1996; Henyey and Seshadri 1982); however, in those cases, no internal states were considered. Thus, our formulation here provides a straightforward way to extend these previous results to more complicated transport processes. We also note that the lattice Green's function for the exterior hexagonal lattice with no internal states or SVs is known (Henyey and Seshadri 1982; Hughes 1996). In Fourier transform space, the Green's function for a hexagonal lattice where each edge is taken in one step, and the transition probabilities at each intersection are all 1/3, is of the form

$$\boldsymbol{p}^{(H)}(\boldsymbol{\omega}, z) = \frac{\begin{pmatrix} 1 & \frac{z}{3}\left(1 + e^{i\boldsymbol{\Delta X}_2\cdot\boldsymbol{\omega}} + e^{i\boldsymbol{\Delta X}_3\cdot\boldsymbol{\omega}}\right) \\ \frac{z}{3}\left(1 + e^{-i\boldsymbol{\Delta X}_2\cdot\boldsymbol{\omega}} + e^{-i\boldsymbol{\Delta X}_3\cdot\boldsymbol{\omega}}\right) & 1 \end{pmatrix}}{1 - \frac{z^2}{9}\left(3 + 2\cos\omega_x + 4\cos\left(\frac{\omega_x}{2}\right)\cos\left(\frac{\sqrt{3}\omega_y}{2}\right)\right)} \tag{B.3}$$

Of course, when we set $n_k = 1$, $n_s = 1$, and replace $\psi(t)$ with z in Eq. (B.2), we would obtain this result. The ij^{th} element of $\boldsymbol{p}^H$ gives the occupation probability for a random walk that started on a type j vertex and is currently on a type i vertex.

Our result here appears to differ slightly from the previous results for this Green's function. This because we have directly included the displacement, $\boldsymbol{\Delta X}_i$ into the computation, rather than just using changes in index $\boldsymbol{\Delta I}_i$, which yield precisely the result previously reported. In other words, Eq. (B.3) gives the probability of being located at position $\boldsymbol{X}_{\boldsymbol{I}}$, whereas previous results give the probability of being located at index $\boldsymbol{I}$.

B.1 The Exterior Hexagonal Lattice with Arbitrary n_k

Here, we consider the hexagonal lattice with n_k SVs and $n_s = 1$. The FPT method from Sect. 4.1 becomes essential here as with arbitrary n_k, directly solving the resulting matrices is non-trivial.

From Appendix B, we found that the form of $\hat{\boldsymbol{T}}(\boldsymbol{\omega})+\hat{\boldsymbol{K}}(\boldsymbol{\omega})$ for the exterior hexagonal lattice. In this example, $n_s = 1$, so $\boldsymbol{K}_{SV} = \boldsymbol{K}_J = \boldsymbol{0}$. We also have that

$$\begin{aligned} \boldsymbol{D}_s &= \frac{\psi}{2}\begin{pmatrix}1\ 0\ \dots\ 0\end{pmatrix} \\ \boldsymbol{D}_e &= \frac{\psi}{2}\begin{pmatrix}0\ \dots\ 0\ 1\end{pmatrix} \end{aligned} \tag{B.4}$$

and

$$\boldsymbol{D}'_s = \frac{\psi}{3}\begin{pmatrix}1\\0\\\vdots\\0\end{pmatrix}, \quad \boldsymbol{D}'_e = \frac{\psi}{3}\begin{pmatrix}0\\\vdots\\0\\1\end{pmatrix}.$$

Lastly, $\boldsymbol{T}_{SV}$ is the matrix for a 1D random walk on a segment of length n_k with absorbing boundaries. This can be written as

$$\boldsymbol{T}_{SV} = \frac{\psi}{2}\begin{pmatrix} 0 & 1 & 0 & \dots & & & \\ 1 & 0 & 1 & 0 & \dots & & \\ 0 & 1 & 0 & 1 & 0 & \dots & \\ \vdots & & \ddots & \ddots & \ddots & 0 & \dots \\ 0 & & \dots & 0 & 1 & 0 & 1 \\ 0 & \dots & & & 0 & 1 & 0. \end{pmatrix}$$

Since there is one internal state, $\boldsymbol{K}_{SV} = \boldsymbol{0}$. Since each edge has the same $\boldsymbol{T}_{SV}$, $\boldsymbol{D}$ and $\boldsymbol{D}'$, we may use the formulation in Appendix D.2 to obtain the effective transition rates, $\boldsymbol{T}^{\text{eff}}_{2,r}$.

To do so, start by noting that since $n_s = 1$, $\boldsymbol{T}^{\text{eff}}_{1,r}$ and $\boldsymbol{K}_r$ are both equal to 0 and $\boldsymbol{T}^{\text{eff}}_{2,r}$ is a scalar-valued function. Since the type I and type II junctions are equivalent in terms of the transitions that occur around them, $\boldsymbol{T}^{\text{eff}}_{2,r}$ is found independent of whether the particle is at a type I or type II junction.

This leaves us with the following matrix equation:

$$\left(\begin{pmatrix}1&0&0&\dots\\0&1&0&\dots\\\vdots&&\ddots&\\0&\dots&&1\end{pmatrix} - \begin{pmatrix}0 & \left(\frac{\psi}{2}\ 0\ \dots\right)\\ \begin{pmatrix}\psi\\0\\\vdots\end{pmatrix} & \boldsymbol{T}_{SV}\end{pmatrix}\right)\begin{pmatrix}\tilde{f}_1\\\tilde{f}_2\\\vdots\\\tilde{f}_{n_k}\end{pmatrix} = \begin{pmatrix}1\\0\\\vdots\\0\end{pmatrix}$$

for $\tilde{f}(s)$. Solving for $\tilde{f}_1$ via a Schur complement yields,

$$\tilde{f}_1 = 1 - 3\boldsymbol{D}_s(\boldsymbol{I} - \boldsymbol{T}_{SV})^{-1}\boldsymbol{D}_s,$$

and the remaining elements of $\tilde{\boldsymbol{f}}$ are found as

$$\tilde{\boldsymbol{f}} = \frac{(\boldsymbol{I} - \boldsymbol{T}_{SV})^{-1}\boldsymbol{D}_s'}{\tilde{f}_1}.$$

Finally,

$$\boldsymbol{T}_{2,r}^{\text{eff}} = \boldsymbol{D}_e\tilde{\boldsymbol{f}} = \frac{\boldsymbol{D}_e(\boldsymbol{I} - \boldsymbol{T}_{SV})^{-1}\boldsymbol{D}_s'}{1 - 3\boldsymbol{D}_s'(\boldsymbol{I} - \boldsymbol{T}_{SV})^{-1}\boldsymbol{D}_s} = \frac{\psi}{2}\tilde{f}_{n_k}.$$

The next step is of course to explicitly solve for this FPT. Since each edge of the lattice is simply a 1D segment with absorbing boundaries, the discussion in Appendix E provides us with an explicit form of the solution to $(\boldsymbol{I} - \boldsymbol{T}_{SV})^{-1}$. After some algebraic simplifications, we find that

$$\boldsymbol{T}_{2,r}^{\text{eff}} = \frac{2}{3}\frac{1}{\left(\frac{1-\sqrt{1-\psi^2}}{\psi}\right)^{n_k+1} + \left(\frac{1-\sqrt{1-\psi^2}}{\psi}\right)^{-n_k-1}}$$

Since $\boldsymbol{K} = 0$ and $\boldsymbol{T}_{1,r}^{\text{eff}} = 0$, this reduces the problem to a single-state CTRW on a hexagonal lattice. Thus, we can make use of formula in Eq. (B.3) with z replaced by $\psi^{\text{eff}} = 3\boldsymbol{T}_{2,r}^{\text{eff}}$. The factor of 3 comes from the fact that $\boldsymbol{T}_{2,r}^{\text{eff}}$ is in fact the effective waiting time distribution multiplied by the probability that the particle actually travels down a particular edge. This probability is 1/3 since each junction connects three edges in the exterior hexagonal lattice, and each edge has the same probability of being traveled on.

With this result, it is possible to directly compute the moments for the hexagonal lattice with n_K SVs. However, assuming each segment has a fixed total length of 1 independent of n_k, the exact formulas become

$$\tilde{m}^{(1)}(s) = 0$$
$$\tilde{m}^{(2)}(s) = \frac{1-\psi^{\text{eff}}}{s}\frac{\psi^{\text{eff}}}{2(1-\psi)^2} = \frac{1}{s}\frac{1-\psi^{\text{eff}}}{(a^{n_k+1} + a^{-n_k-1}) + 4\frac{1}{a^{n_k+1}+a^{-n_k-1}} - 4}$$

with $a = (1 - \sqrt{1-\psi^2})\psi^{-1}$. For a Poisson distributed waiting time $\psi = \lambda e^{-\lambda t}$, we obtain the following results for the first several $n_k = 1, 2, \ldots$

$$m^{(2)}(t) = \frac{1}{2}\lambda t \qquad n_k = 0$$
$$m^{(2)}(t) = \frac{1}{2}\frac{\lambda t}{4} - \frac{1}{16}\left(1 - e^{-2\lambda t}\right) \qquad n_k = 1$$
$$m^{(2)}(t) = \frac{1}{2}\frac{\lambda t}{9} - \frac{2}{27} + \frac{e^{-3\lambda t}}{54}(4 + 3\lambda t) \qquad n_k = 2$$

$$\vdots$$

$$m^{(2)}(t) = \frac{1}{2}\frac{\lambda t}{n_k^2} + \ldots$$

In these results, λ and n_k are independent. However, if this hexagonal lattice is instead interpreted as a discretization of a continuum problem with 1D diffusion along segments of the lattice, then $\lambda \sim n_k^2 D$ where D is the diffusivity along the segment. In that case, the leading-order term for any n_k is

$$m^{(2)}(t) = \frac{1}{2}Dt$$

Although we did not specify the direction of diffusion here, it turns out that for the hexagonal lattice, whether diffusion is considered along the x or y direction, the results are equivalent.

Note that the long-term asymptotics may be obtained easily, at least for a single internal state, from the theory developed in Roerdink and Shuler (1985a). However, the full time dependence is not computable under that theory.

Appendix C: General Form of T and K

Recall from Eqs. (33)–(36) that the solution $\boldsymbol{p}(\boldsymbol{X}, t|\{k_0, \ell_0\})$, to a transport problem depends on the initial concentration distribution, and on the form of the transition matrix. Equation (33) may be written as,

$$\boldsymbol{q}\,(\boldsymbol{X}, t) = \delta(t)\boldsymbol{\delta}_{k_0,\ell_0}\delta(\boldsymbol{X}) + \int_0^t \left[\sum_{\boldsymbol{X}'\in\mathcal{N}(\boldsymbol{X})} \boldsymbol{T}(\boldsymbol{X}-\boldsymbol{X}')\boldsymbol{\phi}(t-\tau)\boldsymbol{q}(\boldsymbol{X}',\tau)\right] d\tau$$
$$+ \int_0^t \boldsymbol{K}\boldsymbol{\Lambda}(t-\tau)\boldsymbol{q}(\boldsymbol{X},\tau,\{k_0,\ell_0\})\,d\tau$$

$$\boldsymbol{p}\,(\boldsymbol{X}, t) = \hat{\boldsymbol{\Phi}}(t)\boldsymbol{\delta}_{k_0,\ell_0}\delta(\boldsymbol{X}) + \int_0^t \hat{\boldsymbol{\Phi}}(t-\tau)\int_0^\tau \left[\sum_{\boldsymbol{X}'\in\mathcal{N}(\boldsymbol{X})} \boldsymbol{T}(\boldsymbol{X}-\boldsymbol{X}')\boldsymbol{\phi}(\tau\right.$$
$$\left.-s)\boldsymbol{q}(\boldsymbol{X}',s,)\right] ds\,d\tau + \int_0^t \hat{\boldsymbol{\Phi}}(t-\tau)\int_0^\tau \boldsymbol{K}\boldsymbol{\Lambda}(\tau-s)\boldsymbol{q}(\boldsymbol{X},s)ds\,d\tau$$

with

$$\hat{\Phi}_{k,\ell}(t) = 1 - \int_0^t \psi_{k,\ell}(t) = 1 - \int_0^t \left(\sum_{\boldsymbol{X}'\in\mathcal{N}(\boldsymbol{X})} \mathbf{1}^T\boldsymbol{T}(\boldsymbol{X}')\boldsymbol{\phi}(\tau)\delta_{k,\ell} + \mathbf{1}^T\boldsymbol{K}\boldsymbol{\Lambda}(\tau)\delta_{k,\ell}\right) d\tau.$$

We now present a general structure for matrices $\boldsymbol{T}$ and $\boldsymbol{K}$ that can include the examples studied, along with other examples that may arise in a variety of applications.

Recall that the number of SVs is n_k, the number of types of edges, n_e, and the number of internal states, n_s. The global matrices $\boldsymbol{T\phi}$ and $\boldsymbol{K\Lambda}$ can be written in block-structured formats, and will be understood here as functions of the Laplace transform variable s. We also will abuse notation here and write $\boldsymbol{T}$ and $\boldsymbol{K}$ rather than $\boldsymbol{T\phi}$ and $\boldsymbol{K\Lambda}$. Recall also that $\boldsymbol{K}$ involves only transitions between internal states, and no spatial movement whereas $\boldsymbol{T}$ involves spatial movement without any change in the internal state. Let $\boldsymbol{K}_J \in \mathbb{R}^{n_s \times n_s}$, $\boldsymbol{T}_{SV}$, $\boldsymbol{K}_{SV} \in \mathbb{R}^{(n_k n_s)\times(n_k n_s)}$, $\boldsymbol{D}'_s, \boldsymbol{D}'_e \in \mathbb{R}^{(n_k n_s)\times n_s}$, and $\boldsymbol{D}_s, \boldsymbol{D}_e \in \mathbb{R}^{n_s \times (n_k n_s)}$ be various blocks of $\boldsymbol{T}$ and $\boldsymbol{K}$. In particular,

- $\boldsymbol{K}_J$ characterizes transitions between the internal states at each junction
- $\boldsymbol{K}_{SV}$ characterizes transitions between internal states associated with the SVs along each edge
- $\boldsymbol{T}_{SV}$ characterizes jumps between SVs on an edge
- $\boldsymbol{D}_s$ and $\boldsymbol{D}_e$ characterize transitions from the SVs to a vertex
- $\boldsymbol{D}'_s$ and $\boldsymbol{D}'_e$ characterize transitions from a junction to an SV

The transitions represented by these matrices are diagrammed in Fig. 5. The indices s and e on $\boldsymbol{D}$ and $\boldsymbol{D}'$ are used to distinguish whether the transfers occur at the "start" or "end" of each edge (see Fig. 5). This is necessary since when the SVs are labeled from $k = 1$ to $k = n_k$, different (but closely related) matrices are needed to describe transfers from $k = 1$ (start) and $k = n_k$ (end). Recall Ex. 2 in Sect. 2.5 where $\boldsymbol{D}_s$ and $\boldsymbol{D}_e$ were explicitly constructed. This labeling does not imply that an edge is directed or undirected, but merely serves as a way of specifying the exact positions of SVs along the edge.

Next, define $\boldsymbol{I}$ as the infinite-dimensional identity matrix over the lattice positions, $\boldsymbol{X}$, and let $\boldsymbol{A}_{s,m}$ and $\boldsymbol{A}_{e,m}$ be infinite-dimensional adjacency matrices that specify which edges start and end at a given vertex. Similarly, let $\boldsymbol{A}'_{s,m}$ and $\boldsymbol{A}'_{e,m}$ specify the vertices that each edge is attached to. Often, $\boldsymbol{A}'_{e,m}$ is the transpose of $\boldsymbol{A}_{s,m}$, and likewise for $\boldsymbol{A}'_{s,m}$ and $\boldsymbol{A}_{e,m}$, so long as the graph is undirected. The index $m = 1, \ldots, n_e$ is used to distinguish between edges of different orientations (e.g., vertical or horizontal), and n_e is the number of different types of edges. For instance, in a square lattice, horizontal edges connect junctions that differ in their x-coordinate, but the vertical edges connect junctions that differ in their y-coordinate. Even if the same types of transition occur regardless of the edge orientation, distinguishing the orientation of each edge is crucial for obtaining spatial moments of the distribution. Furthermore, this formulation lends itself to extensions where not all edges have the same internal transition matrices.

The overall transition matrix is of the form

$$\begin{aligned}\boldsymbol{T} = \boldsymbol{I} \otimes \begin{pmatrix} \boldsymbol{0} & \boldsymbol{T}_{SV} & & \\ & \ddots & & \\ & & \boldsymbol{T}_{SV} \end{pmatrix} + \sum_{k=1}^{n_e} \left(\boldsymbol{A}_{s,k} \otimes \bar{\boldsymbol{D}}_{s,k} + \boldsymbol{A}_{e,k} \otimes \bar{\boldsymbol{D}}_{e,k}\right) \\ + \sum_{k=1}^{n_e} \left(\boldsymbol{A}^T_{s,k} \otimes \bar{\boldsymbol{D}}'_{s,k} + \boldsymbol{A}^T_{e,k} \otimes \bar{\boldsymbol{D}}'_{e,k}\right) \qquad \text{(C.1)}\end{aligned}$$

$$\boldsymbol{K} = \boldsymbol{I} \otimes \begin{pmatrix} \boldsymbol{K}_J & \boldsymbol{K}_{SV} & & \\ & \ddots & & \\ & & \boldsymbol{K}_{SV} \end{pmatrix} \qquad \text{(C.2)}$$

The blocks $\bar{\boldsymbol{D}}_{t,k}$ and $\bar{\boldsymbol{D}}'_{t,k}$ for $k = 1, \ldots, n_e$ and $t = \{s, e\}$ are themselves block matrices of the form

$$\bar{\boldsymbol{D}}_{t,1} = \left(\begin{array}{c|ccc} \mathbf{0} & \boldsymbol{D}_{t,1} & \mathbf{0} & \ldots \\ \hline \mathbf{0} & \mathbf{0} & & \\ \mathbf{0} & & \mathbf{0} & \\ \vdots & & & \ddots \\ \mathbf{0} & & & \mathbf{0} \end{array}\right), \quad \bar{\boldsymbol{D}}_{t,2} = \left(\begin{array}{c|ccc} \mathbf{0} & \mathbf{0} & \boldsymbol{D}_{t,2} & \mathbf{0} \ \ldots \\ \hline \mathbf{0} & \mathbf{0} & & \\ \mathbf{0} & & \mathbf{0} & \\ \vdots & & & \ddots \\ \mathbf{0} & & & \mathbf{0} \end{array}\right), \quad \text{etc.}$$

$$\bar{\boldsymbol{D}}'_{t,1} = \left(\begin{array}{c|ccc} \mathbf{0} & \mathbf{0} & \mathbf{0} \ldots \mathbf{0} & \\ \hline \boldsymbol{D}'_{t,1} & \mathbf{0} & & \\ \mathbf{0} & & \mathbf{0} & \\ \vdots & & & \ddots \\ \mathbf{0} & & & \mathbf{0} \end{array}\right), \quad \bar{\boldsymbol{D}}'_{t,2} = \left(\begin{array}{c|ccc} \mathbf{0} & \mathbf{0} & \mathbf{0} \ldots \mathbf{0} & \\ \hline \mathbf{0} & \mathbf{0} & & \\ \boldsymbol{D}'_{t,2} & & \mathbf{0} & \\ \mathbf{0} & & & \ddots \\ \vdots & & & \mathbf{0} \end{array}\right), \quad \text{etc.}$$

Note that for each type of edge in $k = 1, \ldots, n_e$, it is often possible to label the lattice so that edge $\boldsymbol{J}$ of that type connects to junction $\boldsymbol{J}$ at one terminus. With this in mind, we assume that for each edge, $\boldsymbol{J}$ of type k, the s-end of the edge border junction $\boldsymbol{J}$. Thus, $\boldsymbol{A}_{s,k} = \boldsymbol{A}'_{s,k} = \boldsymbol{I}$, where $\boldsymbol{I}$ is the identity operator on the lattice. If we further assume that the matrices $\boldsymbol{D}_k$ are all equal, then $\boldsymbol{T}$ simplifies nicely,

$$\boldsymbol{T} = \boldsymbol{I} \otimes \begin{pmatrix} \mathbf{0} & \boldsymbol{D}_s & \ldots & \boldsymbol{D}_s \\ \boldsymbol{D}'_s & \boldsymbol{T}_{SV} & & \\ \vdots & & \ddots & \\ \boldsymbol{D}'_s & & & \boldsymbol{T}_{SV} \end{pmatrix} + \sum_{k=1}^{n_e} \left(\boldsymbol{A}_{e,k} \otimes \boldsymbol{D}_{e,k} + \boldsymbol{A}^T_{e,k} \otimes \boldsymbol{D}'_{e,k} \right) \tag{C.3}$$

which resembles the Laplacian-type structure observed previously.

Although $\boldsymbol{I}$, $\boldsymbol{A}_{t,m}$, and $\boldsymbol{A}'_{t,m}$ with $t = \{s, e\}$ were defined as infinite-dimensional matrices, they can also be understood as linear operators over the infinite lattice, e.g., $\boldsymbol{A}_{t,m} = A_{t,m}(\boldsymbol{X}, \boldsymbol{Y})$ where $\boldsymbol{X}$ and $\boldsymbol{Y}$ are two junctions. In all the cases, we have considered, for each fixed $\boldsymbol{Y}$, the lattice operators are only nonzero over a few (or one) values of $\boldsymbol{X}$. The interpretation of $\boldsymbol{A}_{t,m}$ as lattice operators also gives meaning to the notation $\boldsymbol{T}(\boldsymbol{X} - \boldsymbol{X}', s)$ used in Eqs. (33)–(36).

Remark

In some cases there can be more than one type of junction. An example is the exterior hexagonal lattice, which has two types of junctions. When this occurs, additional blocks of rows and columns will augment Eqs. (C.1), (C.2), and the definitions of $\boldsymbol{D}$ and $\boldsymbol{D}'$ to describe internal transitions at each type of junction, transitions from each type of junction to each type of edge, and transitions from each type of edge to each type of junction, c.f. Eq. (B.1).

We see that the dimension of the state-space associated with each junction, $\boldsymbol{X}$ is $n_T = n_s(n_v + n_e n_k)$ where n_v is the number of junction types, and n_e the number of edge types.

C.1 Computation of Spatial Moments in the General Case

We now turn our attention toward computation of the moments for the general evolution equations in Eq. (33). Many properties of CTRWs are most easily analyzed in Laplace transform space. With lattice random walks, it is also often convenient to apply a lattice Fourier transform over $\boldsymbol{X}$, the lattice variable.

To compute the spatial moments (as functions of s, the Laplace transform variable), we start by computing the lattice Fourier transform of Eqs. (C.3) and (C.2) over the lattice spatial variable, $\boldsymbol{X}$, obtaining

$$\hat{\boldsymbol{T}} + \hat{\boldsymbol{K}} = (\mathscr{F} \otimes \boldsymbol{I})(\boldsymbol{T} + \boldsymbol{K})\left(\mathscr{F}^{-1} \otimes \boldsymbol{I}\right) \tag{C.4}$$

$$= \boldsymbol{I} \otimes \left[\begin{pmatrix} \boldsymbol{K}_J & \boldsymbol{D}_e + \boldsymbol{D}_s & \dots & \boldsymbol{D}_e + \boldsymbol{D}_s \\ \boldsymbol{D}'_e + \boldsymbol{D}'_s & \boldsymbol{T}_{SV} + \boldsymbol{K}_{SV} & \boldsymbol{0} & \dots \\ \vdots & \boldsymbol{0} & \ddots & \boldsymbol{0} \\ \boldsymbol{D}'_e + \boldsymbol{D}'_s & \vdots & \boldsymbol{0} & \boldsymbol{T}_{SV} + \boldsymbol{K}_{SV} \end{pmatrix} + \begin{pmatrix} \boldsymbol{0} & \alpha_{e,1}(\boldsymbol{\omega})\boldsymbol{D}_e & \dots & \alpha_{e,m}(\boldsymbol{\omega})\boldsymbol{D}_e \\ \beta_{e,1}(\boldsymbol{\omega})\boldsymbol{D}'_e & \boldsymbol{0} & \dots & \\ \vdots & \vdots & & \\ \beta_{e,m}(\boldsymbol{\omega})\boldsymbol{D}'_e & \boldsymbol{0} & \dots & \end{pmatrix} \right] \tag{C.5}$$

$$= \boldsymbol{I} \otimes \left[\boldsymbol{K}' + \boldsymbol{T}'(\boldsymbol{\omega})\right] \tag{C.6}$$

where

$$\alpha_{e,m}(\boldsymbol{\omega}) = (e^{i\,\Delta \boldsymbol{X}_m \cdot \boldsymbol{\omega}} - 1), \qquad \beta_{e,m}(\boldsymbol{\omega}) = (e^{-i\,\Delta \boldsymbol{X}_m \cdot \boldsymbol{\omega}} - 1)$$

and $\mathscr{F}$ is the Fourier transform operator on the lattice. The vectors $\Delta \boldsymbol{X}_m$ specify the displacements between adjacent junctions along a type m edge. The functions $\alpha_e(\boldsymbol{\omega})$ and $\beta_e(\boldsymbol{\omega})$ are analogous to the functions $(z-1)$ and $(z^{-1}-1)$ discussed in Sect. 3.1.

Since we use a lattice Fourier transform as opposed to a generating function formalism here, we have replaced z by $e^{i\boldsymbol{\omega}}$. With the lattice Fourier transform, it seems somewhat easier to handle cases where $\Delta \boldsymbol{X}_{t,m}$ are not all of the same length for every $t = \{s, e\}$ or $m = 1, \dots, n_s$, although these minutiae could likely be included in a generating function approach with only a few modifications. Lastly, the matrix $\boldsymbol{K}'$ corresponds with $\boldsymbol{K}_0 + \boldsymbol{D}^+ + \boldsymbol{D}^-$, and $\boldsymbol{T}'(\boldsymbol{\omega})$ corresponds with $(z-1)\boldsymbol{D}^+ + (1/z-1)\boldsymbol{D}^-$ from Sect. 3.2.

Due to the translation invariance of the lattice points, we see that the Fourier transform diagonalizes the adjacency matrices, $\boldsymbol{A}_{e,m}$ and $\boldsymbol{A}'_{e,m}$. This reduces an infinite-dimensional matrix problem to an $n_T \times n_T$ problem parameterized by a variable, $\boldsymbol{\omega}$. The spatial moments over the junctions are found by considering derivatives of $(\boldsymbol{I} - \hat{\boldsymbol{K}} - \hat{\boldsymbol{T}})^{-1}$ with respect to $\boldsymbol{\omega}$ in the limit that $\boldsymbol{\omega} \to \boldsymbol{0}$. For instance, on an infinite

one-dimensional lattice, the derivative of the lattice Fourier transform of a function $f(x_k)$ is

$$\lim_{\omega \to 0} \frac{\partial^j \hat{f}(\omega)}{\partial \omega^j} = \sum_{k=-\infty}^{\infty} (-ix)^j f(x_k) = (-i)^j m^{(j)} \qquad j = 0, 1, \ldots$$

Given $\hat{\boldsymbol{T}}$ and $\hat{\boldsymbol{K}}$, in the limit $\boldsymbol{\omega} \to \mathbf{0}$, we have

$$\frac{\partial}{\partial \omega_j} \left[\boldsymbol{I} - \boldsymbol{K}' - \boldsymbol{T}'(\boldsymbol{\omega})\right]^{-1} = \left[\boldsymbol{I} - \boldsymbol{K}'\right]^{-1} \left(\frac{\partial \boldsymbol{T}'}{\partial \omega_j}\right) \left[\boldsymbol{I} - \boldsymbol{K}'\right]^{-1}$$

$$\begin{aligned} \frac{\partial^2}{\partial \omega_j \partial \omega_k} \left[\boldsymbol{I} - \boldsymbol{K}' - \boldsymbol{T}'(\boldsymbol{\omega})\right]^{-1} &= 2\left[\boldsymbol{I} - \boldsymbol{K}'\right]^{-1} \left(\frac{\partial \boldsymbol{T}'}{\partial \omega_j}\right) \left[\boldsymbol{I} - \boldsymbol{K}'\right]^{-1} \left(\frac{\partial \boldsymbol{T}'}{\partial \omega_k}\right) \left[\boldsymbol{I} - \boldsymbol{K}'\right]^{-1} \\ &\quad + \left[\boldsymbol{I} - \boldsymbol{K}'\right]^{-1} \left(\frac{\partial^2 \boldsymbol{T}'}{\partial \omega_j \partial \omega_k}\right) \left[\boldsymbol{I} - \boldsymbol{K}'\right]^{-1} \end{aligned}$$

where derivatives, $\frac{\partial}{\partial \omega_j}$, are taken with respect to $\boldsymbol{\omega}$ and are understood to be evaluated at $\boldsymbol{\omega} = \mathbf{0}$. Since $\boldsymbol{T}'(\boldsymbol{\omega}) = \mathbf{0}$ as $\boldsymbol{\omega} \to \mathbf{0}$, the only matrix inverse required is $\left[\boldsymbol{I} - \boldsymbol{K}'\right]^{-1}$. Averaging over the internal states within a cell, we can compute the average spatial moments of a process with transition matrix, $\hat{\boldsymbol{T}}$ as (c.f. Landman and Shlesinger 1979a)

$$\boldsymbol{m}_j^{(1)} = \left\langle (-i)\hat{\boldsymbol{\Phi}} \left[\boldsymbol{I} - \boldsymbol{K}'\right]^{-1} \left(\frac{\partial \boldsymbol{T}'}{\partial \omega_j}\right) \left[\boldsymbol{I} - \boldsymbol{K}'\right]^{-1} + x_j \hat{\boldsymbol{\Phi}} \left[\boldsymbol{I} - \boldsymbol{K}'\right]^{-1} \right\rangle \tag{C.7}$$

$$\boldsymbol{m}_{jk}^{(2)} = \left\langle -\hat{\Phi} \left[\boldsymbol{I} - \boldsymbol{K}'\right]^{-1} \left(2\left(\frac{\partial \boldsymbol{T}'}{\partial \omega_j}\right) \left[\boldsymbol{I} - \boldsymbol{K}'\right]^{-1} \left(\frac{\partial \boldsymbol{T}'}{\partial \omega_k}\right) + \left(\frac{\partial^2 \boldsymbol{T}'}{\partial \omega_j \partial \omega_k}\right)\right) \left[\boldsymbol{I} - \boldsymbol{K}'\right]^{-1} \right. \tag{C.8}$$

$$\left. + 2(-i) x_j \hat{\boldsymbol{\Phi}} \left[\boldsymbol{I} - \boldsymbol{K}'\right]^{-1} \left(\frac{\partial \boldsymbol{T}'}{\partial \omega_k}\right) \left[\boldsymbol{I} - \boldsymbol{K}'\right]^{-1} + x_j x_k \hat{\boldsymbol{\Phi}} \left[\boldsymbol{I} - \boldsymbol{K}'\right]^{-1} \right\rangle, \tag{C.9}$$

where $\boldsymbol{x} = (x_1, x_2, \ldots, x_d)$ describes the position of SVs relative to a junction and $\langle \ldots \rangle$ is a suitable spatial-summation operator acting over the SVs. In this context, elements of $\hat{\Phi}$ from Eq. (34) are written as

$$\hat{\Phi}_i = \frac{1}{s} \left(1 - \sum_j \boldsymbol{K}'_{ij}(s)\right). \tag{C.10}$$

Many of the same points carry through if the transport process is posed as a generalized differential master equation rather than as an integral master equation. In the differential master equation setting, after Fourier and Laplace transformation, we write

$$(s\boldsymbol{\Gamma} + \boldsymbol{I} - \boldsymbol{H} - \boldsymbol{W}(\boldsymbol{\omega}))\, \boldsymbol{P} = \boldsymbol{\Gamma}\boldsymbol{\delta}$$

with (recall we have set $\boldsymbol{T\phi} \mapsto \boldsymbol{T}$ and $\boldsymbol{K\Lambda} \mapsto \boldsymbol{K}$ in this section)

$$\boldsymbol{W}(\boldsymbol{\omega}) = (\mathscr{F} \otimes \boldsymbol{I})\, \boldsymbol{\Gamma T} \left(\hat{\boldsymbol{\Phi}}\right)^{-1} (\mathscr{F} \otimes \boldsymbol{I})\,, \quad \boldsymbol{H} = \boldsymbol{\Gamma K} \left(\hat{\boldsymbol{\Phi}}\right)^{-1}$$

Similar to the results above, we define the matrix $\boldsymbol{S} = (s\boldsymbol{\Gamma} + \boldsymbol{I} - \boldsymbol{H} - \boldsymbol{W}(\boldsymbol{0}))^{-1}$, and then, we may compute the moments using the matrix derivative formulas above as

$$\begin{aligned}
\boldsymbol{m}_j^{(1)} &= (-i)\boldsymbol{S}^{-1} \left(\frac{\partial \boldsymbol{W}}{\partial \omega_j}\right) \boldsymbol{S}^{-1} \boldsymbol{\Gamma\delta} + \boldsymbol{x}\boldsymbol{S}\boldsymbol{\Gamma\delta} \\
\boldsymbol{m}_{jk}^{(2)} &= \left[-\left(2\boldsymbol{S}\left(\frac{\partial \boldsymbol{W}}{\partial \omega_j}\right)\boldsymbol{S}\left(\frac{\partial \boldsymbol{W}}{\partial \omega_k}\right)\boldsymbol{S} + \boldsymbol{S}\left(\frac{\partial^2 \boldsymbol{W}}{\partial \omega_j \partial \omega_k}\right)\boldsymbol{S}\right) - 2ix_j \boldsymbol{S}\left(\frac{\partial \boldsymbol{W}}{\partial \omega_k}\right)\boldsymbol{S} \right. \\
&\quad \left. + x_j x_k \boldsymbol{S}\right] \boldsymbol{\Gamma\delta}.
\end{aligned}$$

Appendix D: General First-Passage-Time Problems and Secondary Vertex Reductions

In Sect. 4.1, we discussed how the SVs can be eliminated from some problems to form a CTRW involving only the junctions. Here, we discuss how this is done in the general case using the description in See Appendix C and C.1.

D.1 Reduction of SVs in the General Case

Recall the general integral master equation formulation in Eq. (36) with the $n_T \times n_T$ matrices $\boldsymbol{T}$ and $\boldsymbol{K}$ defined in Eqs. (C.1) and (C.2). What we show in this section is that the effective transition rates derived in the previous examples applies more generally as well. In particular, by obtaining effective transition rates, the evolution of a system that has arbitrarily many SVs can be described by a reduced system that only involves internal states at junctions. We first give the resulting evolution equations and moment formulas, and then proceed to describe how to derive the elements of the effective transition matrices that appear in those equations.

In Laplace transform space, we write the n_s-dimensional integral master equation for the reduced system as

$$\begin{aligned}
\boldsymbol{q}_J(\boldsymbol{X}, s) &= \delta(\boldsymbol{X})\delta(t)\boldsymbol{\delta}_k + \sum_{\boldsymbol{X}'} \boldsymbol{A}_2(\boldsymbol{X} - \boldsymbol{X}') \otimes \boldsymbol{T}_2^{\text{eff}} \boldsymbol{q}_J(\boldsymbol{X}', s) \\
&\quad + \left(\boldsymbol{I} \otimes \boldsymbol{K}_J + \boldsymbol{A}_1 \otimes \boldsymbol{T}_1^{\text{eff}}\right) \boldsymbol{q}_J(\boldsymbol{X}, s) \\
\boldsymbol{p}_J(\boldsymbol{X}, s) &= \hat{\boldsymbol{\Phi}}_0(s) \boldsymbol{q}_J(\boldsymbol{X}, s)
\end{aligned} \tag{D.1}$$

where each nonzero element of the diagonal matrix $\hat{\boldsymbol{\Phi}}_0$ is

$$\hat{\Phi}_{0,k} = \frac{1}{s}\left(1 - \mathbf{1}^T\left(\boldsymbol{I} \otimes \boldsymbol{K}_J + \boldsymbol{A}_1 \otimes \boldsymbol{T}_1^{\text{eff}}\right)\boldsymbol{\delta}_k - \sum_{\boldsymbol{X}} \mathbf{1}^T \boldsymbol{A}_2(\boldsymbol{X} - \boldsymbol{X}') \otimes \boldsymbol{T}_2^{\text{eff}}\boldsymbol{\delta}_k\right).$$

The $n_s \times n_s$ matrices $\boldsymbol{T}_1^{\text{eff}}$ and $\boldsymbol{T}_2^{\text{eff}}$ describe effective transition rates for transitions within a junction, and for travel between adjacent junctions. They will be defined precisely in Appendix D.2. The matrix, $\boldsymbol{K}_J$ is the same as that in Eq. (C.2), and it also describes internal transitions at a junction. The infinite-dimensional adjacency matrices $\boldsymbol{A}_1$ and $\boldsymbol{A}_2$ are defined as[10]

$$\boldsymbol{A}_1 = \left(\sum_{m=1}^{n_e} \boldsymbol{A}_{e,m}\boldsymbol{A}'_{e,m} + \boldsymbol{A}_{s,m}\boldsymbol{A}'_{s,m}\right) = 2n_e\boldsymbol{I}$$
$$\boldsymbol{A}_2 = \left(\sum_{m=1}^{n_e} \boldsymbol{A}_{s,m}\boldsymbol{A}'_{e,m} + \boldsymbol{A}_{e,m}\boldsymbol{A}'_{s,m}\right),$$

where n_e is the number of different types of edges in the lattice. The adjacency matrices $\boldsymbol{A}_{e,m}$ and $\boldsymbol{A}_{s,m}$ are those that are introduced in Appendix C, and m ranges over the various types of edges in the system. As described in Appendix C, these matrices can also be understood as operators over the lattice. This leads to the notation in Eq. (D.1) where $\boldsymbol{A}_2(\boldsymbol{X} - \boldsymbol{X}')$ is written as a function of the lattice points.

From Eq. (D.1), the integral master equation for $\boldsymbol{p}_J$ can be derived as

$$\boldsymbol{p}_J(\boldsymbol{X}, s) = \hat{\boldsymbol{\Phi}}_0\delta(\boldsymbol{X})\boldsymbol{\delta}_k + \sum_{\boldsymbol{X}'} \hat{\boldsymbol{\Phi}}_0\left(\boldsymbol{A}_2(\boldsymbol{X} - \boldsymbol{X}') \otimes \boldsymbol{T}_2^{\text{eff}}\right)\hat{\boldsymbol{\Phi}}_0^{-1}\boldsymbol{p}_J(\boldsymbol{X}', s)$$
$$+\hat{\boldsymbol{\Phi}}_0\left(\boldsymbol{I} \otimes \boldsymbol{K}_J + \boldsymbol{A}_1 \otimes \boldsymbol{T}_1^{\text{eff}}\right)\hat{\boldsymbol{\Phi}}_0^{-1}\boldsymbol{p}_J(\boldsymbol{X}, s).$$

Normally, each transition in a random jump process implies a change of internal state or position; however, with effective transitions, we must be able to account for paths where a particle, starting from a junction in internal state ℓ, makes a number of jumps along an edge and then returns to that same junction in state ℓ. The WTDs for such events to occur are given by the diagonal elements of $\boldsymbol{T}_1^{\text{eff}}$, and they involve no change in position or internal state. We will later discuss how to reformulate the effective transition rates so that these self-jumps need not be considered as "transitions" in $\boldsymbol{T}_1^{\text{eff}}$.

It also is the case that unlike $\boldsymbol{T}_J$ and $\boldsymbol{T}_{SV}$ which did not invoke changes in internal states, $\boldsymbol{T}_2^{\text{eff}}$ can include transitions that simultaneously change the position and internal state of a particle. This is because each element of $\boldsymbol{T}_2^{\text{eff}}$ is the aggregate of a number of different steps on an edge. Even though each individual transition on the edge involves only changes in state ($\boldsymbol{K}_{SV}$) or position ($\boldsymbol{T}_{SV}$), the aggregate of many transitions required for a particle to travel between junctions can change both.

[10] The reduction of $\boldsymbol{A}_1$ to $2n_e\boldsymbol{I}$ is valid only under the restrictions discussed below.

Each element of $\boldsymbol{T}_1^{\text{eff}}$ and $\boldsymbol{T}_2^{\text{eff}}$ is found by solving a first-passage-time problem to obtain the distribution of times for a particle to arrive in internal state ℓ at a junction after having started in state ℓ_0 at that junction or an adjacent one without having visited any other junction states in the intervening time. We will discuss the solution to these problems in the next section, but first turn to the computation of the spatial moments for the reduced system.

Note that aside from the exterior hexagonal lattice and a remark in Appendix C, we have only considered lattices with a single type of junction [11] (e.g., the exterior hexagonal lattice does *not* fall into this category since it has type I and type II junctions). This restriction is mostly done for ease of notation and clarity, as there do not appear to be theoretical difficulties with considering multiple types of junctions. In this section, we will make two additional restrictions, also to ensure clarity of the arguments that follow.

Consider a lattice with a single type of junction and n_e types of edges, each type distinguished from the others only by its orientation relative to the x-axis. The first additional restriction is that the transport along each edge is undirected. The second restriction is that we now suppose that the lattice is constructed so that at each junction, one edge of each type starts and one edge of each type ends at that junction. Note that this restriction is also used in Appendix C. Aside from the exterior hexagonal lattice and persistent comb random walk, the examples discussed in this paper have these properties. As an example, in a square lattice, at each junction, one vertical edge and one horizontal edge start (have their s-terminus) at that junction, and one vertical and one horizontal edge end (have their e-terminus) at that junction. Thus, there are $n_e = 2$ types of edges (vertical and horizontal), and each junction is connected to $4 = 2n_e$ edges in the square lattice.

Recall that the lattice Fourier transform of a function is

$$\hat{f}(\boldsymbol{\omega}) = \sum_{\boldsymbol{X}\in\mathscr{G}} f(\boldsymbol{X}) e^{i\boldsymbol{X}\cdot\boldsymbol{\omega}}$$

with $\boldsymbol{\omega}$ defined over a d-dimensional cube, $\left[-\frac{\pi}{|\Delta X|}, \frac{\pi}{|\Delta X|}\right]^d$. Here, d is the dimension of the space and $\boldsymbol{\Delta X}$ the lattice spacing.

Applying the lattice Fourier transform to the matrix,

$$\left(\boldsymbol{I}\otimes\boldsymbol{K}_J + \boldsymbol{A}_1\otimes\boldsymbol{T}_1^{\text{eff}}\right) + \boldsymbol{A}_2(\boldsymbol{X})\otimes\boldsymbol{T}_2^{\text{eff}},$$

from Eq. (D.1), and keeping in mind the restrictions above, we obtain

$$\boldsymbol{I}\otimes\left[\boldsymbol{K}_J + 2n_e(\boldsymbol{T}_1^{\text{eff}} + \boldsymbol{T}_2^{\text{eff}})\right] + \boldsymbol{I}\otimes\left[\sum_{j=1}^{2n_e}(e^{i\Delta\boldsymbol{X}_j\cdot\boldsymbol{\omega}} - 1)\boldsymbol{T}_2^{\text{eff}}\right]$$

[11] Each junction can still have arbitrarily many internal states. A *single type* of junction refers to all junctions in a lattice having the same connectivity, via a single edge, to other junctions in that lattice. For example, in a square lattice, each junction is connected to its neighbors to the north, south, east, and west. This differs from the exterior hexagonal lattice where type I junctions are connected to their neighbors to the north, southeast, and southwest; and type II junctions to neighbors to their south, northeast, and northwest.

$$\equiv \boldsymbol{I} \otimes \boldsymbol{K}_0 + \boldsymbol{I} \otimes \boldsymbol{T}_0^{\text{eff}}(\boldsymbol{\omega}).$$

To find the moments, we differentiate in Fourier space as in Appendix C.1. Differentiating $\tilde{\boldsymbol{p}}_J(\boldsymbol{\omega}, s)$, we obtain

$$\tilde{\boldsymbol{m}}_j^{(1)} = (-i)\hat{\boldsymbol{\Phi}}_0 [\boldsymbol{I} - \boldsymbol{K}_0]^{-1} \left(\frac{\partial \boldsymbol{T}_0^{\text{eff}}}{\partial \omega_j} \right) [\boldsymbol{I} - \boldsymbol{K}_0]^{-1} \tag{D.2}$$

$$\tilde{\boldsymbol{m}}_{jk}^{(2)} = -\hat{\boldsymbol{\Phi}}_0 [\boldsymbol{I} - \boldsymbol{K}_0]^{-1} \left(2 \left(\frac{\partial \boldsymbol{T}_0^{\text{eff}}}{\partial \omega_j} \right) [\boldsymbol{I} - \boldsymbol{K}_0]^{-1} \left(\frac{\partial \boldsymbol{T}_0^{\text{eff}}}{\partial \omega_k} \right) + \left(\frac{\partial^2 \boldsymbol{T}_0^{\text{eff}}}{\partial \omega_j \partial \omega_k} \right) \right) [\boldsymbol{I} - \boldsymbol{K}_0]^{-1} \tag{D.3}$$

with $j, k = 1, 2, \ldots, d$. Notice that there is no summation over the n_k SVs since details regarding the SVs have been condensed into the elements of $\boldsymbol{T}_2^{\text{eff}}$ which describes transfers between adjacent junctions. Likewise we do not need any information about how the internal states are situated relative to a junction. We can also write $\hat{\boldsymbol{\Phi}}_0$ from above as

$$\left(\hat{\Phi}_0(s) \right)_i = \frac{1}{s} \left(1 - \sum_j \boldsymbol{K}_{0,ij}(s) \right).$$

Unlike the SVs, the internal states have not been summed over, so the moments are still written as vectors over these states.

Remark 1 It is important to note that since no summation is done over the SVs, the value of $\boldsymbol{p}_J(\boldsymbol{X}, t)$ at junction $\boldsymbol{X}$ is now the aggregate probability density of all particles that have reached that junction, but not yet arrived at any other junctions. In other words, a particle located on an edge after exiting junction $\boldsymbol{X}$, but not having yet reached an adjacent junction, would contribute to $\boldsymbol{p}_J(\boldsymbol{X}, t)$. This is a reflection of the fact that in the reduced process, the fine details of the exact location of a particle along an edge have been suppressed. Nonetheless, if one uses the elements of $\hat{\boldsymbol{\Phi}}$ associated with junctions from the full system (e.g., Eq. (34)) rather than $\hat{\boldsymbol{\Phi}}_0$ for the reduced system, the probabilities *at* junction $\boldsymbol{X}$ are obtained (c.f. the difference between $\hat{\boldsymbol{\Phi}}$ and $\hat{\boldsymbol{\Psi}}$ in Ex. 4).

Remark 2 When the FPT procedure is applied to a Markov process, this result is typically a non-Markovian process with a reduced number of degrees of freedom (Kampen 1992). The non-Markovian character arises since even if all the transitions in the original process have Poisson distributed waiting times, the aggregate waiting-time distribution for several sequential Poisson processes to occur is not a Poisson distribution. As noted above, this leads to an overall non-Markovian process since the only continuous waiting-time distributions which leads to a Markov process are Poisson distributions.

D.2 General First-Passage-Time Problems

It now remains to describe the general first-passage-time (FPT) problem which must be solved to obtain $\boldsymbol{T}_1^{\text{eff}}$ and $\boldsymbol{T}_2^{\text{eff}}$ in Eq. (D.1). The elements of $\boldsymbol{T}_{1,2}^{\text{eff}}$ are closely related to FPTs for a random walk to reach state ℓ at a junction given that it started in state ℓ_0 at one of the junctions bordering that edge and did not leave the edge yet.

Recall that we assume that all edges have the same set internal transitions and spatial jump transitions. Also recall that the transition matrices for internal state changes and spatial jumps on an edge are $\boldsymbol{K}_{SV}$ and $\boldsymbol{T}_{SV}$, respectively. Since a particle starting out on an edge can eventually jump to a vertex at the "s" or "e" end of that edge, the matrix $\boldsymbol{T}_{SV} + \boldsymbol{K}_{SV}$ cannot conserve particle number. Thus, the matrix $\boldsymbol{T}_{SV} + \boldsymbol{K}_{SV}$ is the transition matrix for a random walk confined to an edge and subject to absorbing boundary conditions. Since particles are absorbed at the boundaries, the rate at which particles are absorbed can be defined. In the full matrix system, these absorption rates correspond to the rate at which particles arrive at the vertices at either end of an edge.

In order to define the arrival rates, we consider the nonzero elements of $\boldsymbol{D}_e$ and $\boldsymbol{D}_s$ which describe transitions from an edge to a vertex. As depicted in Fig. 5, there are typically at most n_s distinct transitions from each end of an edge, one from each internal state at $k = 1$ and $k = n_k$. Thus, there are typically at most n_s nonzero entries in $\boldsymbol{D}_s$ and $\boldsymbol{D}_e$. Considering $\boldsymbol{D}_s$ first, each nonzero element of $\boldsymbol{D}_s$ can be written as $d_\ell \psi_{d,\ell}(t)$. Here, d_ℓ is the probability for a particle at the first SV ($k = 1$) in state ℓ to jump to state ℓ at the adjacent junction, and $\psi_{d,\ell}(t)$ is the WTD for the jump when it does occur. The same description holds for nonzero elements of $\boldsymbol{D}_e$, except in that case the particle is jumping from the n_kth SV, $k = n_k$ rather than $k = 1$.

Then, the Laplace transform of the FPT density for a particle to reach the junction attached to the "s"-end of an edge in state ℓ after starting in state (k_0, ℓ_0) on the edge is of the form

$$\tilde{f}_\ell(s|\{k_0, \ell_0\}) = d_\ell \psi_{d,\ell}(s) \boldsymbol{\delta}_{1,\ell}^T \left(\boldsymbol{I} - \boldsymbol{T}_{SV} - \boldsymbol{K}_{SV}\right)^{-1} \boldsymbol{\delta}_{k_0,\ell_0}$$

where $\boldsymbol{\delta}_{k_0,\ell_0}$ and $\boldsymbol{\delta}_{1,\ell}$ are Kronecker deltas over the state-space of the edge. But $\tilde{f}_\ell(s|\{k_0, \ell_0\})$ is just the ℓ^{th} component of a vector $\tilde{\boldsymbol{f}}(s|\{k_0, \ell_0\})$ over the internal states at a junction. The FPT densities to reach each of the n_s internal states at a junction defined easily by decomposing $\boldsymbol{D}_s$ as a sum of rank one matrices,

$$\boldsymbol{D}_s = \sum_{\ell=1}^{n_s} d_\ell \psi_{d,\ell}(s) \boldsymbol{\delta}_\ell \boldsymbol{\delta}_{1,\ell}^T$$

and writing

$$\tilde{\boldsymbol{f}}(s|\{k_0, \ell_0\}) = \boldsymbol{D}_s \left(\boldsymbol{I} - \boldsymbol{T}_{SV} - \boldsymbol{K}_{SV}\right)^{-1} \boldsymbol{\delta}_{k_0,\ell_0}.$$

This describes the FPT densities to reach the vertex adjacent to the "s"-end of the edge for a particle starting at some SV on edge, and the FPT densities at the "e"-end can

be found similarly. However, the effective transition rates we seek describe how long it takes a particle to jump between vertices, not from an SV to a vertex.

Let us consider the n_k^{th} SV on an edge. Each internal state associated with this SV is directly connected to the junction at the "e"-end of the edge, and jumps from that junction to the edge are governed by $\boldsymbol{D}'_e$. Like $\boldsymbol{D}_e$, $\boldsymbol{D}'_e$ typically has at most n_s nonzero entries and we can write $\boldsymbol{D}'_e$ as

$$\boldsymbol{D}'_e = \sum_{\ell=1}^{n_s} d'_\ell \psi'_{d,\ell}(s) \boldsymbol{\delta}_{n_k,\ell} \boldsymbol{\delta}_\ell^T$$

where d'_ℓ is the probability of a particle in state ℓ at the junction jumping to the edge, and $\psi'_{d,\ell}$ is the WTD when the jump occurs.

With this, the elements of the vector,

$$\tilde{\boldsymbol{f}}(s|\ell_0\}) = \boldsymbol{D}_s \left(\boldsymbol{I} - \boldsymbol{T}_{SV} - \boldsymbol{K}_{SV}\right)^{-1} \boldsymbol{\delta}_{n_k,\ell_0} \psi'_{d,\ell_0}$$

are the FPTs for a particle jumping from state ℓ_0 at the junction at the "e"-end of an edge to reach state ℓ at the junction at the "s"-end of the same edge. Elements of $\boldsymbol{T}_2^{\text{eff}}$ are then found by multiplying these FPTs by d'_{ℓ_0} which gives the probability of the jump occurring. Collecting all of these FPTs into a matrix, we obtain,

$$\boldsymbol{T}_2^{\text{eff}} = \boldsymbol{D}_s \left(\boldsymbol{I} - \boldsymbol{T}_{SV} - \boldsymbol{K}\right)^{-1} \boldsymbol{D}'_e \tag{D.4}$$

By similar arguments, we find the elements of $\boldsymbol{T}_1^{\text{eff}}$ by replacing $\boldsymbol{D}_s$ with $\boldsymbol{D}_e$,

$$\boldsymbol{T}_1^{\text{eff}} = \boldsymbol{D}_e \left(\boldsymbol{I} - \boldsymbol{T}_{SV} - \boldsymbol{K}\right)^{-1} \boldsymbol{D}'_e. \tag{D.5}$$

Notice that we could have replaced $\boldsymbol{D}_s$ and $\boldsymbol{D}'_e$ by $\boldsymbol{D}_e$ and $\boldsymbol{D}'_s$ in the computation of $\boldsymbol{T}_2^{\text{eff}}$. Either combination is valid since we have assumed that transport along each edge is undirected. Note that many useful examples involve just two types of effective transitions (return to origin, and jump to other states) in which case the matrices above will be rank two.

The presence of condensed paths over the SVs that return a particle to its starting state prior to jumping is a peculiarity that arises here. However, as we will now show, these self-jumps can be eliminated by solving an extended first-passage-time problem which results in a rescaling of the values of $\boldsymbol{T}_2^{\text{eff}}$ and the off-diagonal elements of $\boldsymbol{T}_1^{\text{eff}}$ to account for the contingency of multiple returns to the starting point. This was done implicitly in Ex. 4.2 when we solved for the FPT to reach $X_{i\pm1}$ from X_i in the a 1D lattice. In that case, no self-jumps were possible since the effective WTD was defined such that it described sojourns on edges that started (at X_i) and ended (at $X_{i\pm1}$) at different points in space. This same principle holds in general.

It turns out the form of the rescaled transition rates is relatively simple. We first give the result and then discuss its derivation. To obtain the rescaled transition rates,

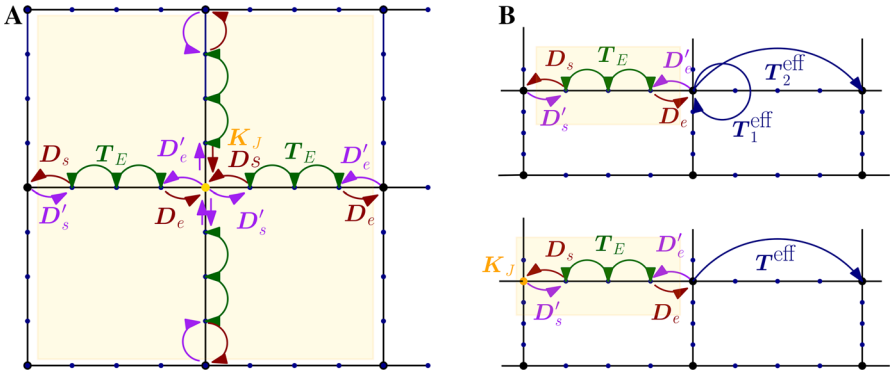

Fig. 13 Random walk first-passage-time problems with $n_\ell = 1$. **A** The most general type of FPT problem involving the full set of states in between any two adjacent lattice states. **B** The two simplifications. In the first simplification (top), only the internal states within an edge are considered, the FPT matrix here is $\boldsymbol{D}\,(\boldsymbol{I} - \boldsymbol{T}_{SV} - \boldsymbol{K}_{SV})^{-1}\,\boldsymbol{D}'$. Self-returns and jumps to adjacent junctions are highlighted. In the second case, the junction is considered as well. This rescales the problem to eliminate self-jumps. It can be understood as equivalent to the general FPT problem when all edges exhibit the same set of transitions including those to and from a lattice point. In (a) and (b), the highlighted boxes are used to indicate the states involved in the FPT computation

we additively decompose $\boldsymbol{T}_1^{\text{eff}}$ into diagonal and off-diagonal components,

$$\boldsymbol{T}_1^{\text{eff}} = \boldsymbol{T}_{1,d}^{\text{eff}} + \boldsymbol{T}_{1,o}^{\text{eff}}.$$

The subscripts d and o indicate the diagonal and off-diagonal components of $\boldsymbol{T}_1^{\text{eff}}$. The self-jumps are characterized by $\boldsymbol{T}_{1,d}^{\text{eff}}$, and jumps that change the state or position of a particle are given by $\boldsymbol{K}$, $\boldsymbol{T}_{1,o}^{\text{eff}}$, and $\boldsymbol{T}_2^{\text{eff}}$. The rescaled internal transitions and first-passage-times are then of the form

$$\begin{aligned} \boldsymbol{K}_r &= \boldsymbol{K}\left(\boldsymbol{I} - 2n_e\boldsymbol{T}_{1,d}^{\text{eff}}\right)^{-1}, \quad \boldsymbol{T}_{1,r}^{\text{eff}} = 2n_e\boldsymbol{T}_{1,o}^{\text{eff}}\left(\boldsymbol{I} - 2n_e\boldsymbol{T}_{1,d}^{\text{eff}}\right)^{-1}, \\ \boldsymbol{T}_{2,r}^{\text{eff}} &= \boldsymbol{T}_2^{\text{eff}}\left(\boldsymbol{I} - 2n_e\boldsymbol{T}_{1,d}^{\text{eff}}\right)^{-1} \end{aligned} \tag{D.6}$$

As noted before, this rescaling is equivalent to the solution of an extended first-passage-time problem that does not terminate when a particle returns to its starting state. Consider a particle starting at state ℓ at vertex $\boldsymbol{X}$. To exclude self-jumps, consider the transition matrix for a particle in a system that includes state ℓ at vertex $\boldsymbol{X}$ and all of the SVs and internal states on the edges that are attached to $\boldsymbol{X}$ (see Fig. 13).

The transition matrices for each ℓ are of the form

$$\boldsymbol{T}_{r,\ell}+\boldsymbol{K}_{r,\ell} = \begin{pmatrix} 0 & \boldsymbol{\delta}_\ell^T\boldsymbol{D}_{t_1} & \dots & \boldsymbol{\delta}_\ell^T\boldsymbol{D}_{t_{2n_e}} \\ \boldsymbol{D}'_{t_1}\boldsymbol{\delta}_\ell & \boldsymbol{T}_{SV}+\boldsymbol{K}_{SV} & \boldsymbol{0}\dots & \\ \vdots & \vdots & \ddots & \vdots \\ \boldsymbol{D}'_{t_{2n_e}}\boldsymbol{\delta}_\ell & \boldsymbol{0} & \dots & \boldsymbol{T}_{SV}+\boldsymbol{K}_{SV} \end{pmatrix}, \quad \ell = 1,\dots,N_\ell \tag{D.7}$$

where $t_k = \{s, e\}$ specifies which end of edge k connects to vertex, $\boldsymbol{X}$, see Fig. 13a. We see that a particle starting on $\boldsymbol{X}$ in state ℓ can exit the system by 1) reaching $\boldsymbol{X}$ in any internal state except for ℓ, or 2) by reaching a junction adjacent to $\boldsymbol{X}$ in any internal state including ℓ. Since the particle cannot exit this system from the same position and state at which it started, no effective self-jumps occur.

The resulting matrix for the FPT problem is much larger in this case than the matrix $\boldsymbol{T}_e + \boldsymbol{K}_e$ which was needed to find $\boldsymbol{T}^{\text{eff}}_{1,2}$. This is disadvantageous since solutions may be more difficult to compute. However, a significant simplification is possible due to assumptions we have made. In the case, we have been considering, all edges have the same set of transitions and WTDs. Given this, we find that since the particle starts at the junction, the probabilities, $\tilde{p}_{k,\ell}(s)$ along each edge are equal. This allows us to write

$$\boldsymbol{T}_{r_0,\ell} + \boldsymbol{K}_{r_0,\ell} = \begin{pmatrix} 0 & (\boldsymbol{D}_{t_1})_\ell \\ 2n_e(\boldsymbol{D}'_{t_1})^T_\ell & \boldsymbol{T}_{SV} + \boldsymbol{K}_{SV} \end{pmatrix}.$$

Given this matrix, FPTs to reach an adjacent vertex or return to $\boldsymbol{X}$ in a state other than ℓ may be found using the techniques discussed above. After simplification, one can show that Eq. D.7 are the resulting solutions.

Likewise, one can substitute $\boldsymbol{T}^{\text{eff}}_{1,r}$ and $\boldsymbol{T}^{\text{eff}}_{2,r}$ into Eqs. (D.2) and (D.3) for the spatial moments. However, since both approaches end up computing approximate moments for the same initial system which includes SVs and junctions, they must both yield very similar results. The distinction is that in the latter case, the definition of a single jump has been redefined to only include jumps where the position or state of the particle changes. This distinction is important in regard to interpreting the elements of $\boldsymbol{T}^{\text{eff}}$. In the former case, they cannot be considered as jump probabilities multiplying waiting-time distributions in the standard sense, but after rescaling, they can.

Appendix E: Random Walks on Segments with Various Boundary Conditions

Consider a random walk on $\mathbb{Z}$ where at each $k \in \mathbb{Z}$, there is a 1/2 probability of jumping to the left or right. If the random walk starts at $\ell \in \mathbb{Z}$, the probability generating function for the probability of finding the walker at m is (Hughes1996)

$$u^{(F)}(z, m|\ell) = \sum_{n=0}^{\infty} z^n p_n(m|\ell) = (1 - z^2)^{-1/2} x^{|m-\ell|} \tag{E.1}$$

with

$$x \equiv z^{-1}\left(1 - \sqrt{1 - z^2}\right)$$

and $p_n(m|\ell)$ being the probability of reaching m after starting at ℓ on the nth step of the walk. For a periodic segment with $m, \ell = 0, 1, \ldots, N$, the solution is given by

using the method of images (Montroll and Greenberg 1964) as

$$u^{(P)}(z,m|\ell) = \sum_{k=-\infty}^{\infty} u^{(F)}(z,m+Nk|\ell) = \left(\frac{x^{m-\ell}+x^{N-(m-\ell)}}{1-x^N}\right)(1-z^2)^{-1/2}.$$

It is also possible to find solutions with other types of boundary conditions (Hughes 1996; Weiss and Rubin 2007). For instance, the image points for a random walk on a segment with two absorbing boundaries are of the form $\{2kN \pm \ell\}$, and the method of images solution yields

$$u^{(AA)}(z,m|\ell) = \frac{x^{|m-\ell|} - x^{|m+\ell|} + x^{2N}(x^{-|m-\ell|} - x^{-|m+\ell|})}{\sqrt{1-z^2}\left(1-x^{2N}\right)}. \tag{E.2}$$

Moments of $u^{(F)}(z,\cdot|\cdot)$ can be found by summing over m and using identities related to geometric series:

$$\begin{aligned}
\sum_{n=0}^{N} r^n &= \frac{1-r^{N+1}}{1-r} \\
\sum_{n=0}^{N} n r^n &= r\frac{d}{dr}\left[\frac{1-r^{N+1}}{1-r}\right] = r\frac{1-(N+1)r^N+Nr^{N+1}}{(1-r)^2} \\
\sum_{n=0}^{N} n(n-1) r^n &= r^2\frac{d^2}{dr^2}\left[\frac{1-r^{N+1}}{1-r}\right] \\
&= r^2\frac{2-N(1+N)r^{N-1}+2(N^2-1)r^N-N(N-1)r^{1+N}}{(1-r)^3} \\
\sum_{n=0}^{N} n(n-1)\ldots(n-k) r^n &= r^k\frac{d^k}{dr^k}\left[\frac{1-r^{N+1}}{1-r}\right]
\end{aligned}$$

For finite N, these formulas are valid (if one uses L'Hopitals rule at $r = 1$) for all r, and in the case that $N \to \infty$, the results are valid if $0 \le r < 1$. In particular, the variance of $u^{(F)}$ over the integers is

$$\sigma^2(z) = \frac{z}{(1-z)^2}. \tag{E.3}$$

In the CTRW setting, one can find the arrival probabilities, $q(x,t|y)$ by substituting the Laplace transform of $\psi(t)$ for z in the formulas in this section. Likewise, upon multiplying by $\hat{\Phi}(s)$, the probability, $p(x,t|y)$ and time-dependent moments can be found. For instance, for an unbiased 1D CTRW with nearest neighbor jumps,

$$\sigma(s) = L^2\frac{1-\psi}{s}\frac{\psi}{(1-\psi)^2} = \frac{L^2}{s}\frac{\psi}{1-\psi}$$

as was found in Eq. (43) by different techniques.

The first-passage-time probability generating function may also be found by making use of the definition in Eq. (E.1) for $u^{(F)}$. As derived in Montroll and Weiss (1965),

$$f^{(F)}(z, m|\ell) = \frac{u^{(F)}(z, m|\ell) - \delta_{m,\ell}}{u^{(F)}(z, 0|0)}.$$

Furthermore, this result is easily extended to much more general cases such as multi-state random walks, and walks on complicated structures (Hughes 1996).

References

Akiyama T, Kamimura K, Firkus C, Takeo S, Shimmi O, Nakato H (2008) Dally regulates Dpp morphogen gradient formation by stabilizing Dpp on the cell surface. Dev Biol 313(1):408–419

Iomin A (2011) Subdiffusion on a fractal comb. Phys Rev E 83(5):052106

Iomin A (2019) Richardson diffusion in neurons. Phys Rev E 100(1):010104

Iomin A, Zaburdaev V, Pfohl T (2016) Reaction front propagation of actin polymerization in a comb-reaction system. Chaos Solitons Fract 92:115–122

Kicheva A, Pantazis P, Bollenbach T, Kalaidzidis Y, Bittig T, Jülicher F, Gonzalez-Gaitan M (2007) Kinetics of morphogen gradient formation. Science 315(5811):521–525

Berezhkovskii AM, Dagdug L, Bezrukov SM (2014) From normal to anomalous diffusion in comb-like structures in three dimensions. J Chem Phys 141(5):054907

Berezhkovskii AM, Dagdug L, Bezrukov SM (2015) Biased diffusion in three-dimensional comb-like structures. J Chem Phys 142(13):134101

Bracewell RN (1986) The Fourier transform and its applications, vol 31999. McGraw-Hill, New York

Bressloff PC, Kim H (2018) Bidirectional transport model of morphogen gradient formation via cytonemes. Phys Biol 15(2):

Bressloff PC, Newby JM (2013) Stochastic models of intracellular transport. Rev Mod Phys 85(1):135

Gadgil C, Lee CH, Othmer HG (2005) A stochastic analysis of first-order reaction networks. Bull Math Biol 67:901–946

Cox DR (1967) Renewal theory, vol 1. Methuen, London

Entchev EV, Schwabedissen A, Gonzalez-Gaitan M (2000) Gradient formation of the TGF-beta homolog Dpp. Cell 103(6):981–91

Feller W (1968) An introduction to probability theory. Wiley, New York

Mainardi F, Raberto M, Gorenflo R, Scalas E (2000) Fractional calculus and continuous-time finance II: the waiting-time distribution. Phys A 287(3–4):468–481

Aurenhammer F, Klein R, Lee DT (2013) Voronoi diagrams and Delaunay triangulations. World Scientific Publishing Company, Singapore

Gibson WT, Gibson MC (2009) Cell topology, geometry, and morphogenesis in proliferating epithelia. Curr Topics Dev Biol 89:87–114

Gibson MC, Lehman DA, Schubiger G (2002) Lumenal transmission of Decapentaplegic in Drosophila imaginal discs. Dev Cell 3(3):451–60

Goldhirsch I, Gefen Y (1987) Biased random walk on networks. Phys Rev A 35(3):1317

Haerry TE, Khalsa O, O'Connor MB, Wharton KA (1998) Synergistic signaling by two BMP ligands through the SAX and TKV receptors controls wing growth and patterning in Drosophila. Development 125(20):3977–3987

Hamid T, Kolomeisky AB (2013) All-time dynamics of continuous-time random walks on complex networks. J Chem Phys 138(8):084110

Harris TJC, Tepass U (2010) Adherens junctions: from molecules to morphogenesis. Nat Revs Mol Cell Biol 11(7):502–514

Henyey FS, Seshadri V (1982) On the number of distinct sites visited in 2 d lattices. J Chem Phys 76(11):5530–5534

Hu J, Othmer HG (2011) A theoretical analysis of filament length fluctuations in actin and other polymers. J Math Biol 63(6):1001–1049

Hughes BD (1996) Random walks and random environments. Clarendon Press, Oxford
Iomin A, Méndez V (2013) Reaction-subdiffusion front propagation in a comblike model of spiny dendrites. Phys Rev E 88(1):
Goldhirsch I, Gefen Y (1986) Analytic method for calculating properties of random walks on networks. Phys Rev A 33(4):2583
Isaacson SA (2009) The reaction-diffusion master equation as an asymptotic approximation of diffusion to a small target. SIAM J Appl Math 70(1):77–111
Gou J, Lin L, Othmer HG(2018) A model for the Hippo pathway in the Drosophila wing disc. Biophys J 115(4):737–747 PMID: 30041810
Gou J, Stotsky JA, Othmer HG (2020) Growth control in the Drosophila wing disk. Wiley Interdisciplinary Reviews, New York, Systems biology and medicine, p e1478
Kang HW, Zheng L, Othmer HG (2012) A new method for choosing the computational cell in stochastic reaction-diffusion systems. J Math Biol 2012:1017–1099
Karlin S, Taylor HM (1975) A first course in stochastic processes, 2nd edn. Academic Press, New York
Kim H, Bressloff PC (2018) Direct vs. synaptic coupling in a mathematical model of cytoneme-based morphogen gradient formation. SIAM J Appl Math 78(5):2323–2347
Kornberg TB (2014) Cytonemes and the dispersion of morphogens. Wiley Interdiscip Rev Dev Biol 3(6):445–463
Kornberg TB, Roy S (2014) Cytonemes as specialized signaling filopodia. Development 141(4):729–736
Choi KW (2018) Upstream paths for Hippo signaling in Drosophila organ development. BMB Reports 51(3):134
Lin L, Othmer HG (2017) Improving parameter inference from frap data: an analysis motivated by pattern formation in the Drosophila wing disc. B Math Biol 79(3):448–497
Lubashevskii IA, Zemlyanov AA (1998) Continuum description of anomalous diffusion on a comb structure. J Exp Theor Phys 87(4):700–713
Ciocanel MV, Fricks J, Kramer PR, McKinley SA (2020) Renewal reward perspective on linear switching diffusion systems in models of intracellular transport. Bull Math Biol 82(10):1–36
Matthaus F, Jagodic M, Dobnikar J (2009) E. coli superdiffusion and chemotaxis-search strategy, precision, and motility. Biophys J 97(4):946–957
Metzler R, Klafter J (2000) The random walk's guide to anomalous diffusion: a fractional dynamics approach. Phys Reports 339(1):1–77
Montroll EW, Weiss GH (1965) Random walks on lattices II. J Math Phys 6(2):167–181
Montroll EW, West BJ (1979) On an enriched collection of stochastic processes. Fluct Phen 66:61
Montroll EW (1969) Random walks on lattices. III. calculation of first-passage times with application to exciton trapping on photosynthetic units. J Math Phys 10(4):753–765
Montroll EW, Greenberg JM (1964) Proceedings of the symposium on applied mathematics. Am Math Soc Providence 16:193
Mundt MG (2013) Characterization of a unique basolateral targeting domain in the Drosophila TGF-β type II receptor punt. Master's thesis, University of Minnesota
Othmer HG, Painter K, Umulis D, Xue C (2009) The intersection of theory and application in biological pattern formation. Math Mod Nat Phenom 4(4):3–82
Othmer HG (1983) A continuum model for coupled cells. J Math Biol 17:351–369
Othmer HG, Scriven LE (1971) Instability and dynamic pattern in cellular networks. J Theor Biol 32:507–537
Othmer HG, Dunbar SR, Alt W (1988) Models of dispersal in biological systems. J Math Biol 26(3):263–298
Pavliotis G, Stuart A (2008) Multiscale methods: averaging and homogenization. Springer, Berlin
Roerdink JBTM, Shuler KE (1985) Asymptotic properties of multistate random walks. I. theory. J Stat Phys 40(1):205–240
Roerdink JBTM, Shuler KE (1985) Asymptotic properties of multistate random walks. II. applications to inhomogeneous periodic and random lattices. J Stat Phys 41(3):581–606
Churchill RV (1958) Operational Mathematics. McGraw-Hill
Scher H, Wu CH (1981) Random walk theory of a trap-controlled hopping transport process. Proc Natl Acad Sci 78(1):22–26
Zhou S, Lo WC, Suhalim JL, Digman MA, Enrico G, Qing N, Lander AD (2012) Free extracellular diffusion creates the Dpp morphogen gradient of the Drosophila wing disc. Curr Biol 22(8):668–675
Shlesinger MF (1974) Asymptotic solutions of continuous-time random walks. J Stat Phys 10(5):421–434
Havlin S, Ben-Avraham D (1987) Diffusion in disordered media. Adv Phys 36(6):695–798

Roy S, Huang H, Liu S, Kornberg TB (2014) Cytoneme-mediated contact-dependent transport of the Drosophila decapentaplegic signaling protein. Science 343(6173):1244624
Harmansa S, Alborelli I, Dimitri B, Caussinus E, Affolter M (2017) A nanobody-based toolset to investigate the role of protein localization and dispersal in Drosophila. Elife 6:
Subrahmanyan C (1943) Stochastic problems in physics and astronomy. Rev Mod Phys 15(1):1
Landman U, Shlesinger MF (1977) Cluster motion on surfaces: a stochastic model. Phys Rev B 16(8):3389
Landman U, Shlesinger MF (1979) Stochastic theory of multistate diffusion in perfect and defective systems. I. mathematical formalism. Phys Rev B 19(12):6207
Landman U, Shlesinger MF (1979) Stochastic theory of multistate diffusion in perfect and defective systems. II. case studies. Phys Rev B 19(12):6220
Landman U, Montroll EW, Shlesinger MF (1977) Random walks and generalized master equations with internal degrees of freedom. Proc Natl Acad Sci 74(2):430–433
Van Kampen NG (1992) Stochastic processes in physics and chemistry, vol 1. Elsevier, London
Wartlick O, Mumcu P, Jülicher F, Gonzalez-Gaitan M (2011) Understanding morphogenetic growth control - lessons from flies. Nat Rev Mol Cell Biol 12(9):594–604
Weiss GH, Havlin S (1986) Some properties of a random walk on a comb structure. Phys A 134(2):474–482
Weiss GH, Rubin RJ (2007) Random walks: theory and selected applications. Wiley-Blackwell, London, pp 363–505
Widmann TJ, Dahmann C (2009) Wingless signaling and the control of cell shape in Drosophila wing imaginal discs. Dev Biol 334(1):161–173
Yamazaki Y, Palmer L, Alexandre C, Kakugawa S, Beckett K, Gaugue I, Palmer RH, Vincent JP (2016) Godzilla-dependent transcytosis promotes Wingless signalling in Drosophila wing imaginal discs. Nat Cell Biol 18(4):451–457